EFFECT OF POZZOLANIC MATERIAL ON THE RESTRAINED SHRINKAGE BEHAVIOR OF SELF-CONSOLIDATING CONCRETE

by

UFUK ATES

A Thesis submitted to the

Graduate School – New Brunswick

Rutgers, The State University of New Jersey

in partial fulfillment of the requirements

for the degree of

Master of Science

Graduate Program in Civil and Environmental Engineering

written under the direction of

Dr. Hani H. Nassif

and approved by

_____

_____

_____

New Brunswick, New Jersey

May 2010

ABSTRACT OF THE THESIS

Effect of Pozzolanic Material on the Restrained Shrinkage Behavior of Self-Consolidating Concrete

by UFUK ATES

Thesis Director:

Dr. Hani H. Nassif

Self-consolidating concrete (SCC) has been the subject of various research projects, and its use has been a source of increasing interest in industry. The very early phase of SCC research mainly focused on mechanical and fresh concrete properties. The area of SCC research was then enlarged with the inclusion of shrinkage behavior. This was necessary because SCC as a concrete type was always presumed to exhibit higher levels of free and restrained shrinkage due to its higher cementitious material content. Given that concrete in general has very low tensile strength capacity, especially the deformations caused by restrained shrinkage behavior are among the primary concerns related to SCC.

Restrained shrinkage behavior of SCC is investigated in this study, with the emphasis on cracking ages and patterns. The AASHTO-T334 test setup is used to evaluate the cracking potential of the SCC mixes. In addition to the steel ring data

collection method of AASHTO-T334, Vibrating Wire Sensor Gages (VWSG) were also implemented to collect concrete strain measurements. Many other laboratory tests such as the compressive strength, splitting tensile strength, modulus of elasticity, and free shrinkage were performed in companion with the restrained shrinkage test. The resistance to restrained shrinkage cracking of the SCC was found to be weak since all the SCC mixes cracked under restrained shrinkage before day 56 after casting. Moreover, except for one SCC mix, the cracking was observed only between day 19 and 31 after casting. Amount of total cementitious material was found to have the greatest effect on the restrained and free shrinkage performance of the SCC mixes. Partial replacement of Portland cement with high percentages of fly ash was found to have the potential to increase the elapsed time until cracking. If silica fume was used as a replacement, the cracking performance was slightly worse whereas the free shrinkage strain increased 10 % at day 56 after casting.

ACKNOWLEDGEMENTS

I would like thank my advisor Dr. Hani H. Nassif for his support throughout all my study at Rutgers. It was an honor to work with him and be exposed to his engineering and life experience.

I would also like to thank Dr. Husam Najm and Dr. Kaan Ozbay for being in my thesis committee and for their valuable advice.

I would like to thank my parents for their infinite support and care throughout my life.

I would like to thank John Montemerano for his help at the early stages of my laboratory experience. His help was very important at the outset of my research. I would like also like to thank my graduate partner Dan Su for being helpful throughout my study.

I would like to thank Christopher Kirchner, Michael Leonard, Parth Oza, Carl Fleurimond and all my friends in the lab for their help with the various laboratory tasks involved during my study. Their continuous efforts enabled me to complete this work.

Special thanks are due to Sami Demiroluk, and Ozan Etkin Kara for their invaluable help and hard work at the later ages of my study.

TABLE OF CONTENTS

LIST OF TABLES

LIST OF FIGURES

CHAPTER I

INTRODUCTION

1.1 PROBLEM STATEMENT

Self-Consolidating Concrete (SCC) has many advantages over High Performance (HPC) and Ordinary Portland Cement Concrete (OPC). Its biggest advantage is the improved workability provided by its self-flowing nature. This aspect of SCC inherently reduces the need for consolidation work, and thus decreases construction costs in large scale projects. Workability of concrete is very important for avoiding improper settlement of the material. In cases where the reinforcement is congested or the formwork irregularities create obstructions for consolidating the concrete, the casted sections will not only deviate from their actual design sections but also deteriorate faster because the reinforcement will be more vulnerable to environmental effects. Such vulnerability becomes a durability issue if the structure is exposed to severe environmental conditions. To avoid these types of problems, special care needs to be taken while applying external vibration to consolidate the concrete. In the case of SCC, this task is less burdensome in that the material is already able to flow through the formwork if properly designed and batched.

Although SCC is very appealing from a constructability point of view, there are still many concerns, especially those mainly related to its visco-elastic aspects. For

instance, SCC is presumed to undergo greater free and restrained shrinkage deformations because SCC mix designs incorporate very large amounts of cementitious material compared to HPC and OPC mixes. Previous research findings presented in the next sections of this thesis support this presumption for both types of shrinkage phenomena. In the case of free shrinkage, SCC will experience only a level of length change and no other deformations will occur since concrete by its nature is already very efficient at compression. On the other hand, if restraints are exerted against concrete shrinkage, internal tensile stresses will build up and may result in tensile cracking of concrete. Although SCC is a high strength concrete type such as HPC, tensile cracking is most likely to occur because the cracking capacity of concrete is very limited. So, given that SCC will shrink faster than HPC and OPC, the risk of tensile cracking under restrained conditions is very high.

The growing demand for SCC also increases the need for establishing an extensive range of standards. As discussed above, there is a great need to better understand the shrinkage performance of this material under restrained conditions. By overcoming this disadvantage through research and established standards, the use of SCC in various structural applications will eventually be disseminated.

Since SCC is more likely to exhibit more shrinkage than HPC and OPC, the optimization of the mix designs is very important in order to reduce the shrinkage deformations. The minimization of shrinkage is particularly important for extending the time until cracking under restrained conditions. Therefore, the influence of individual mix design parameters should be extensively studied in both cases, that is, whether or not there is restraint for concrete shrinkage.

1.2 RESEARCH OBJECTIVES AND SCOPE

This primary goal of this study is to evaluate the restrained shrinkage cracking behavior of the produced SCC mixes. The evaluation was conducted by comparing the cracking ages of concrete specimens and the cracking patterns as well. Visual crack observations were used as a part of this evaluation. In addition, free shrinkage measurements of the SCC mixes were compared to each other and correlated with restrained shrinkage measurements. Mechanical properties such as the compressive strength, splitting tensile strength, and the modulus of elasticity were also tested in companion with the shrinkage measurements. SCC mixes were grouped into 3 categories to study the effect of different mix design parameters. The studied parameters included the total cementitious material content, percentage of fly ash, and the percentage of silica fume replacement in the mix designs. The total amount of cementitious material content for the SCC mixes was between 800 and 900 pounds per cubic yard of each batch. The fly ash replacement was between 10% and 30%, whereas the silica fume replacement was between 0 and 10% among the studied SCC mixes.

1.3 THESIS ORGANIZATION

This thesis consists of 5 chapters and is organized in the following manner:

Chapter 1 covers the introduction including the problem statement, research objectives and scope, and thesis organization.

Chapter 2 covers the literature review for SCC including the background, previous research work related to free and restrained shrinkage, and also a review of SCC's mechanical properties.

Chapter 3 covers the experimental program including the source material properties and all the testing procedures used for the SCC mixes.

Chapter 4 covers all the laboratory test results for mechanical properties, free and restrained shrinkage, cracking patterns, and the analysis conducted from the test results.

Chapter 5 covers the conclusions and the recommendations of the study along with the scope of research.

CHAPTER II

LITERATURE REVIEW

2.1 INTRODUCTION

Self-Consolidating Concrete (SCC) initially emerged from the interest of Professor Hajime Okamura, Kochi University of Technology in investigating the durability performance of concrete structures. The durability of the structures was observed to be below the desired level as a result of the poor consolidation at casting. The deficiencies in the consolidation of concrete were mainly attributed to the difficulty in sustaining the number of skilled workers in the job market. [24]

One can better understand the abovementioned concrete research interest by looking at the various sources of that interest. In the case of concrete durability, the motivation behind the research could be the various aspects of the material that need to be improved. If a high seismic zone is a matter of concern, for instance, the heavily reinforced sections have to go under proper consolidation since the controversy will lead to corrosion problems or create structural members that are not complying with their actual design. Not surprisingly, the concrete durability issue triggered the need for a new concrete technology, Self-Consolidating Concrete, in Japan where the structures are vulnerable to high seismic activities.

In 1988, Okamura and his research team achieved the first prototype of Self-Consolidating Concrete. This new concrete technology was first entitled as “High-

Performance Concrete" but then changed to "Self-Compacting Concrete" to distinguish the new concrete technology from its predecessors. The term "High Performance Concrete" refers to a type of concrete which simultaneously has adequate strength and durability capacities, while "Self-Compacting Concrete" refers to a type of "High Performance Concrete" having high flowability characteristics.

Okamura's study attracted considerable attention when the work was presented at the Second East-Asia and Pacific Conference on Structural Engineering, EASEC-2 (1989). The knowledge of SCC technology continued to spread after Ozawa's presentation at CANMET & ACI International Conference in Istanbul (1992). After attracting global attention, SCC started to be a subject of research in Europe, Korea, Thailand, and Canada. Okamura's "Ferguson Lecture" at the ACI Fall Convention held in New Orleans was also a milestone that drew the attention of researchers in North America. The RILEM committee on SCC formed in 1997, and the 1998 first international workshop on SCC held in Kochi, Japan were other early global activities that expedited the globalization of SCC. More detailed information on chronological recognition of SCC can be found in Okamura and Ouchi (2003).

2.2 TECHNOLOGY OVERVIEW: SELF CONSOLIDATING CONCRETE

2.2.1 Structural Applications of SCC

Some early applications of SCC use as structural concrete can be found in Ouchi et al. (2003). Ritto Bridge in Japan was shown to be one of the earliest experiences for the SCC use in structures. This bridge, with columns as high as 65 meters and with a

congested reinforcement design, presented an SCC option to provide adequate workability. During the project, the initial slump was targeted as 600mm, but then increased to 650 due the obstacles in pumping.

Another example of SCC structural applications presented by Ouchi et al. (2003) is the Higashi-Oozu viaduct also built in Japan. The difficulties in girder construction due to the dimensional obstructions as well as the complaints regarding excessive vibration and noise led to the choice of SCC over conventional concrete. Thus, prestressed T-girders were used, and the cost estimations revealed that the total construction cost was reduced by approximately 7% with SCC use.

Experience with SCC in the Sodra Lanken Project in Sweden was also reviewed by Ouchi et al. (2003). In this large-scale infrastructure project, SCC was used in concrete rock linings, underground installation structures, rock tunnel entrances, and retention walls with negative and relief structures. Low slump values such as 450-500mm were encountered in the early stages of each concrete cast, and therefore superplasticers were introduced to the agitating trucks to bring the slump to the desired levels. Despite all the difficulties in casting some of the sections such as the arches and walls, later observations revealed that SCC performed better in terms of surface evenness and porosity than sections casted with conventional concrete.

After a variety of structural applications of SCC in different countries, SCC gained the attention of the precast industry in the United States. NCHRP Project 18-12 was initiated in the early 2000's to provide guidelines for the use of precast, prestressed structural elements in bridge construction. In the meantime, several State Department of Transportation's (SDOT's) conducted research programs to investigate the possible

advantages and disadvantages of SCC use in this area. One of these investigations was undertaken by Larson et al. (2007) to evaluate the material properties, the bond characteristics, and the time-dependent deformations of bridge girders casted with SCC. The first phase of this research consisted of testing 15 pretensioned flexural sections to evaluate the transfer and development lengths. In the second phase, elastic shortening, creep, and shrinkage deformations were evaluated for the SCC mix design. In the last phase, the bridge girders used in the field were monitored for prestress losses. For this phase, a five-span bridge was selected and 7 girders were instrumented, three of which were casted using SCC. One of the conclusions reached by Larson et al. (2007) was that the effective prestress losses for the SCC girders correlated with the AASHTO, ACI/PCI, and Kansas DOT design equations. In other words, the authors found out that the prestress loss calculations for SCC girders did not require any special provisions.

Another study related to precast bridge beams was performed by Ozyildirim (2008). In this study, the performance of SCC Bulb - T beams was evaluated both prior to and during construction. First, 2 beam specimens were casted using SCC, and loaded to different modes of failure. The sections were found to develop the nominal flexural capacity in accordance with the initial analysis. And observed strand-concrete bond development was found to be adequate.

Ozyildirim (2008) also instrumented 2 of the actual SCC and 2 conventional concrete bridge girders with sensors. The average cambers measured at the SCC girders were found to be slightly higher, whereas the in-service cambers and strains were similar for both SCC and conventional concrete girders. In general, SCC girder placement and behavior were rated as successful, and it was acknowledged that the design of such

members can be performed using methods similar to those of conventional concrete girder designs.

Along with the bridge superstructure element construction, SCC was found to have the potential to improve the drilled shat installations because of its high flowability. Hodgson (2005) presents the research conducted to evaluate the performance of drilled shafts casted using SCC. Two SCC and three conventional concrete shafts were constructed to compare the performance of the two concrete types. Two of the conventional concrete mixes were batched with No.57 crushed limestone, whereas the third one and the SCC mixes were batched with No. 7 uncrushed rounded river gravel. Fresh and hardened concrete tests were performed for the SCC and the conventional concrete shafts. Four months after the construction, the drilled shafts were exhumed and visually inspected. Any possibility of segregation was attributable to aggregates trapped inside the congested reinforcement cages. The hardened state performance of the concrete was evaluated in terms of compressive strength, modulus of elasticity and the Poisson's ratio. After the investigations, drilled shafts built with No. 7 aggregate showed more even and consistent cross sections and also less aggregate blocking compared to other drilled shafts incorporating No. 57 aggregate.

2.2.2 Specifications and Recommended Practice

Although Japan, Europe, and China have established specifications and guidelines for the design and testing of SCC in the first half of 2000's, such progress has still not been frequently achieved in the United States. However, the NCHRP Project 18-12 has recently provided an extensive guideline in the bridge construction area. One of the many challenging objectives of this study was to evaluate AASHTO models in the case of SCC,

and to recommend revisions. The first of the three phases from this research program involved a parametric study on different mix design parameters and material components. The parametric study aimed to provide assistance in developing SCC mix design recommendations. Forty three mixes were produced with different slump flow, aggregate type, and binder types. Twenty four of these mixes were non-air entrained.

In the second phase of NCHRP Project 18-12 the influence of mixture proportioning and material characteristics on both fresh and hardened concrete properties were evaluated. The studied SCC properties included temperature rise, autogenous and drying shrinkage, creep, and as well as the pull-out bond strength. Also, the effect of air-entrainment on the fresh and hardened concrete properties was evaluated. Moreover, 3.6 feet high PVC column forms were casted and installed with pressure sensors to record the initial formwork pressure exerted by SCC.

Phase 3 of NCHRP Project 18-12 consisted of the structural performance tests for full-scale AASHTO precast prestressed bridge girders. SCC bridge girders were evaluated in terms of constructability, temperature variations, transfer length, camber, flexural and shear cracking, and shear strength characteristics. Two AASHTO Type-II SCC girders, along with the same two types of HPC girders, were casted. Fresh, hardened, visco-elastic, and rheological properties of the batches were also tested along with the structural performance tests performed.

Based on the extensive laboratory testing program, Khayat and Mitchell (2009) presented their findings and recommendation about the relative effects of material constituents and designs, and the structural performance testing results of the AASHTO girders. The authors also developed guidelines for SCC use in precast prestressed bridge

girders based on the experimental program implemented and on literature review survey results. These SCC guidelines included the early age and mechanical properties, durability and structural performance of the material. Detailed information on the guidelines and conclusions can be found in Reference 12.

Some of the research findings of Khayat and Mitchell (2009) that are relevant to the current study are briefly mentioned to provide a reference for some of the following thesis sections.

- Drying shrinkage of 16 SCC and 2 HPC mixes ranged between 495 and 975 micro strains after 300 days.
- With 18 hours of steam curing, drying shrinkage of SCC was found to be 5% to 30% higher than that of HPC at day 300.
- The increase in the binder content worsened the drying shrinkage behavior.
- SCC with high Sand to Total Aggregate Ratio can exhibit higher drying shrinkage in long term.
- The type of binder used does not affect the drying shrinkage significantly.

Also, Khayat and Mitchell's (2009) research findings related to the effect of entrained air percentage, as well as the mix fluidity, on the mechanical properties of SCC are shown in Figure -2-1 and Figure 2-2. The global performance and rankings shown in the figures are based on the selected parameter weights considered by the authors. For example, the weight of 56 day compressive strength is assumed to have a weight of 2, whereas 18 hour steam curing had a weight of 3. Also, "++" represented compressive strength be at a medium level (8-10ksi), while "+++" represented a high strength level (higher than 10ksi)

SCC Behavior	Fluidity level		
	Low	Medium	High
HRWRA demand (×1)	NA	NA	NA
Slump flow retention (×1)	+++	+++	+
Passing ability (×1)	+	++	+++
Filling capacity (×2)	+	++	+++
Static stability (×2)	+++	++	+
Total fresh properties	**12**	**13**	**12**
18-hour compressive strength steam-cured (×3)	+++	+++	++
18-hour compressive strength air-cured (×1)	+++	+++	++
56-day compressive strength (×2)	+++	+++	++
18-hour modulus of elasticity (×2)	+++	+++	++
Total hardened properties	**24**	**24**	**16**
Global performance	**36**	**37**	**28**
Ranking	**II**	**I**	**IV**

Figure -2-1 SCC Performance with Respect to Fluidity, Khayat and Mitchell (2009)

SCC Behavior	*w/cm*		Air entrainment	
	0.33	0.38	without AEA	with AEA
HRWRA demand (×1)	++	+++	NS	NS
Slump flow retention (×1)	++	+++	NS	NS
Passing ability (×1)	++	+++	++	+++
Filling capacity (×2)	++	+++	++	+++
Static stability (×2)	+++	++	+++	++
Total fresh properties	**16**	**19**	**12**	**13**
18-hour compressive strength steam-cured (×3)	+++	++	+++	++
18-hour compressive strength air-cured (×1)	++	+++	++	+++
56-day compressive strength (×2)	+++	++	+++	++
18-hour modulus of elasticity (×2)	+++	+++	+++	++
Total hardened properties	**23**	**19**	**23**	**17**
Global performance	**39**	**38**	**35**	**30**
Ranking	**I**	**I**	**I**	**III**

Figure 2-2 SCC Performance with Air Entrainment, Khayat and Mitchell (2009)

2.3 REVIEW OF PREVIOUS RESEARCH ON MATERIAL PROPERTIES OF SELF COMPACTING CONCRETE

2.3.1 Mechanical Properties

Since SCC is considered a high performance type of concrete, it is expected to provide high compressive and tensile strength similar to HPC. This assumption is based mainly on the high w/b ratio, in other words, the high cementitious material content used in SCC mix designs to provide flowability during the fresh state. From strength point of view, the improvements in SCC relative to OPC or HPC have been widely searched and different levels of improvement can be seen compared to the previous research findings.

Nakin et al. (2006) provide the results of mechanical testing performed on SCC, HPC, and OPC types of mixes. In their experimental program, a total of 8 mixes including one OPC, two HPC and five SCC types were evaluated. Except for one SCC mix, all the mixes had a water to cementitious material ratio of 0.39. ASTM C39, C4622 and C496 were followed to perform compressive strength, modulus of elasticity, and splitting tensile strength tests, respectively. The authors reported that the compressive strength difference between SCC and OPC was not significant whereas the splitting tensile difference was approximately 10 %. Modulus of elasticity for SCC was found to be approximately 5% lower than OPC.

Another comparison between SCC and conventional concrete was completed by Naito et al. (2005). The authors compared the hardened state properties of an SCC mix design with a conventional high early strength concrete (HESC) mix design. Six batches of each concrete type were produced. Water to cement ratios of the mix designs were 0.32 and 0.34 for SCC and HESC, respectively, and all the batches varied from the actual

mix designs by less than 1%. Average slump flow for the SCC mixes was 21.3 inches whereas the average slump of the HESC mixes was 6.3 inches.

ASTM C39 compressive strength test results at day 28 reported by Naito et al. (2005) were 7366psi for HESC and 8276psi for SCC mixes. Modulus of elasticity testing results both at day 14 and at later testing ages for HESC were relatively higher than those for SCC. At day 14, the modulus of elasticity of HESC was approximately 12% higher for the SCC. This stiffness difference was mainly attributed to the fact that the amount and gradation of coarse aggregate used in HESC were higher. For tensile strength capacity, ASTM C496 and C78 were performed, and the direct tension capacity as well as the modulus of rupture for SCC was found to be higher than for HESC.

Nowak et al. (2005) performed a comparison of mechanical properties between several SCC mix designs and a conventional concrete mix design, which was derived from an ACI 211.1 mix design approach and was a typical concrete mix for reinforced concrete bridge slabs. The target compressive strength for this conventional concrete mix design was 4ksi and the water to cement ration was 0.54. On the other hand, the SCC mixes had a low water to cementitious material ratio of 0.29. At day 28, SCC mixes developed a compressive strength of 9ksi, where as the conventional concrete had a strength of 4.5ksi. The authors also reported that the splitting tensile strength, modulus of rupture, and the modulus of elasticity of SCC mixes was 30% to 45% higher than those of conventional concrete mix.

In general, the w/c ratio of the SCC mixes is the dominant factor in affecting mechanical properties, especially compressive strength. Domone (2005) reported a range of SCC compressive strength test results between 2.9ksi and 14.5ksi by analyzing 68 case

studies of SCC. In this analysis, 80% of the SCC mixes were found to have a compressive strength above 5.8ksi.

In this study presented herein this thesis, the range of test results at day 28 for compressive strength was found to be 6.8 to 9.6 ksi, while the range of splitting tensile strength was 537 to 700 psi. All the SCC mixes fell into these ranges depending on their total cementitious material content and the pozzolanic material replacement percentage. Also, modulus of elasticity testing results of the SCC mixes in this study ranged from 3543 ksi to 4785 ksi. The difference in the modulus of elasticity results for different SCC mixes was mainly dependent on the percentage of entrained air, cementitious material content and type.

2.3.2 Free Drying Shrinkage

Shrinkage of concrete can be defined as the decreasing change in volume starting shortly after production. As simple as this definition is, the complexity of the concrete shrinkage has been the underlying reason for the extensive amount of research conducted on this topic. Many studies focused on understanding the mechanisms, types, measures to quantify, level of controllability, and so on.

In this section, a review of the literature relevant to free shrinkage is presented. Free shrinkage, also widely defined as drying shrinkage, has been a primary concern for researchers in this area since it is more likely to create superior problems. More information about other types of concrete shrinkage can be reviewed in detail in Ref. 1 and 19.

Drying shrinkage of the concrete occurs when there is a difference between the relative humidity of the pores in the concrete capillary system and the environment where

the concrete is placed. This difference initiates an evaporation process which can continue for varying periods depending on the severity of certain factors. There are direct and indirect factors affecting this severity (i.e., the rate and magnitude of the shrinkage), from the external environment where the concrete is placed and also from the internal characteristics of the concrete mix. The difference in the relative humidity, the temperature, and the wind effect can be considered the dominant external factors, whereas the type and size of aggregate , amount of cementitious material, and amount of mixing water are the dominant internal factors affecting the drying shrinkage. Many researchers have studied the effect of these dominant factors on the drying shrinkage of concrete. Despite this being a relatively new concrete technology, numerous studies also been conducted for SCC, and selected studies are detailed further in the following sections.

Among the aforementioned key parameters that have either a beneficial or a negative effect on the drying shrinkage of SCC, the total amount of cementitious material in a given mix design is a primary concern in the case of SCC. Since SCC mixes generally require more cementitious material than conventional concrete mixes, it has always been presumed that the drying shrinkage would be more problematic in the case of SCC. While the past research supports this presumption, there are different findings about the level of shrinkage increase induced by the large amount of cementitious material.

Loser and Leemann (2008) studied the effect of water to binder ratio on the free and restrained shrinkage by comparing 13 SCC mixes to three conventional concrete mixes. 120mm×120mm×360mm prism samples were casted to evaluate the free drying

shrinkage of produced mixes. The free shrinkage samples were stored at 20°C with 90% R.H. for one day and at 20°C with 70% R.H. for 90 days. The authors reported a difference of 10% to 40% in the shrinkage potential between the investigated SCC mixes and the conventional concrete mixes compared at day 91.

Hwang and Khayat (2009) used the ASTM C157 standard free shrinkage test as a companion to the ASTM C1581 restrained shrinkage test. The purpose of ASTM C 157 was mainly to evaluate the visco-elastic properties of the studied mixes while the primary purpose of the study was to find out the cracking potential of SCC mixes under restrained conditions. Free shrinkage samples were immersed in water for six days after demolding at 24 hours. Samples were kept under 23±1°C with a R.H. of 50±3 and measured until day 56. Ten SCC mixes were produced under the experimental program with varying w/b ratios, HRWRA and binder type. Also, one typical high performance concrete (HPC) mix and one ordinary concrete (OC) mix were produced. One of the ten SCC mixes was designed and casted in a way that facilitated comparison with the HPC and OC mixes. This single SCC mix incorporated a low dosage of HRWRA and had a slump flow of 180 mm The results of this comparison were found to be approximately 25% between HPC and SCC, and 27% between OC and SCC. The authors also reported a slight difference of 15 to 25 micro strains in free shrinkage of SCC mixes with 0.42 w/b ratio and SCC mixes with 0.35 w/b ratios, which was mainly attributed to the higher paste content.

Ng et al. (2007) compared both the autogenous and drying shrinkage of an ordinary concrete mix to five different SCC mixes. The authors produced a Portland cement only ordinary concrete mix and five SCC mixes incorporating fly ash and silica

fume as partial replacement of cement. Prismatic concrete specimens with the dimensions of 75mm×75×200mm were cast and fiber optic sensors were instrumented at the center of each specimen. The specimens were demolded at 24 hours after casting and then saturated curing was applied until day seven. After curing, the samples were sealed with impermeable coating at both ends and two of the side surfaces in order to direct the moisture loss to the top and bottom of the specimen. This was assumed to be a simulation of one-directional moisture loss by the authors.

One of the findings by Ng et al. (2007) was that the autogenous shrinkage results of SCC mixtures were found to be 1.8 to 5.5 times larger than that of ordinary concrete mix. This fact was attributed to the low w/c ratio used for the SCC mixes. Meanwhile, the authors found that one year drying shrinkage of all SCC mixes were lower than that of those for ordinary concrete mixes, which ranged from 17% to 36%. This finding was tied to the fact that the lower w/c ratio of SCC mixes accelerates the self desiccation, and thus the loss of relatively more capillary water during curing, whereas the mixes with higher w/c ratio are more likely to lose moisture after the curing is removed.

Another finding of Ng et al. was related to the use of fly ash and silica fume as partial replacements of cement. Two SCC mixes, one of which had 20% Portland cement replaced with fly ash, were compared, and they showed that fly ash replacement decreased the autogenous and one-year drying shrinkage by 40% and 10%, respectively. On the other hand, two of the other SCC mixes were investigated to find out the effect of 5% silica fume replacement. The mix incorporating 5% silica fume replacement exhibited 10% and 4% higher values for autogenous and one-year drying shrinkage, respectively.

Besides the experimental research, one can find several shrinkage prediction models that are used to estimate long-term behavior of concrete. Gomez and Landsberger (2007) used an experimental database of shrinkage results and evaluated the applicability of shrinkage prediction models in the case of SCC. The experimental database used by the authors included 25 different studies that had been already presented at various conferences on SCC and other published articles. The total number of mixes from the selected publications was 123, of which 93 were SCC designs and 30 were OC designs. Fresh concrete properties, testing methods and conditions, compressive strength, and shrinkage results were extracted from the 25 studies.

After compiling the database, the authors then calculated the shrinkage strain by various prediction models, such as CEB-FIP 1990, EHE, ACI 209R, B3 and GL 2000. The generalized equations of these models are given as follows;

$$(\varepsilon_{sh})_t = \frac{t}{35+t}(\varepsilon_{ht})u \quad ACI\,2009R-32 \tag{2.1}$$

where $(\varepsilon_{sh})_t$ is the shrinkage strain at the age of t given that the concrete is cured for one to three days, and $(\varepsilon_{sh})_u$ is the ultimate shrinkage strain.

$$\varepsilon_{cs} = \varepsilon_{cs0}\beta_s \quad CEB-FIP\,1990 \tag{2.2}$$

where ε_{cs} is the shrinkage strain at time t recorded since t_s, ε_{cs0} is the basic shrinkage coefficient, and β_s is the coefficient for shrinkage development.

$$\varepsilon_s = (570-5f_{ck})10^{-6} \quad EHE \tag{2.3}$$

where ε_s is the shrinkage strain at f_{ck} is the compressive strength. The Spanish EHE shrinkage estimation equation is adopted from CEB-FIP 1990.

$$\varepsilon_{sh}(t,t_0) = -\varepsilon_{sh\infty} k_h S(t) \quad B3 \tag{2.4}$$

where ε_{sh} is the shrinkage strain measured at time t, $\varepsilon_{sh\infty}$ is the ultimate shrinkage strain k_h is the humidity dependence factor, and S(t) is the time function for shrinkage.

$$\varepsilon_{sh} = \varepsilon_{shu}\beta(h)\beta(t) \quad GL2000 \tag{2.5}$$

where ε_{sh} is the shrinkage strain, ε_{shu} is the notional ultimate shrinkage strain β(h) is the correction coefficient for the effect of humidity, β(t) is the correction coefficient for the effect of time.

The comparative analysis between predicted and experimental results was then conducted using different statistical techniques including best-fit line, residual analysis, and coefficient of variation. As an overall conclusion, the authors stated that all the models predicted the shrinkage with similar accuracy for SCC and OC. Nonetheless, B3 and ACI 209R was pointed out to be the best estimation methods evaluated at the aforementioned statistical models. CEB-FIP 1990, EHE, and GL2000 models were found out to be accurate when the f_c was lower than 6525psi, while ACI 209R and B3 was at the same level of accuracy when f_c was either lower or higher than 6525 psi.

2.3.3 Restrained Shrinkage

Restrained shrinkage of concrete occurs when the concrete undergoing drying shrinkage is subject to restraints that are resisting the volumetric changes. This would create reactant tensile stresses in the concrete element, and, in most of the cases, lead to cracking due to the poor tensile strength of concrete as a material. Even in the case of no restrained shrinkage cracking, a portion of concrete tensile capacity will be utilized by the additional shrinkage stresses, and thus the element will more likely to be over-stressed

after other stresses are also imposed. For a more specific example of how the shrinkage induced tensile stresses can create over-stressing or cracking , one can consider the negative moment regions of reinforced concrete bridge decks where the material is already expected to utilize its tensile capacity under design loads. Although design of RC decks or slabs includes the effect of shrinkage as a stress component, the approximations in shrinkage prediction models indicate the need to improve the material to account for unexpected circumstances.

Bridge deck elements, as illustrated in the previous paragraph, are a typical example of how the shrinkage of concrete can be restrained. The reinforcement in the deck, or the shear studs that are usually very closely spaced to provide composite girder-deck action are sources of restraints for concrete shrinkage. Reinforced pavements or slabs can also be considered as susceptible locations where restraint of concrete shrinkage can create cracking problems.

Throughout the last couple decades, during which concrete material has been a wide topic of research, researchers have looked at the restrained shrinkage problem in order to mitigate its effects. Meanwhile, the scale of restrained shrinkage studies has been widened and applied to new material technologies. Similarly in the case of SCC, the restrained shrinkage problem has been widely studied starting from the early 2000s. Selected studies in this regards are reviewed and presented in the following section.

2.3.3.1 Testing Methods of Restrained Shrinkage and Past Research Relevant to Self-Consolidating Concrete

Different types of testing setups have been used in the past for assessing the restrained shrinkage behavior of concrete. The linear restrained shrinkage test, or the flat

panel test, can be cited as former examples of these types. After the early 1990s, an important advance in the restrained shrinkage testing methodology was achieved with the implementation of the ring test. Especially after being made a part of AASHTO standard tests after 1997, the ring test has been the handiest testing tool in this area. ASTM also established the ring test as a standard in 2004 by applying slight changes to AASHTO test dimensions. The ring test can be considered relatively inexpensive and easy to use in laboratory conditions. One way to use the ring test is by correlating the changes in the mix design parameters with the associated cracking performance in the hardened state. This can provide useful information in ranking different concrete mix designs in terms of their susceptibility to restrained shrinkage cracking. Another advantage of the ring test is its ability to enable stress level predictions using data collected from steel ring strain sensors.

Although the purpose is similar, there are differences in ASSHTO PP-34 and ASTM C1581 ring tests in terms of specimen and steel ring dimensions. The steel ring used in AASHTO PP-34 has a wall thickness of 12.7 mm ± 0.4 mm (1/2 in. ± 1/64 in.), an outer diameter of 305 mm (12 in.), and a height of 152 mm (6 in.). The total outer diameter of the setup adds up to 457 mm (18 in.) after 3inches of concrete are casted around the ring. The steel ring is instrumented with 4 foil strain gages (FSG) such that the gages are at the mid-height of the steel ring and spaced equally.

The main dimensional differences between the ASTM C1581 and AASHTO PP-34 tests are the concrete and steel ring thickness. The steel ring used in ASTM setup has a wall thickness of 13 ± 0.12 mm (0.5 ± 0.05 in), an outer diameter of 330 ± 3.3 mm (13.0 ± 0.12 in), and a height of 152 ± 6 mm (6.0 ± 0.25 in). The total outer diameter

of the setup adds up to 406 ± 3 mm (16.0 ± 0.12 in) after 1.5 inches of concrete are casted around the ring. ASTM test also requires the instrumentation of the steel ring with at least 2 foil strain gages. The main purpose of decreased concrete thickness along with increased steel ring thickness is to expedite the crack formation since more restraint is exerted to concrete with a stiffer steel ring.

Many studies can be found in the literature where ring tests are used as a tool for measuring restrained shrinkage of concrete. However, the research related to SCC only goes back to the early 2000s since SCC is a relatively new concrete type.

See and Attiogbe (2005) used the ASTM C1581 ring-test while studying the effect of different parameters on the restrained shrinkage performance of 12 SCC and 2 comparative ordinary concrete (OC) mixes. The parametric study included the effects of sand-to-aggregate ratio (S/A), paste content, aggregate shape, and use of shrinkage reducing-admixtures (SRA) on the cracking potential of SCC mixes compared to OC mixes. The effect of S/A ratio was studied by casting 3 mixes with ratios of 0.43, 0.48, and 0.54. The effect of paste content was evaluated through 3 mixes having 430, 490, and 550 kilograms of nominal cement contents per cubic meter of volume. Also, 3 SCC mixes were casted using rounded river gravel, while 3 other SCC mixes were casted using crushed angular limestone to identify any effect of difference.

The authors tested the SCC mixes by ASTM C157 for free drying shrinkage along with the ring test. Shrinkage strain data was collected after demolding the samples at day 1. The experimental program also included compressive strength, modulus of elasticity and splitting tensile tests in the line with ASTM procedures.

One of the conclusions of See and Attiogbe (2005) was that the high fluidity characteristics of SCC were not unfavorable since the compared OC mixes exhibited very similar cracking performance. The reduction in the S/A ratio was found to be beneficial, as well as the minimization of the paste content. Four comparative sets each including 2 SCC mixes were compared to evaluate the effect of paste content. The difference in the total elapsed time until cracking between 493 kg/m^3 and 554 kg/m3, 428 kg/m^3 and 494 kg/m^3, 426 kg/m^3 and 497 kg/m^3, 425 kg/m^3 and 500 kg/m^3 were found to be 3.25, 1, 3.25, and 5.5 days, respectively. See and Attiogbe (2005) also concluded that the utilization of SRA for the SCC mixes increased the elapsed time to cracking as much as 67% to 109%, and SCC mixes with rounded river gravel performed better under restrained shrinkage compared to mixes with crushed angular limestone.

Turcry et al. (2006) used the ring test setup but with relatively smaller dimensions compared to ASTM C1581 and AASHTO PP-34. Figure 2-3 shows the plan and side view of the ring test setup used by Turcy et al. (2006). The purpose of the study was to compare the cracking potential of produced SCC and OC mixes by analyzing their mechanical properties and fracture parameters.

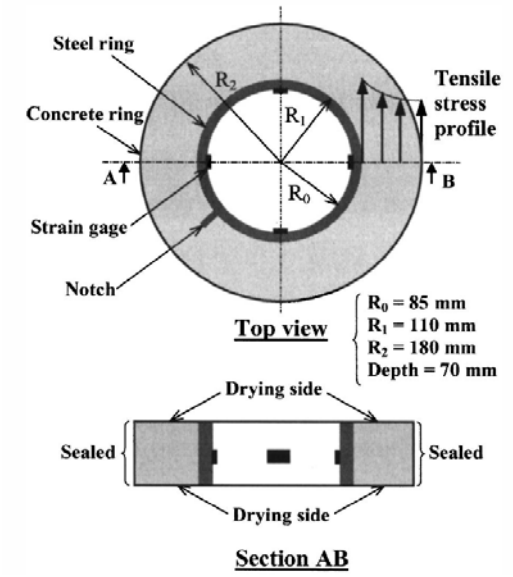

Figure 2-3 Dimensions of the ring specimen casted by Turcy et. al. (2006)

Along with the mechanical properties tests such as the compressive strength, splitting tensile strength, modulus of elasticity, free drying and autogenous shrinkage measurements were taken from 70×70×280mm prism specimens that were allowed to dry on their lateral surfaces after one day of wet curing. The authors also measured the creep strain using the 20% of the loading level obtained from 7-day compression testing.

Turcry et al. (2006) compared three SCC mixes to three ordinary concrete mixes where each SCC mix was associated with one OC mix. These mix designs were selected from different ready-mix concrete plants, and the link between a SCC and an OC mix was related to their 28-day compressive strength testing results.

Restrained shrinkage cracking potential was also predicted by numerical models using the tested material properties. For this purpose, the authors used the approach by Weiss et al. (2000). The authors also used a model to calculate the age at cracking of the ring specimens. The R curve approach proposed by Ouyang and Shah (1991) was adapted

for this purpose. Detailed information about these approaches can be reviewed from Ref. [28] and [38].

Turcry et al. (2006) reported very similar behaviors for 2 out of 3 comparisons made between SCC and OC mixes. The first 2 mixes cracked almost at the same age and exhibited similarly in terms of shrinkage strain magnitude measured from the steel rings. However, the third SCC mix exhibited cracking at day 21 while the associated OC mix cracked at day 56. Similar to its cracking performance, the magnitude of shrinkage strain recorded from this last SCC mix was significantly greater than that of the OC mix.

Hwang and Khayat (2008) used ASTM C1581 to study the restrained shrinkage performance of the SCC mixes produced. The authors evaluated SCC as a material to be used in repair applications where mix proportions and raw material characteristics become very sensitive in reaching the demanded concrete properties. Thus, the focus while studying restrained shrinkage cracking was on the effects of different mix design approaches and binder types. Besides the main matters of investigation, different types of high range water reducing agents (HRWRA) were used to see the relative effect of their base chemical compounds. The difference in mix design approaches was evaluated by means of using two different water to cement ratios (w/c). The first set of SCC mixes was casted with a w/c ratio of 0.35 while the second set was casted using a ratio of 0.42 and with the addition of viscosity enhancing agents (VEA). Three different types of binders incorporating varying amounts of fly ash, slag, and silica fume were used with the second set of SCC mixes while one type of binder blended with fly ash and silica fume was used for the first set of SCC mixes. Besides the SCC mixes, one ordinary concrete mix and one

high performance concrete mix, both used in past repair applications, were produced to provide a comparison.

The experimental program of Hwang and Khayat (2008) included ASTM C157 free drying shrinkage, ASTM C39 compressive strength, and ASTM C469 modulus of elasticity testing, along with the restrained shrinkage ring test. The sampled ring specimens were moist cured using wet burlaps for the first 3 days and then the drying process was initiated right after sealing the top and bottom of the ring. The authors used the prismatic free shrinkage specimens instrumented with a WVSG to simulate the free drying shrinkage of the concrete casted around the ring. This calculated strain, donated as ε_{sh}, was referred to as the total shrinkage resultant from autogenous and drying shrinkage. The authors approached equilibrium of deformations as;

$$\varepsilon_{sh}(t) = \varepsilon_{e}(t) + \varepsilon_{cp}(t) + \varepsilon_{st}(t) \tag{2.6}$$

where $\varepsilon_{sh}(t)$ is the free drying shrinkage, $\varepsilon_{e}(t)$ is the elastic concrete strain, $\varepsilon_{cp}(t)$ is the tensile creep strain, and $\varepsilon_{st}(t)$ is the elastic steel strain.

Using the above-mentioned approach and testing methods, the authors provided comparisons between the investigated parameters. One of the findings was the 26 to 37% extension of elapsed time until cracking with the use of w/c ratio of 0.42 instead of 0.35. This was attributed to the extra stress relaxation linked to the low modulus of elasticity. The authors found out that the mixes produced with polycarboxylate-based HRWRAs cracked much earlier than the mixes produced with polynaphthalene sulfonate-based HRWRAs. The HPC and OC mixes were found to have better cracking resistance

compared to SCC mixes. The authors associated this finding with the relatively higher paste volume of the SCC mixes.

Hwang and Khayat (2008) presented their findings from another parametric study where they investigated the effect of high-range water-reducing admixture types, content of synthetic fibers, dosage of shrinkage-reducing admixtures, and also the use of hybrid fibers on the restrained shrinkage cracking of SCC. The authors produced 13 SCC mixes to investigate the studied parameters. All the investigated mixes had 5% silica fume and 25% class F fly ash by weight of the total 800lbs cementitious material per cubic yard of volume. In addition, some mixes had different types of fibers or fibers with shrinkage reducing admixtures. Restrained shrinkage evaluation was done by casting 2 ASTM C1581 rings for each mix. Free drying shrinkage measurements were taken from 75×75×285mm prism specimens according to ASTM C157. Prism specimens with the same dimensions were installed with strain gages to calculate the free drying shrinkage of ring specimens. Compressive strength and modulus of elasticity of the mixes produced were also measured using cylindrical specimens.

The authors derived a methodology where they interrelated the measured modulus of elasticity values with drying shrinkage strain level and the cracking potential expressed in terms of percentages. To achieve this type of relationship, % cracking potential of the SCC mixes was related to drying shrinkage and specific creep values by generating a multiple regression at 95% confidence level. The relationship was expressed as;

$$\begin{aligned} \textit{Cracking Potential}\ (\%) = 15.9 + 0.268\textit{drying shrinkage}(\mu\varepsilon) \\ -1.57\textit{specific creep}(\mu\varepsilon / MPA) \end{aligned} \tag{2.7}$$

where the drying shrinkage values used are measured after the initial 3 days of curing and at the age of 10 days after casting. Then the specific creep was correlated to the degree of restraint as follows;

$$Specific\,Creep\,(\mu\varepsilon / MPa) = 404.6 \times R_m^{\,13.48}. \tag{2.8}$$

where R_m is the degree of restraint, and was expressed as ;

$$R_m = 1 - \frac{\varepsilon_{st}}{\varepsilon_{sh}}. \tag{2.9}$$

where the ε_{sh} and ε_{st} are referred measured from the instrumented free shrinkage specimens and the steel ring, respectively. Afterwards, the authors correlated the R_m values evaluated at initial 3 days of curing and at the age of 10 days after casting with the modulus of elasticity measured at day 3. Using this correlation with equation 1.3, and substituting equation 1.3 in equation 1.2, the authors eventually expressed the % cracking potential in terms of the modulus of elasticity, and the drying shrinkage of concrete. After the final derivations, the authors expressed the % cracking potential as;

$$\begin{aligned} Cracking\ Potential\ (\%) = {} & 1.58 + 0.161 drying\ shrinkage\,(\mu\varepsilon) - \\ & 526 \times \left[-0.0122 MOE\,(GPa) + 1.059\right]^{13.48} - 1.57 specific\ creep\ (\mu\varepsilon / MPA) \end{aligned} \tag{2.10}$$

where MOE is the measured modulus of elasticity at the end of 3 days of wet curing, and drying shrinkage is the ASTM C157 free shrinkage strain values measured 56 days after the drying was initiated.

Based on the derived equations, Hwang and Khayat (2008) pointed out a new way to predict the cracking potential of concrete by using the drying shrinkage values at day 7 or 56 of drying together with the modulus of elasticity measured at the age of ring specimen's drying initiation. The authors also reported that increasing the synthetic fiber

amount from 0 to 0.25% and from 0.25% to 0.50% improved the cracking performance of SCC mixes by 40% on average. Similarly, the utilization of shrinkage reducing agents was found to be significantly advantageous in terms of extending the time elapsed until cracking. The authors attributed this time extension to the 37% difference in the shrinkage magnitude between the mixes with and without SRA.

Loser and Leemann (2008) used a different test setup to evaluate the restrained shrinkage cracking performance of SCC. In this study, a steel square with specific breaking points was used to simulate restrained conditions. The steel square had a cross section of 100 mm × 100mm except for the breaking points being 60mm ×100mm. Dimensions and a sampled specimen with an observed crack are illustrated in Figure 2-4.

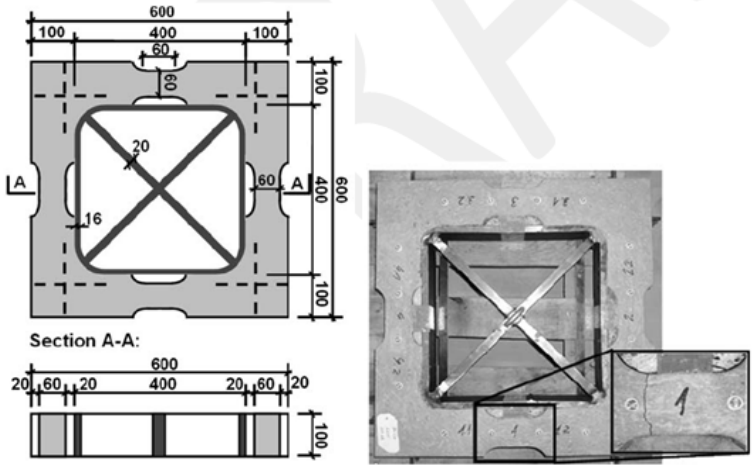

Figure 2-4 Restrained Shrinkage Test Setup by Loser and Leemann (2008)

The purpose of this study was to evaluate the effects of paste, water content, type of binder, grain size distribution, and the shrinkage reducing admixtures on the cracking performance of SCC mixes. Thirteen SCC mixes were produced along with 3 comparable OC mixes. Types of testing under the experimental program included 28 day compressive strength, flexural strength, and modulus of elasticity measured using 120×120×360mm

prisms specimens, creep and free drying shrinkage deformations measured using 120×120×360 prisms as well. Creep and free shrinkage samples were wet cured at 20°C with a R.H. of 90% for 1 day and then stored in 20°C with a R.H. of 70%, whereas varying curing conditions were applied to restrained shrinkage samples from different mixes to see the significance of curing conditions.

Loser and Leemann (2008) found out that the variations in w/b ratio or partial replacement of cement using fly ash or limestone powder did not substantially influence the shrinkage magnitude and the cracking potential of the studied SCC mixes. Once the curing time of the compared SCC and OC mixes was increased from 2 to 14 days, the authors found that the difference of 21 days in the elapsed time until cracking tended to decrease although the shrinkage of the SCC mix was still higher. One of the mechanisms used to explain this behavior was the increased modulus of elasticity and the decreased creep relaxation with additional curing time. In the case of OC, the total drying shrinkage was the same regardless of the curing time, so the decreased creep relaxation and the increased shrinkage rate shortened the time until cracking. In the case of SCC, though, the cracking age was almost the same. Since the autogenous shrinkage is more of an issue for the SCC mix, the long curing time pushed the drying shrinkage stresses beyond the curing period, while the initial autogenous shrinkage stresses were accommodated by creep relaxation. This way the stress development decreased, and the SCC mix exhibited a roughly similar cracking performance to the combined effect of reduced creep relaxation and increased stiffness gained by longer curing time.

CHAPTER III

EXPERIMENTAL SETUP

3.1 INTRODUCTION

Several SCC mixes were produced to evaluate the effect of selected parameters on the cracking potential of concrete under restrained conditions. The study was focused on three variables: the total amount of cementitious (material, the amount of fly ash, and the amount of silica fume. Seven SCC mixes were produced in this regard, and distributed into 3 groups such that at least one mix of each group was common to 2 groups, yet all 3 groups had at least 3 mixes to evaluate.

The most important test used in the study was a modified AASHTO Ring test. The concept of measuring the actual concrete strain, first proposed by Nassif et. al. (2008) was implemented in the studied SCC mixes. The details of the modified ring test are provided later in this chapter.

Along with the ring test, mechanical properties such as the compressive strength, the tensile strength, and the modulus of elasticity of the produced SCC mixes were tested. Also, free shrinkage tests were performed using concrete prisms in accordance with ASTM C157.

One can find the restrained shrinkage cracking potential expressed in terms of cracking age and the cracking area in the literature. In this regard, visual crack observations performed on the ring samples were an important aspect of this study.

3.2 MATERIAL PROPERTIES

All the SCC mixes were casted using 3/8" crushed stone and masonry sand provided by Weldon Construction Materials. Portland Cement Type I is provided by Lafarge in Whitehall, Pennsylvania, whereas fly ash is provided by Titan American in North Jersey. Force 10,000 type of silica fume provided by WR Grace Construction Products is also used in 6 of the 7 SCC mixes in this study. Table 3-1 lists the types of cementitious materials and their suppliers.

Table 3-1 Types of Cementitious Materials and Suppliers

	Material	Supplier
Cement	Portland Type I	LaFarge
Silica Fume	Force 10,000 D	Grace Construction
Fly Ash	Pro-Ash	Titan American

Table 3-2 lists the aggregate types used in the study and their suppliers. Mechanical properties of the aggregates such as the specific gravity, absorption, and the fineness modulus are listed in Table 3-3 and Table 3-4.

Table 3-2 Types of Aggregates and Suppliers

	Material	Supplier
Coarse Aggregate	3/8" Crushed Stone	Weldon Materials
Fine Aggregate	C33 Fine Aggregate	Weldon Materials

Table 3-3 Properties of Fine Aggregate

Bulk Specific Gravity	2.54
Bulk Specific Gravity (SSD)	2.56
Apparent Specific Gravity	2.56
Absorption	0.266
Fineness Modulus	2.34

Table 3-4 Properties of Coarse Aggregate

Bulk Specific Gravity	2.81
Absorption	1.94

A polycarboxylate based superplasticiser supplied by WR Grace Construction Products is used in all the SCC mixes. The air entraining agent selected is a complex mixture of organic acid salts and is also provided by WR Grace Construction Products. Table 3-5 lists the chemicals used in the SCC mixtures produced in this study.

Table 3-5 Types of Concrete Admixtures and Suppliers

	Material	**Supplier**
Air-Entrainment	Darex II	WR Grace
Super Plasticizer	ADVA 405	WR Grace

3.3 MIX PROPORTIONS

A total of 7 SCC mix designs were formulated for this study. These 7 mixes were distributed in 3 groups so that that each group had 3 mixes. Table 3-6 describes the way that the mixes were grouped and labeled.

Table 3-6 Definitions of Mix Groups

Group	Definition
G1 Cementitious Material	Variable amount of cementitious material, 800, 850,900 lbs w/c = 0.39, s/a = 0.5
G2 Fly Ash Volume	Variable amount of fly ash, %10, %20, %30 by weight w/c = 0.39, s/a = 0.5, total cement. =900 lbs
G3 Silica Fume Volume	Variable amount of silica fume, %0, %5, %10 by weight w/c = 0.39, s/a = 0.5, total cement. =850 lbs

Table 3-7 includes all the abbreviations related to materials used in the mixes.

Table 3-7 Abbreviations Used in the Mix Designs

Abbreviation	Definition
SF	Silica Fume
FA	Fly Ash
CS	Crushed Stone
S	Masonry Sand
S/A	Sand/Total Aggregate
G1	Group 1 Mixes
G2	Group 2 Mixes
G3	Group 3 Mixes

Table 3-8 shows the mix proportions of Group 1 mixes. The only variable parameter in this group is the total amount of cementitious material. For Group 1, three different mixes having 800, 850, and 900 lbs of cementitious material were produced to study the effect of this parameter. All the mixes in this group have the same the water cement ratio and the S/A ratios are both fixed at 0.39 and 0.5, respectively.

Table 3-8 Group 1 Mix Proportions

(Lb/cu yd.)	Group 1		
	G1-M1	G1-M2	G1-M3
	5SF20FA	5SF20FA	5SF20FA
Portland Cement Type I, lbs	600	637.5	675
	75%	75%	75%
Silica Fume, lbs	40	42.5	45.00
	5%	5%	5%
Class F Fly Ash, lbs	160	170	180
	20%	20	20%
Total Cementitious Material, lbs	800	850	900
Course Aggregate, lbs	1362	1330	1244
Fine Aggregate, lbs	1363	1328	1238
S/A	0.5	0.5	0.5
Water	295.2	322.1	352.3
W/(C+P)	0.39	0.39	0.39
Superplasticizer (oz/cu yd.)	202	194	118
AEA (oz/ cu yd.)*	5.5	5	6.5
Slump Flow, inches	22	24	25
J-Ring , inches	20	23	23
L-Box, % passing ability	56%	71%	70%
Entrained Air, %	4.7%	5%	8.0%

Table 3-9 shows the mix proportions of group 2 mixes. In this group of 3 mixes, the amount of Fly Ash relative to the total cementitious material weight is the investigated parameter. The total amount of Fly Ash is fixed at 900lbs among the 3 produced mixes while the water to cement ratio and the S/A ratio was fixed at 0.39 and 0.5, respectively. The difference in the amount of Fly Ash is expressed in the mix designation labels in terms of percentages (%10FA, %20FA, and % 30FA).

Table 3-9 Group 2 Mix Proportions

(Lb/cu yd.)	Group 2		
	G2-M1	G2-M2	G2-M3
	5SF10FA	5SF20FA	5SF30FA
Portland Cement Type I, lbs	765	675	585
	85%	75%	65%
Silica Fume, lbs	45.00	45.00	45.00
	5%	5%	5%
Class F Fly Ash, lbs	90	180	270
	10%	20%	30%
Total Cementitious Material, lbs	900	900	900
Course Aggregate, lbs	1279	1244.4	1241
Fine Aggregate, lbs	1299.4	1237.5	1294.8
S/A	0.5	0.5	0.51
Water	315.4	352.3	347.5
W/(C+P)	0.39	0.39	0.39
Superplasticizer (oz/cu yd.)	187	118	143.5
AEA (oz/ cu yd.)*	7	6.5	7
Slump Flow, inches	23	25	24
J-Ring , inches	21.5	23	21
L-Box, % passing ability	69%	70%	50%
Entrained Air, %	6%	8.0%	4%

Table 3-10 shows the mix proportions of group 3 mixes. The amount of silica fume is studied for the 3 mixes produced. One of the group 3 mixes has no silica fume while the other 2 mixes have 5% and 10% of their total cementitious material as silica fume. The water to cement ratio and the S/A ratio of group 1 mixes is the same as the group 1 and 2 mixes. The amount of total cementitious material is 850lbs in all 3 mixes for group 3.

Table 3-10 Group 3 Mix Proportions

(Lb/cu yd.)	Group 3		
	G3-M1	G3-M2	G3-M3
	20FA	5SF20FA	10SF20FA
Portland Cement Type I, lbs	680	637.5	595
	80%	42.5	70%
Silica Fume, lbs	0.00	42.5	85.00
	0%	5%	10%
Class F Fly Ash, lbs	170	170	170
	20 %	20	20%
Total Cementitious Material, lbs	850	850	850
Course Aggregate, lbs	1319.3	1330	1306.9
Fine Aggregate, lbs	1342.1	1328	1319
S/A	0.5	0.5	0.5
Water	294.2	322.1	298.4
W/(C+P)	0.39	0.39	0.39
Superplasticizer (oz/cu yd.)	176	194	229
AEA (oz/ cu yd.)*	6.5	5	7
Slump Flow, inches	22.5	24	24
J-Ring , inches	22	23	21
L-Box, % passing ability	65%	71%	60%
Entrained Air, %	6.5%	5%	5.4%

3.4 MIXING AND FRESH SAMPLING OF CONCRETE

3.4.1 Mixing (ASTM C - 192)

Trial mixes using small volumes were produced for all the mix designs used in this study. These pre-mixes were batched according to the actual mix design presented in the previous sections. The purpose was to simulate the original mixes with minimum loss of material since there was a need to adjust the amount of concrete admixtures required for the given mix design.

Both the trial and actual mixes are produced according to the same procedure. First the mixer is filled with only the coarse and the fine aggregate, and run for 30 seconds. Then 2/3 of the water is poured in the mixer along with the air entraining agent, and the mixer is spun for another 30 seconds. All the cementitious material and the rest of the water is added after this point and mixed for 3 to 4 minutes. The concrete is then let to hydrate in the mixer for 3 minutes while the mixer is stopped and the lid of the mixer is kept closed to prevent moisture loss. Following the 3 minutes resting period, the superplasticer is introduced into the mixer and run for another 3 to 4 minutes. The first slump flow is measured at the end of last run, and the mixing is stopped if the measured initial slump flow is at the desired level. If not, additional superplasticiser is immediately introduced to the concrete, and the mixer is run for an additional minute and a half. Figure 3-1 shows the concrete drum mixers used for the trial and actual batches.

Figure 3-1 Concrete Mixers Used for Trial and Actual Batches

3.4.2 Slump Test (ASTM C1611M-05)

The slump flow of the fresh concrete is tested according to ASTM-C1611/C1611M. A 4' × 4' slump board is used as flat surface to operate the test. The slump cone is placed with its smaller opening facing down. No rodding is applied while filling the slump cone. Once the slump cone is filled, it is leveled with a strike-off bar and the slump cone is pulled upwards to a distance of approximately 10 inches from ground level. The concrete is then let to flow freely until it stops. The largest and the average diameter of the spread are measured immediately after the stop of the flow. The resulting slump flow of the concrete is considered to be the average of these 2 measurements rounded to the nearest ½".

The concrete is also evaluated visually after the slump flow measurements are taken. The presence of any segregation or bleeding is inspected by observing the perimeter of the circular spread. Cutting the concrete spread with a metal bar is also performed as a rule of thumb to observe the stability of the produced concrete. The SCC mix is considered to be stable enough if this gap created by the cut is quickly filled back by the concrete. A couple of cuts were introduced to the spread to determine how stable and homogeneous the produced SCC mixes.

Figure 3-2 shows the testing apparatus and a typical slump flow observed.

Figure 3-2 Slump Flow Testing (ASTM C1611M-05)

3.4.3 J – Ring Test (ASTM C 1621 / C 1621M)

The J- Ring test is performed according to ASTM C 1621. A regular slump cone is used with a J – Ring to operate the test. The J – Ring used has 16 steel bars spaced at 2.4” center to center. The J-Ring test is performed immediately after the slump flow test, approximately about 5-10 minutes after the concrete mixer is stopped. The slump cone is placed inversely; and the J – Ring is placed as the slump cone would be centered in the middle of it. The slump cone is filled with concrete without introducing any rodding or vibration. The concrete is leveled with the strike-off bar and the cone is pulled upwards approximately 10 inches. The concrete is let to flow freely on the flat surface. The largest and the average diameter of the circular concrete spread are measured after the concrete flow stops. The average of the 2 measurements is considered to be the J–Ring flow of the concrete.

The actual evaluation of the concrete passing ability is based on the difference between the slump flow and the J-Ring flow diameters. Table 3-11 shows the ASTM C

1621 Standard criteria for evaluating this difference between the diameters measured in these 2 tests.

Table 3-11 ASTM Blocking Criteria for J – Ring Test (ASTM ASTM C 1621)

Blocking Assessment	
Difference Between Slump Flow and J - Ring	**Blocking Assessment**
0 to 1 in. [0 to 25 mm]	No visible blocking
>1 to 2 in. [>25 to 50 mm]	Minimal to noticeable blocking
>2 in. [>50mm]	Noticeable to extreme blocking

Visual observations similar to the slump flow test are also performed after the diameter measurements are taken. Figure 3-3 shows the J-Ring testing apparatus and an example from the test.

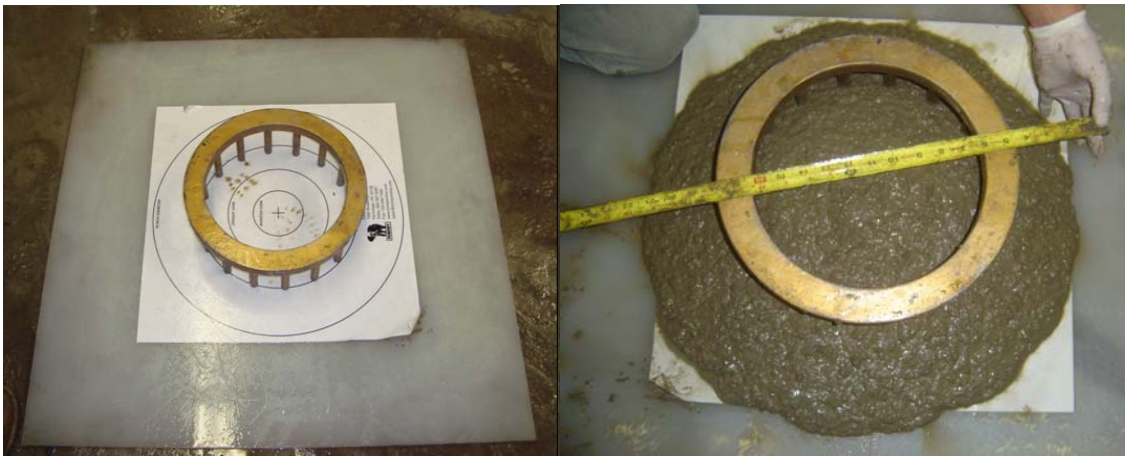

Figure 3-3 J-Ring Test Apparatus and the Illustration of the Flow Measurement

3.4.4 L – Box Test

Although not been established as a standard, L –Box test is a widely used method for evaluating the passing ability of fresh concrete through congested steel rebars. The L-Box test has been used in many countries for both laboratory and field testing of self-consolidating concrete. Thus, different dimensions of the L- Box can be observed throughout the industry and the academia. A commercially available L-Box was obtained and used throughout this study. Figure 3-4 shows the view and the dimensions of the L-box used in this study.

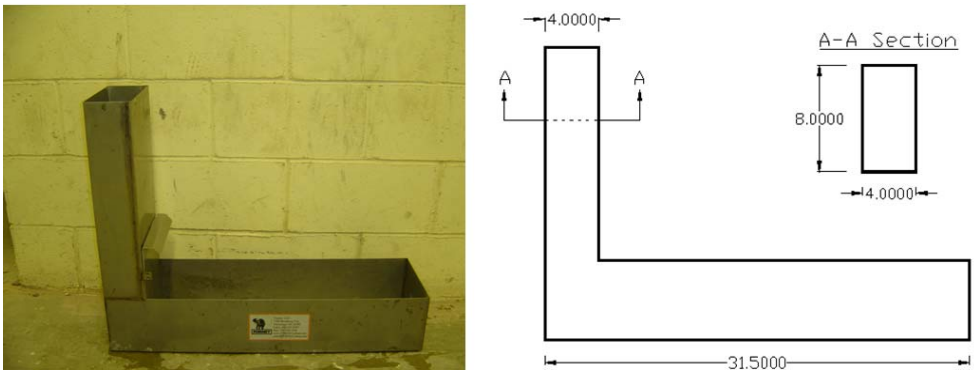

Figure 3-4 Dimensions and View of the L-Box

The L-box test is performed within 10-15 minutes after the concrete mixer is stopped. To perform the test, the L-box is first located on a level surface. The reservoir of the L-box is fulfilled without any rodding or vibration, and the top of the box is leveled with a strike-off bar. Then, the gate is pulled upwards with a single and quick move allowing the concrete to flow through the rebars. The concrete is then let to flow until it reaches the end of the L-box and stops flowing.

The height of the set concrete at both ends of the L-box is measured with a ruler. The result of L-box test is then reported as a ratio derived from dividing the concrete height at the end of the L-box by the concrete height leftover at the reservoir (h_2/h_1).

3.4.5 Air Content (ASTMC – 231)

The air content of the fresh concrete is measured according to ASTM C 231 using a Type-B Pressure meter, as shown in Figure 3-5. The test is performed within the first 5 minutes after the target slump flow is achieved. The container of the air-meter is filled with fresh concrete without any rodding or external vibration. Once the container is filled with concrete, its sides of are cleaned with a sponge to provide a proper seal between the air-meter lid and the container. Afterwards, clean water is injected into the container through one of the petcocks until the injected water is flushing out of the opposite petcock. Then, the petcocks are closed and the air is pumped into the container up to the initial pressure line set up at the gauge calibration. (Usually 3%) The gauge is tapped gently, and finally the air release lever is pressed down to assess the air content of the concrete. The final air percentage reading is obtained after waiting a couple of seconds, and then tapping the gauge gently.

Figure 3-5 ASTM C – 231 Type B Pressure Meter

Since the accuracy of the air measurement with this method is very much dependent on the precise calibration of the gauge, periodic checks were made on the gauge to ensure that the air meter is functioning properly.

3.4.6 Pouring Specimens

The volumes of the produced concrete mixes are pre-calculated by taking into account the required number of samples and mold sizes. Thirty six 4in×8in cylinder specimens are casted to perform the mechanical tests. For free shrinkage, three 3in×3in×10in steel molds are casted to perform the ASTM C157 test. Two ring specimens were casted using the AASHTO Ring test dimensions in order to evaluate the restrained shrinkage performance of the mixes. No rodding was applied to any of the test specimens mentioned.

3.4.7 Curing of Specimens

All the test specimens are demolded 24 ±4 hours after casting and wet cured for 14 days. Curing was applied to ring specimens with wet burlap and polyethylene sheet was used to cover the rings. Figure 3-6 shows 2 ring specimens wet cured with burlap and covered with polyethylene sheet. Special care was taken while covering the rings to ensure that no moisture was lost. Mechanical and free shrinkage testing samples were moist cured until day 14. At the end of curing, these samples are transferred to an environmental chamber with 74±4 degrees temperature and 50% relative humidity until they are tested. Similarly, ring specimens were stored in the same environmental chamber after the wet burlap curing is removed on day 14.

Figure 3-6 Ring Specimens Covered with Burlap and Sealed with Polyurethane Sheet

3.5 LABORATORY TESTING PROCEDURES

A summary of all the laboratory tests performed in companion with AASHTO T-334 restrained shrinkage test is tabulated in Table 3-12. Associated standards designations and timing of tests are also shown. In addition to all the fresh and hardened concrete tests listed in the Table 3-12, the coarse and fine aggregates are tested to determine the specific gravity, absorption and gradation characteristics. The aggregate tests are conducted once a new batch of aggregate is obtained.

Table 3-12 Summary of the Performed Laboratory Tests

Test	Number of Specimens	Applicable ASTM Standard	Curing Conditions	Age of Concrete
Slump Flow	1 Per Mix	C 1611M	-	Fresh Concrete
J – Ring Test	1 Per Mix	C 1621/ C 1621M	-	Fresh Concrete
L – Box Test	1 Per Mix	N/A	-	Fresh Concrete
Fresh Air Content	1 Per Mix	C231	-	Fresh Concrete
Free Shrinkage	3 Per Mix	C157	14 Days	14 to 91 days
Restrained Shrinkage	2 Per Mix	AASHTO T-334	14 Days	14 to age of cracking
Compressive Strength	12 Per Mix	C39	14 Days	14, 21,28, 56, 91 days
Splitting Tensile Strength	12 Per Mix	C496	14 Days	14, 21,28, 56, 91 days
Modulus of Elasticity	12 Per Mix	C469	14 Days	14, 21,28, 56, 91 days

3.5.1 Specific Gravity and Absorption of Fine Aggregate (AASHTO T 84-04)

Because all the mix designs in this research were calculated by using volumetric method, there was a need to determine the specific gravity and absorption values of the concrete aggregate prior to mixing. For the fine aggregates, AASHTO T-84-04 test provisions were followed.

The test apparatus consisted of a scale, pyncometer, metal mold, and a tamper. To perform the test, fine aggregate is sampled in accordance with AASHTO T 248 and dried in oven until it reaches constant mass conditions. Afterwards, it is removed from the oven and let cool until it could be safely handled. The sampled aggregate is then immersed into a bucket of clean water and kept immersed for 15 to 19 hours. Once the immersion of the

aggregate is complete and the aggregate is fully saturated, the aggregate is removed from the water and let to surface dry. During this period, special care is taken not to over dry the sample, and to ensure that it only reached a saturated surface dry (SSD) condition. The metal mold is used to check whether the sample has reached the surface dry conditions or not. Afterwards, 500 grams of the SSD sample is introduced in the pyncometer and filled with water. The pyncometer is agitated for 10 to 15 minutes, filled to the calibration mark and weighed using a digital scale. The sample in the pyncometer is then dried again in an oven till it reached a constant mass, whereupon it was weighed again.

After all the above-mentioned steps are completed, the equations provided in AASHTO T84 are followed to determine the specific gravity and absorption values of the fine aggregate.

3.5.2 Specific Gravity and Absorption of Coarse Aggregate (AASHTO T 85-04)

Except for slight differences, AASHTO T-85 is very similar to AASHTO T-84 test provisions. After sampling, the aggregate is oven dried until it reaches a constant mass. Then, the sample aggregate is immersed in a bucket of clean water and kept immersed for 15 to 19 hours. Afterwards, the coarse aggregate sample is surface dried such that all the visible films of water are removed from the aggregate surface. The sample is then scaled both in air and in water. Finally, the sample aggregate is oven dried and re-weighed. The specific gravity and absorption of the coarse aggregate is calculated using the SSD weight in air, in water, and the final oven dry weight.

3.5.3 Compressive Strength of Cylindrical Concrete Specimens (ASTM C-39-05)

ASTM C-39-05 compressive strength test is performed at the ages of 14, 21, 28, 56 and 91 days after casting the concrete specimens. A minimum of 2 4×8in cylinder specimens were tested at each testing day. The cylinders were first capped using high-strength capping compound to provide a uniform concentric loading area. Then the cylinders were loaded with a constant speed of 4000pounds per 9 seconds using the Forney 1-Million Pound Compression Machine shown in Figure 3-7.

Figure 3-7 Forney 1-Million Pound Compression Machine

The ultimate breaking load and the ASTM mode of compression failure are recorded at the end of each test. If the breaking load of 2 specimens varied more than the ASTM specified tolerances, a third sample was tested. Out of the 3 samples tested, the 2 closest to each other were used as final results.

3.5.4 Standard Test Method for Splitting Tensile Strength of Cylindrical Concrete Specimens (ASTM C – 496 –04e1)

Splitting Tensile Strength test in accordance with ASTM C-496-04e1 was performed at the ages of 14, 21, 28, 65, and 91. The 4×8in. cylinder specimens were positioned on a 400,000 pounds Tinius Olsen Compression machine as shown in Figure 3-8. The applied load is transferred to the cylinder through 1/8" thick wood strips that are placed on the sides of the specimen. Also, a steel rectangular load cell is placed under the bottom wood strip to provide an appropriate clearance. Two cylinder specimens are loaded at each testing day using a rate of 100 pounds per second until splitting of the cylinders occurs. The load level where the splitting takes place is recorded as the splitting tensile strength of the cylinders.

Figure 3-8 Splitting Tensile Strength Test Setup

3.5.5 Modulus of Elasticity (ASTM C-469-02e1)

Modulus of Elasticity test for all the SCC mixes was performed in accordance with ASTM C-469. Prior to modulus of elasticity test, compressive strength test is

required to acquire an appropriate load level. After 2 cylinders are tested for compression, %40 of the ultimate breaking load is calculated and used in modulus of elasticity test as the upper threshold of loading. Once the 4×8 in cylinder specimens are capped with high-strength sulfur capping compound, a compressometer with a gage is attached to them as shown in Figure 3-9.

Figure 3-9 Modulus of Elasticity Test Setup

The tested specimen is loaded for three times using a rate of 4000 pounds per 9 seconds. The compressmeter gage readings are recorded for the second and third runs at every 4000 pounds until the maximum load level. The gage lengths are also recorded before each run using a digital caliper. Once the change in length readings is recorded for 2 cylinder specimens, stress-strain curves are generated for each cylinder specimen. Thus, the modulus of elasticity is calculated using the slope of the curve.

3.5.6 Free Shrinkage Test (ASTM C – 157)

Free drying shrinkage of SCC mixtures was measured using ASTM C-157 provisions. In compliance with the standard test, three 3×3×10in beam specimens were sampled using steel forms shown in Figure 3-10. Prior to mixing, two gage studs are screwed into the end plates of the steel forms. After the beam specimens are moist cured for 14 days, the length change between the 2 gage studs is measured at various ages using a length comparator. While measuring the change in length, the specimens are placed in the length comparator and gently spun until the lowest reading is found. Once the length change is recorded at various ages, the free shrinkage strain at any age of measurement is calculated using the following relationship:

$$L = \frac{\left[\left(L_f - L_i\right)\times 100\right]}{L_0}$$

Where,

L_f = the difference between the length of the specimen and the reference bar at any age of testing.

L_i = the difference between the length of the specimen and the reference bar at the age of 14 days. (The age when the drying is initiated)

L_0 = the original length of the test specimen= 10 inches.

Since the specimens are moist cured until day 14 after casting, no shrinkage is assumed to be taking place during this curing period. Thus, the free shrinkage measurements are started once the curing is removed and the drying of the samples are initiated.

Figure 3-10 Steel Free Shrinkage Molds

3.5.7 Restrained Shrinkage Ring Test

The ring test of AASHTO-T334 is used to assess the cracking potential of the SCC mixes. In this test setup, the restraint to concrete is provided by a steel ring with 12" diameter and 0.5" wall thickness. Once the concrete starts shrinking, compressive stresses develop on the steel ring. The steel ring compressive stresses are balanced by the tensile stresses developed in concrete until these tensile stresses exceeds the tensile strength of the concrete. The possibility of tensile cracking on the concrete ring is visually inspected every 2-3 days after the curing period ends. Consistent with the AASHTO T-334 provisions, four strain gages are also installed on the inner circumference of the steel ring at the mid-height. The compressive strain around the steel ring is monitored by these foil gages.

In addition to the foil gages installed on the steel ring, the modified test setup used by Aktas (2007) and Montemerano (2008), where vibrating wire sensor gages (VWSG) were used to monitor the concrete strain, is adopted for monitoring the restrained shrinkage behavior of SCC mixes. VWSG sensors are instrumented in the concrete

section using bolts. More information on the VWSG installation is given in the following section. With the VWSG installation, actual concrete strain is monitored during the test period. Also, VWSG data is very helpful in determining the actual location where the restrained shrinkage cracking will occur.

3.5.7.1 Sensors and Instrumentation

As mentioned above, vibrating wire strain gages are used to monitor strain data from the concrete ring specimens. Geokon Model 4000 gages, shown in Figure 3-11, with a gage length of 6 inches are selected for this purpose. The sensor is attached to 2 mounting blocks at both ends and fixed into the concrete using threaded bolts. The sensor has a steel wire inside the tubing and any relative movement of the sensor ends is recorded by this wire in terms of change in frequency. This change in frequency is recorded by a pluck coil attached to a shielded cable, and then transferred into strain readings after going through a vibrating wire gage interface. These readings are downloaded from the data logger and used as strain measurements of concrete shrinkage.

Figure 3-11 Geokon Model 4000 VWSG's and Modified Mounting Blocks

The FSG's used to collect strain data from the steel rings are shown in Figure 3-12. The full bridge strain gages have a resistance of 120 ohms with a tolerance of ±0.6%. The gages and the adhesives are both provided by Vishay Micromeasurements Inc. Prior to gage installation; the surfaces of the ring where the sensors will be positioned are sanded and cleaned with the surface cleaning compounds. Then the adhesives are applied to the steel ring and the gage is positioned on the steel ring. Finally, the gage is covered with a special gage coating to protect it from environmental and other external effects. The sensor cables are then connected to the data logger to collect continuous strain measurements from the steel rings.

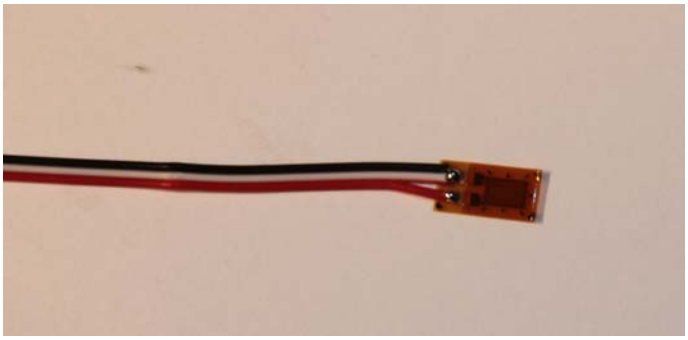

Figure 3-12 Foil Strain Gage for Steel Strain Data Collection

3.5.7.2 Vibrating Wire Sensor Gage Setup

The ring test setup used in this study includes the implementation of VWSG sensors in addition to the FSG sensors used in the original version of AASHTO-T334. The vibrating wire sensor gage setup is prepared before casting the ring specimens. A 2-inch threaded bold is used to connect the adjacent VWSG sensors. After all the 6 VWSG 's are positioned on a board on which the exact sensor lengths are marked, the 2-inch bolts are tightened using ¼" nuts at the top and bottom mounting blocks. This way, all the 6

sensors form a closed hexagonal loop and connected together. A view of 6 sensors connected together can be seen in Figure 3-13a.

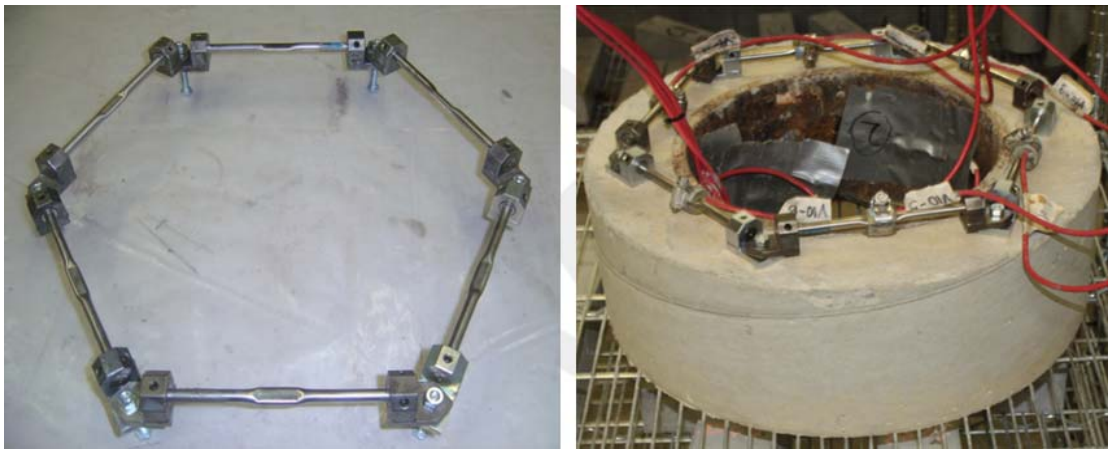

(a) (b)

Figure 3-13 Vibrating Wire Sensors Gages Setup a) 6 Sensors Connected Prior to Mixing b) A view of VWSG sensors During Data Collection Period

After the concrete is mixes and the fresh concrete tests are performed, the following sequence is followed for sampling and curing:

1) The Free and Restrained Shrinkage Specimens molds are filled with fresh SCC without applying any vibration of rodding.
2) Cylinder molds to be used for hardened concrete tests are filled and capped with plastic lids.
3) The VWSG's that are prepared prior to mixing are inserted in the fresh concrete. Because the FSG sensors are pre-labeled, the VWSG 1 is placed in the concrete such that it centers the FSG 1. The WVSGs are labeled from 1 to 6 following the

clockwise direction as a rule of thumb. Figure 3-14 shows both the label configuration of FSG and VWSG sensors.

4) Samples are then covered with burlap and polyethylene sheeting to prevent moisture loss. The strain profile of the ring specimens are monitored starting from the casting of concrete.

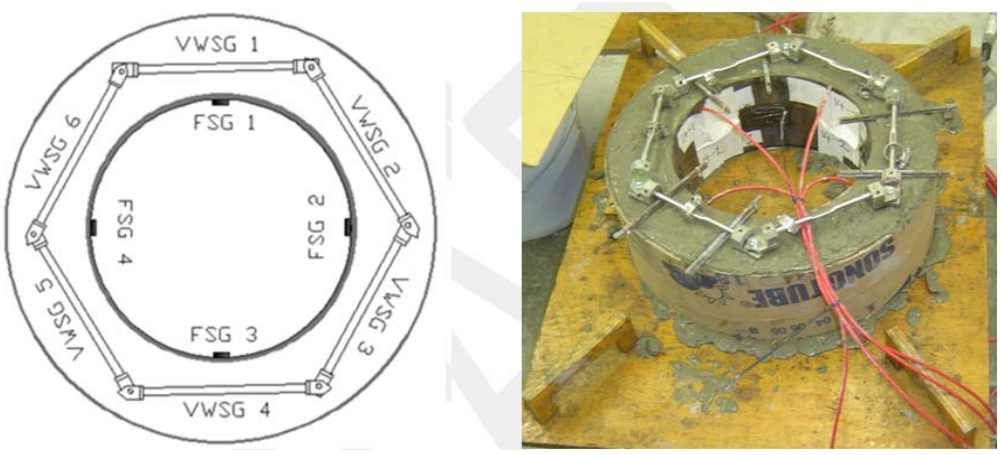

(a) (b)

Figure 3-14 a)Labeling Configuration of the FSG and VWSG sensors, b) View of the Ring Specimen Shortly after Casting

The specimens are demolded at 24±4 hours after casting, and the molds are removed and burlaps are replaced. For the rest of the14 day curing period, the burlaps are replaced at least once too provide enough moisture. Once the curing period is over, the ring specimens are moved to shelves where they are monitored for the remainder of the test.

3.5.7.3 Data Collection and Analysis

A data acquisition system (DAQ) manufactured by Campbell Scientific Inc. is used to continuously record the shrinkage strain from the ring specimens. Both VWSG and FSG modules are programmed in the same unit to collect steel and concrete stain data from the same source. The unit is also set for auto data download daily and the data is then transferred to another computer for plotting. A view of the DAQ unit is shown in Figure 3-15.

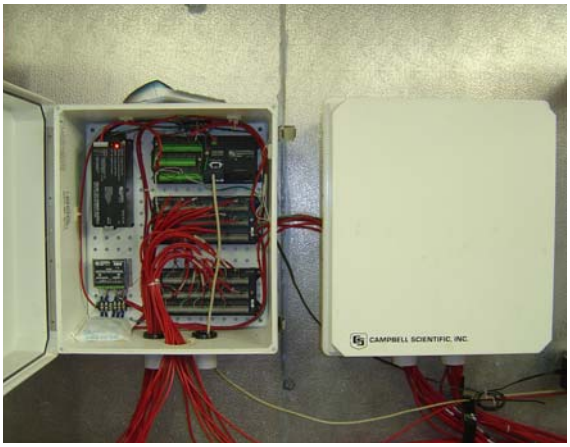

Figure 3-15 Data Acquisition System for Restrained Shrinkage Test Setup

The strain records from the DAQ are monitored daily after curing is removed. The data is updated and plotted in spreadsheet to follow up on the rate of shrinkage and compare the tensile shrinkage strain to the cracking strain of the mix. The tensile cracking strain of the mixes are obtained from the mechanical tests performed .Since the splitting tensile and modulus of elasticity of the SCC mixes are known from the testing days, the cracking strain is calculated from the following equation:

$$\varepsilon_{ten.} = \frac{\sigma_t}{E}$$

Where,

σ_t , is the splitting tensile strength,

E, is the modulus of elasticity

ε_{ten}, is the tensile cracking strain

While the strain profile of the ring specimens are monitored, visual crack observations are also performed every 2-3 days. A microscope is used to identify the small drying shrinkage cracks on the ring specimens. Most often, the strain profile of the ring specimen indicates the cracking location since the crack will most likely occur around the region where a VWSG exceeds the cracking strain. Figure 3-16 is a schematic sequence of the data collection procedure and also illustrating the visual crack observations.

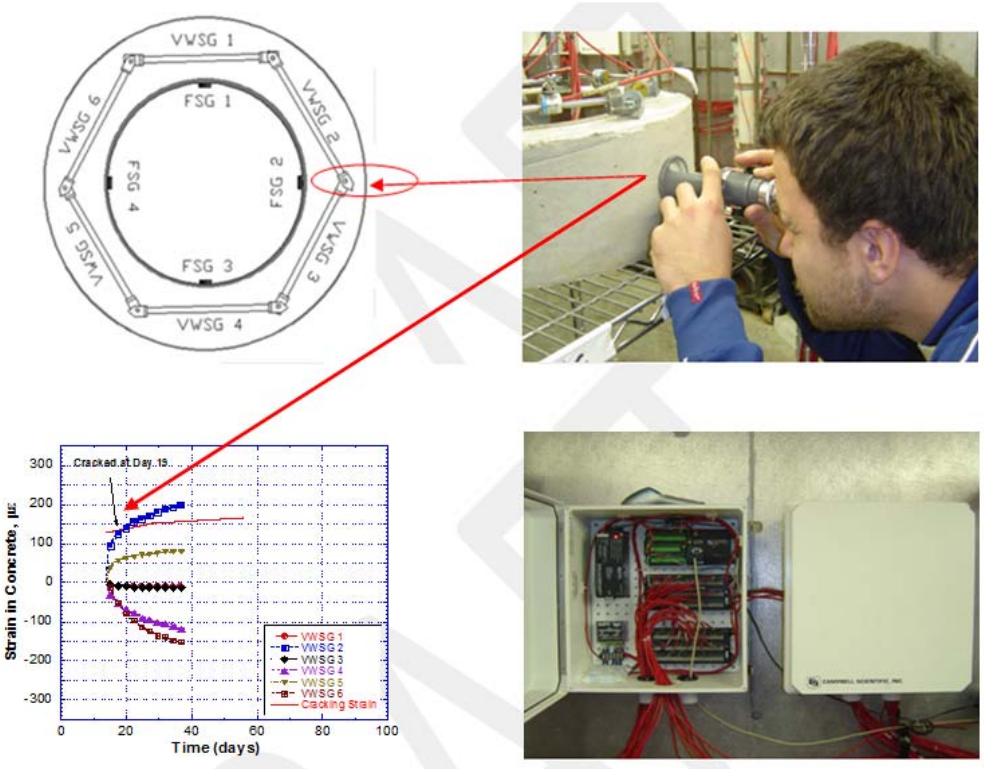

Figure 3-16 Illustration of Restrained Shrinkage Crack Monitoring

The length of the data collection period depends on the strain profile gained from the VWSG and FSG records, and the cracking behavior of the ring specimens. If the ring specimen exhibits drying shrinkage cracking at multiple locations propagated towards the steel ring, and the strain data shows a release in the shrinkage rate, the specimen is assumed to fail under restrained conditions. Therefore, the ring specimen is removed and a final visual observation is performed to generate the crack map drawings of the concrete ring.

3.5.7.4 Environmental Chamber

The relative humidity and temperature of the environment where the concrete specimens are kept is very important in the shrinkage behavior of concrete. Thus, all the concrete specimens are kept in an environmental chamber, where the relative humidity and temperature is at the levels specified by standard test method provisions. This environmental chamber is 24×16×8ft room, where the temperature is kept constant at 74±3 and the relative humidity at 50±4. The room is also insulated with thick aluminum walls to prevent any types of external interference. The temperature and the humidity in the chamber are measured by sensors that are positioned to detect the overall conditions of the room. Then the sensor readings are monitored from a digital controller unit located outside the room. A view from the environmental chamber is given in Figure 3-17.

Figure 3-17 Ring Specimens Monitored in Environmental Chamber

CHAPTER IV

RESULTS

4.1 INTRODUCTION

Laboratory testing results of the 7 SCC mixes are presented in this chapter. The testing results for fresh concrete, compressive strength, splitting tensile, modulus of elasticity, free shrinkage and, restrained shrinkage are listed respectively along with the discussions. The following sections in this chapter are organized in a way that for any of the performed tests, the results from the first group of mixes are provided, and then followed by the test results from the following group of mixes. Thus, the effect of the studied group parameters can be seen step by step for all the different tests.

4.2 FRESH CONCRETE TESTING RESULTS

All the SCC mixes produced throughout this research was tested for slump flow, J-ring, L-box, and entrained air percentage at the fresh state. Table 4-1 shows the results of all SCC fresh concrete testing, and as well as the amount of superplasticiser used in each mix.

The fresh concrete testing results for Group 1 mixes point out the effect of total amount of cementitious material with regard to the flowability of concrete. The flowability, in other words, the workability of the mix, is enhanced as the total amount of cementitious material is increased from 800 pounds to 850 pounds.

Table 4-1 Fresh Concrete Testing Results for all the SCC Mixes

Mix ID	Slump Flow, in.	J - Ring, in.	L- Box , %	% Entrained Air	Superplasticiser, ml/cy
G1-M1	22	20	56%	4.7%	202
G1-M2	24	23	71%	5.0%	194
G1-M3	25	23	70%	8.0%	118
G2-M1	23	21.5	69%	6.0%	187
G2-M2	25	23	70%	8.0%	118
G2-M3	24	21	50%	4.0%	143.5
G3-M1	22.5	22	65%	6.5%	176
G3-M2	24	23	71%	5.0%	194
G3-M3	24	21	60%	5.4%	229

The slump flow of the SCC mixes ranged between 22 and 25 inches (559 to 635mm) with an average of 23.5 inches (597mm). Except for the G3M3 and G2M3, all the SCC mixes falls into the first 2 categories of ASTM J-Ring blocking assessment category where there is either “visible blocking” or “minimal to noticeable blocking”.

The L-Box test results for all the SCC mixes ranged between %56 and %71, with an average of %63. The relationship between the L- box and J-ring results obtained from the SCC mixes produced are represented in Figure 4-1. The correlation of the results points out a good relationship between these tests by an R value of 0.79.

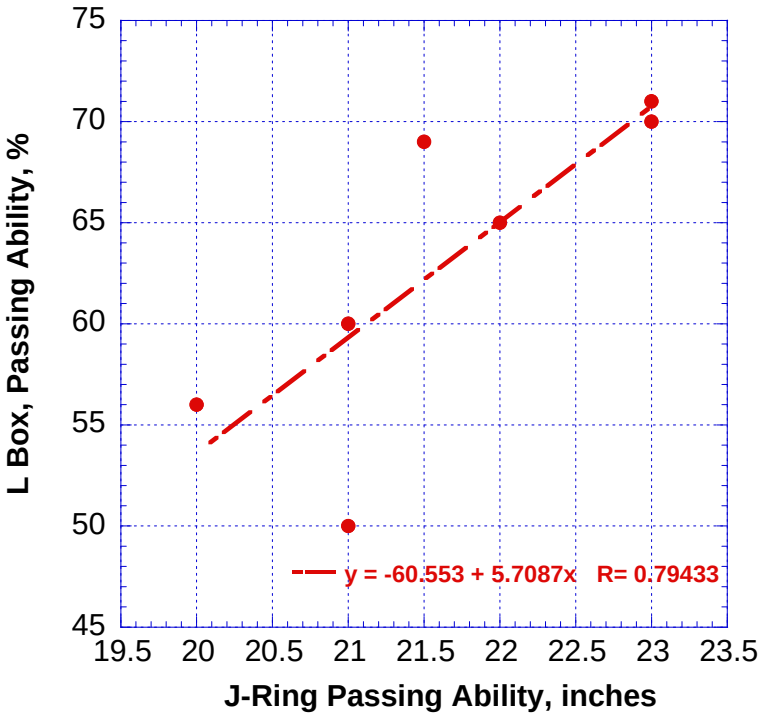

Figure 4-1 Correlation of L- box and J-Ring Test Results for all SCC mixes

The fresh concrete was also tested for entrained air percentage for all the batches produced in this study. The target of the entrained air of all the mix designs in this study was selected as %5 with a margin of ±2%, and the results varied between 4% and 8%. Only one of the 7 SCC mixes produced exhibited percentage of entrained air higher than 7%, and the rest of the 7 mixes were within the target range.

4.3 MECHANICAL PROPERTIES

4.3.1 Compressive Strength

Table 4-2 and Figure 4-2 shows the compressive strength testing results for group 1 mixes having varying amounts of cementitious material. All the group 1 mixes have 5%

silica fume and 20% fly ash replacement in their total cementitious material content. Although the first mix of group 1 has the least amount of cementitious material with 800 pounds, it exhibited the highest compressive strengths compared to other group mixes. The relatively low compressive strength development of the third G1M3 is mainly attributed to the high entrained air percentage of the other 2 group mixes. Since the compressive strength of concrete tends to decrease as the percentage of entrained air increases, compressive strength differences are likely to occur. Another reason is the difference in the slump flow, in other words, the fluidity of the mixes relative to each other created differences in compressive strength as previously discussed in the literature review section. G1M1 had a lower slump flow compared to G1M2 and G1M3 as shown the fresh concrete testing results section, this type of difference in fluidity can affect the compressive strength. Also, the slight differences in the aggregate characteristics such as the specific gravity or the fineness modulus can be effecting the strength development. G1M1 was batched with a slight different type of aggregate batch, while G1M2 and G1M3 were batched using the same source of aggregate.

Table 4-2 Compressive Strength of Group 1 Mixes (psi)

Testing Day	5SF20FA 800 lbs	5SF20FA 850 lbs	5SF20FA 900lbs
14	6822	6478	5211
21	8154	7975	6146
28	8373	8194	6802
56	9149	8771	6822
91	9208	-	6762

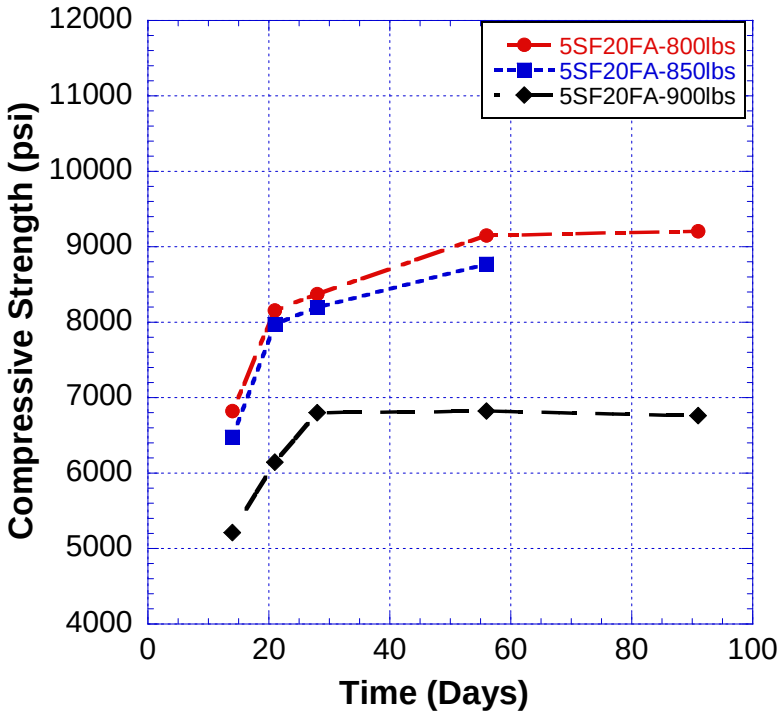

Figure 4-2 Compressive Strength of Group 1 Mixes (psi)

The compressive strength testing results for group 2 mixes are illustrated in Table 3-1 and plotted in Figure 4-3 as well. The highest compressive strength measured at the age of 28 from this group mixes was for G2M1. This mix incorporated 900 pounds of cementitious material with 5% silica fume and only 10% fly ash replacement. Since the fly ash replacement is the lowest for this mix, the early or mid age compressive strength development is the highest for this mix. This is expected since fly ash reacts slower compared to Portland cement or silica fume.

Table 4-3 Compressive Strength of Group 2 Mixes (psi)

Testing Day	5SF10FA	5SF20FA	5SF30FA
14	7094	5211	5969
21	8207	6146	-
28	8738	6802	7239
56	8791	6822	8115
91	9547	6762	-

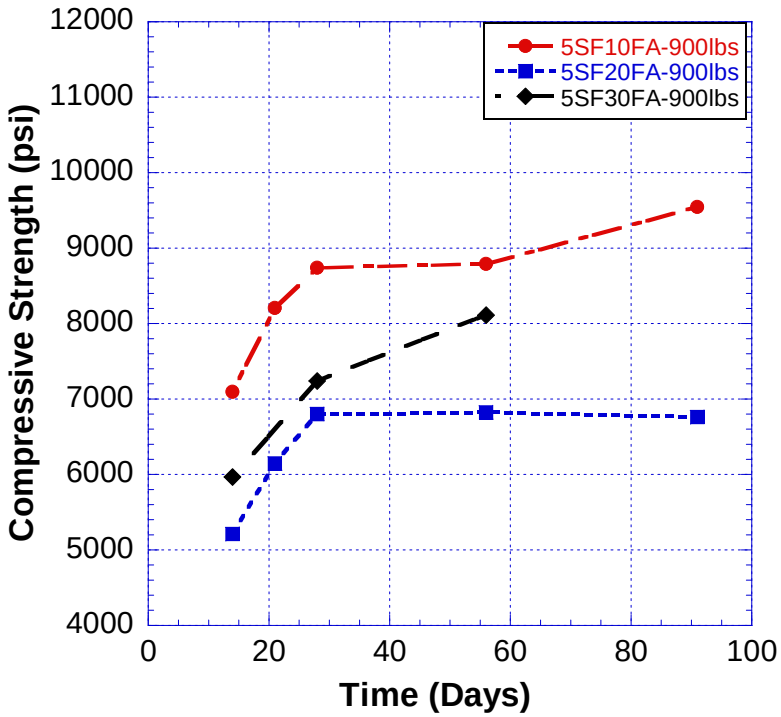

Figure 4-3 Compressive Strength of Group 2 Mixes

Table 4-4 and Figure 4-4 shows the compressive strength testing results for group 3 mixes. Table 4-4, we can see that the difference between G3M1 and G3M3 evaluated at day 28 is 27% and this can be can be attributed to the use of silica fume as a replacement of cement in G3M3 mix design. On the other hand, G3M2 had similar compressive strength results with G3M3 although it had 5% silica fume in its mix design.

This was mainly attributed to the difference in the fluidity of 2 mixes. G3M2 had a higher slump compared to G3M3, thus the fluidity level had a negative effect on the compressive strength development.

Table 4-4 Compressive Strength of Group 3 Mixes

Testing Day	20FA	5SF20FA	10SF20FA
14	6627	6478	7558
21	8022	7975	9029
28	8194	8194	9547
56	8075	8771	10004
91	8433	-	9905

It can be noted from Table 4-4 that the compressive strength of G3M3 at day 28 is highest among all the SCC mixes evaluated in this study. The second highest compressive strength was gained from G2M1, which had 50 pounds more cementitious material than G3M3, but only 5% silica fume replacement. Thus, silica fume was found to be more effective to achieve higher compressive strength values.

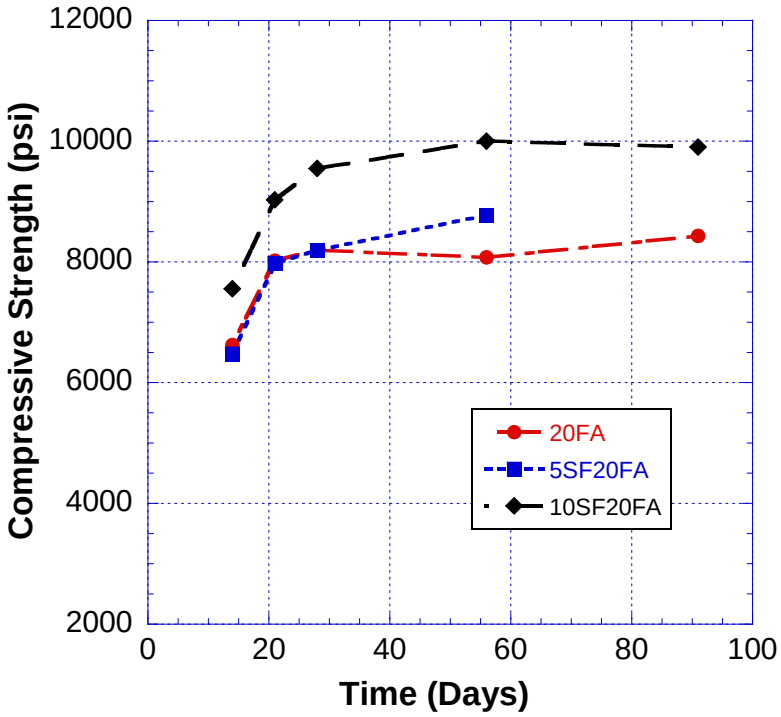

Figure 4-4 Compressive Strength of Group 3 Mixes

4.3.2 Splitting Tensile Strength

The splitting tensile test results of the SCC mixes showed similar trends compared to the compressive strength test results. For Group 1mixes, the slitting tensile strength of the mixes is shown in Table 4-5 and Table 4-5. The effect of high entrained air percentage and difference in the fluidity level of the mixes is also clear in the tensile strength results since the G1M3 and G1M2 exhibited lower tensile strengths relative to G1M1. G1M1 had the lowest slump flow among all the mixes, thus developed high tensile strength, whereas G1M3 did not perform as well as expected due to its high air percentage.

Table 4-5 Splitting Tensile Strength of Group 1 Mixes (psi)

Testing Day	5SF20FA	5SF20FA	5SF20FA
14	596	534	527
21	647	599	567
28	657	629	585
56	716	652	564
91	741	-	570

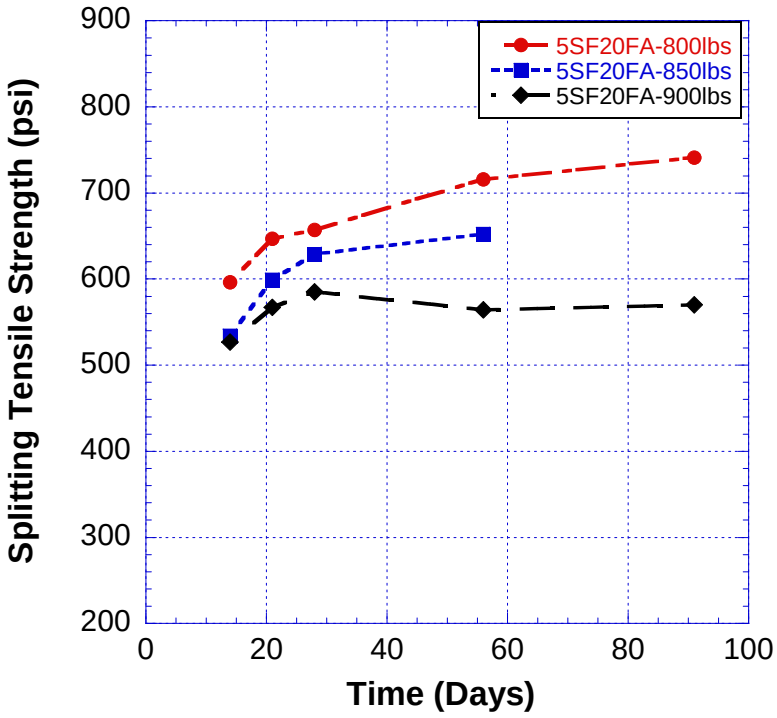

Figure 4-5 Splitting Tensile Strength of Group 1 Mixes

Splitting tensile strength of group 2 mixes are tabulated in Table 4-6 and displayed in Figure 4-6 as well. As expected, G2M1 with the least amount of fly ash replacement exhibited higher splitting tensile strength compared to the other group mixes.

Table 4-6 Splitting Tensile Strength of Group 2 Mixes (psi)

Testing Day	5SF10FA	5SF20FA	5SF30FA
14	588	527	463
21	-	567	-
28	700	585	537
56	758	564	541
91	761	570	-

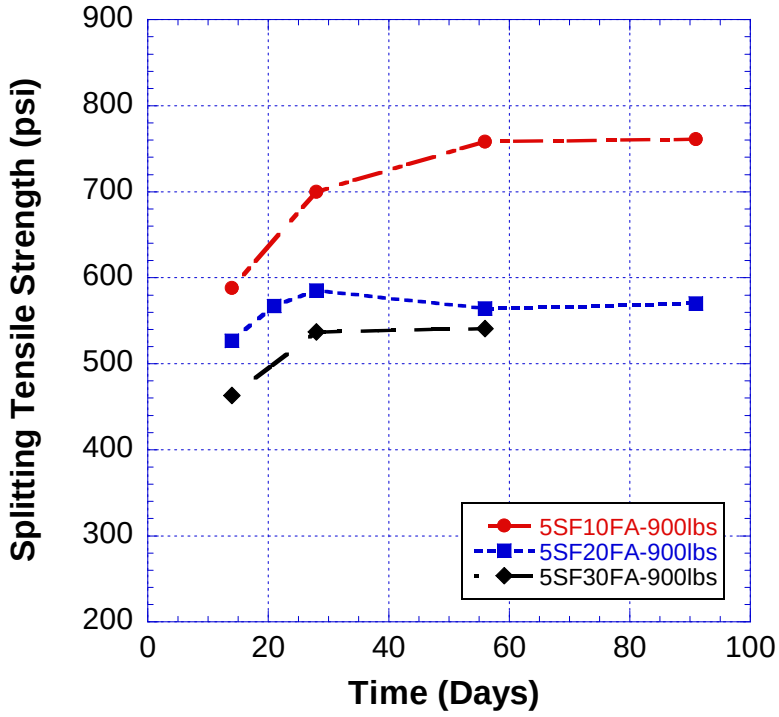

Figure 4-6 Splitting Tensile Strength of Group 2 Mixes

Table 4-7 and Figure 4-7 illustrates the splitting tensile strength testing results for group 3 mixes. The difference in the splitting tensile strength of the 10% silica fume and 0% silica fume was not found to be as significant as it was in compressive strength. At day 28, the 3 mixes of this group exhibited slight differences in the tensile strength development.

Table 4-7 Splitting Tensile Strength of Group 3 Mixes (psi)

Testing Day	20FA	5SF20FA	10SF20FA
14	506	534	542
21	-	599	576
28	570	629	610
56	703	652	696
91	727	-	752

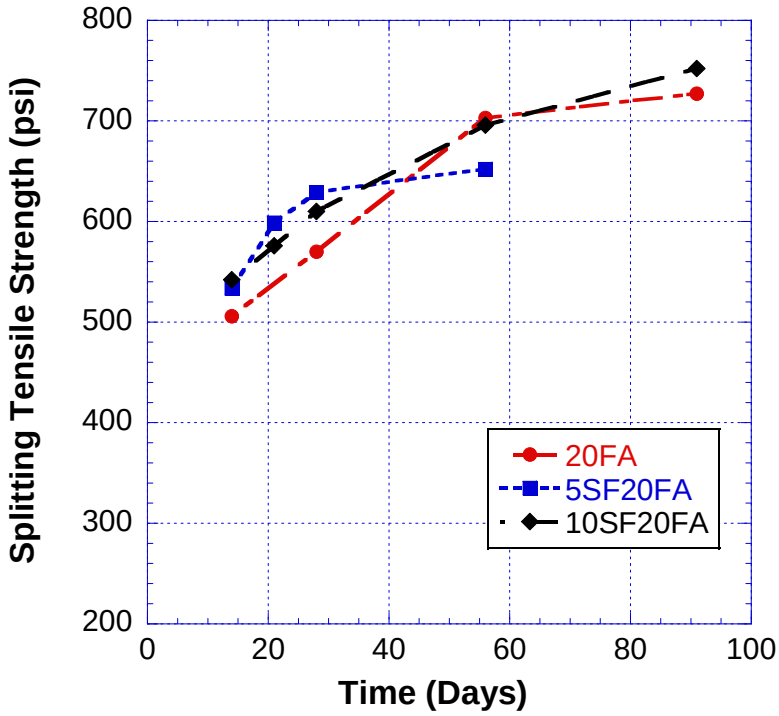

Figure 4-7 Splitting Tensile Strength of Group 3 Mixes

4.3.3 Modulus of Elasticity

Instead of using the ACI 318 Modulus derivation, laboratory tests were performed for extract the modulus of elasticity of SCC mixes. The tensile cracking strain of concrete ring specimens are then calculated using the modulus of elasticity test results along with the splitting tensile test results.

After day 14, the modulus of elasticity tends to remain at the same level rather than increasing rapidly, or in some cases decreases slightly .This manner is mainly attributed to the moist state of the concrete specimens during the long curing period going into dry conditions.

Table 4-8 and Figure 4-8 shows the modulus of elasticity testing results for Group 1 mixes. It can be noticed that the mix 5SF20FA with 900 pounds exhibited very low modulus of elasticity due to the high entrained air percentage as discussed in the previous sections. The difference between G1M3 with G1M1and G1M2 was 26% and 35% at day 28.

Table 4-8 Modulus of Elasticity of Group 1 Mixes (ksi)

Testing Day	5SF20FA	5SF20FA	5SF20FA
14	4917	4289	3388
21	4717	4573	3583
28	4785	4460	3543
56	4751	4455	3345
91	4792	-	3516

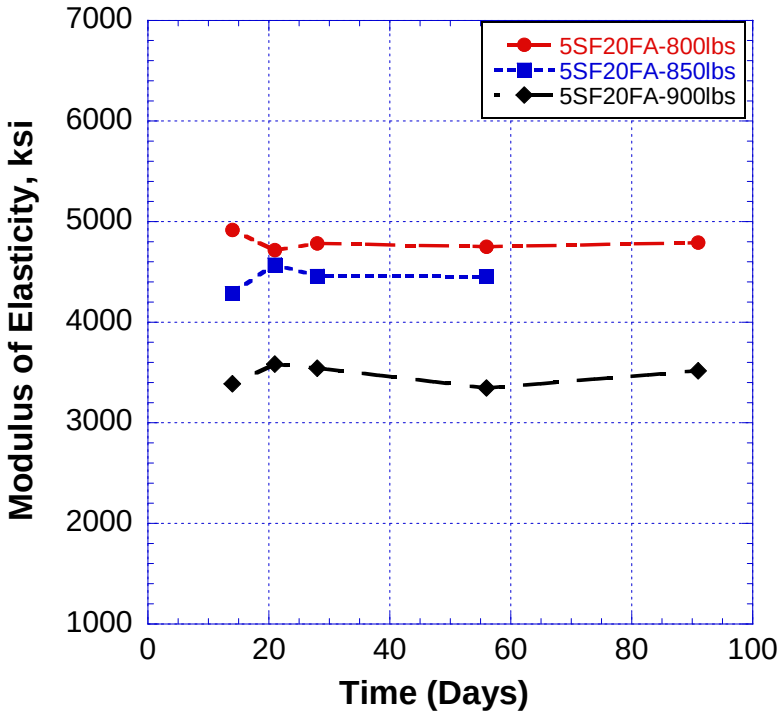

Figure 4-8 Modulus of Elasticity of Group 1 Mixes

Modulus of Elasticity test results for group 2 mixes is shown in Table 4-9 and Figure 4-9. It can be seen from Figure 4-9 that the modulus of elasticity for G2M1 slightly decreases after the curing is removed while G2M2 and G2M3 shows a slight increase or remains the same. Since the difference in the 3 mix designs of this group is the amount of fly ash as a replacement, this replacement difference can be attributed to the relative changes in modulus of elasticity. G2M1 having the least amount of fly ash gains its strength faster than the other group mixes, and thus the modulus of elasticity slightly decreases after curing.

Table 4-9 Modulus of Elasticity of Group 2 Mixes (ksi)

Testing Day	5SF10FA	5SF20FA	5SF30FA
14	4637	3388	4008
21	4567	3583	-
28	4591	3543	4087
56	4563	3345	3993
91	4376	3516	-

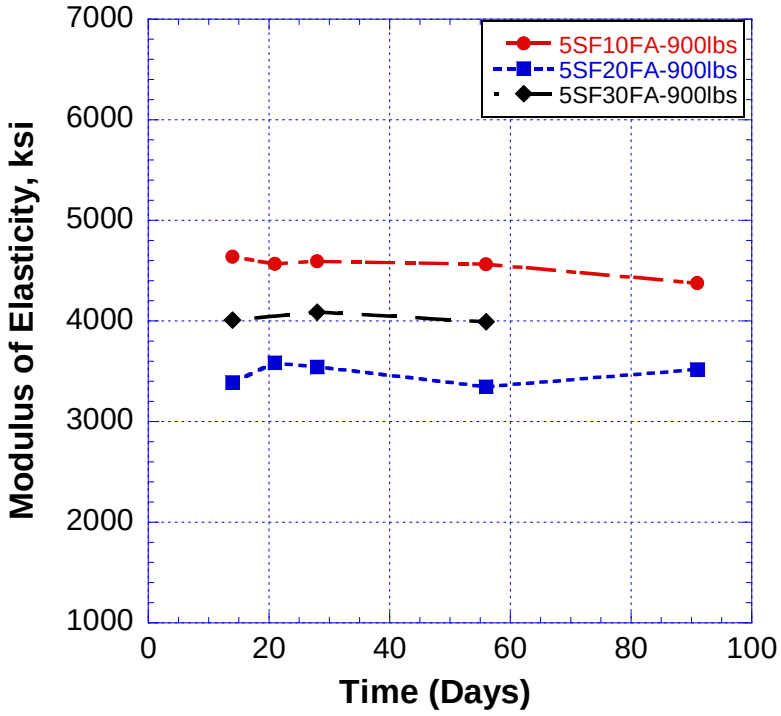

Figure 4-9 Modulus of Elasticity of Group 2 Mixes

Table 4-10 and Figure 4-10 shows the modulus of elasticity test result for the group 3 mixes. The trend after day 14 is similar to other group mixes since the group 3 mixes showed very slight increases or decreases after day 14. Similar to the splitting tensile strength, the 10% and 0% silica fume mixes exhibited very close modulus of elasticity results. Compared to the other 2 group mixes, 5% silica fume mix had slightly

lower modulus of elasticity at day 14, whereas all the 3 mixtures had similar results on day 21 and 28.

Table 4-10 Modulus of Elasticity of Group 3 Mixes (ksi)

Testing Day	20FA	5SF20FA	10SF20FA
14	4790	4289	4724
21	4830	4573	4628
28	4599	4460	4722
56	4875	4455	4632
91	4563	-	4643

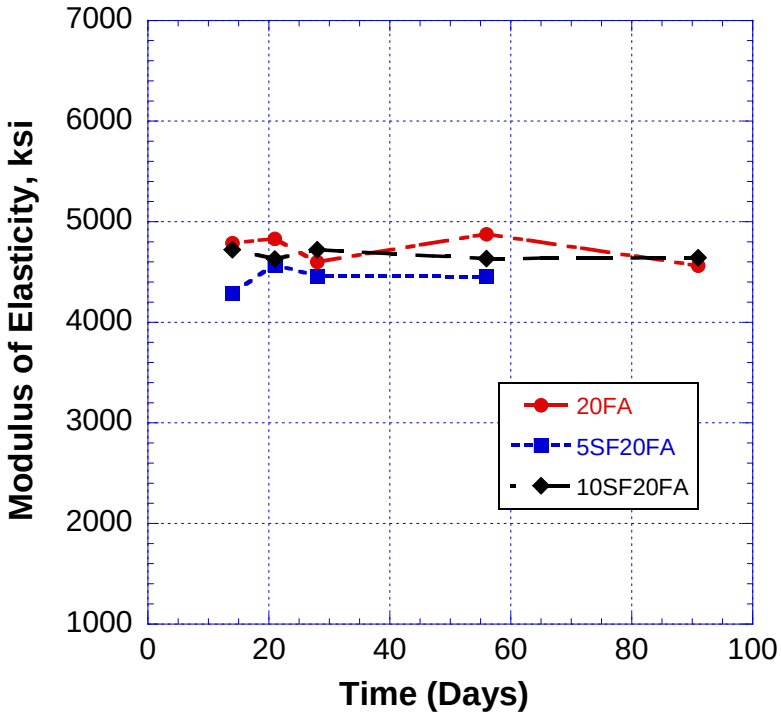

Figure 4-10 Modulus of Elasticity of Group 3 Mixes

4.4 FREE SHRINKAGE

Self consolidating concrete is assumed to exhibit higher levels of free shrinkage compared to conventional or high performance concrete mixes. This is mainly due to its high cementitious material content, in other words the low w/c ratio. In this sense, any improvements in the mix design to decrease the shrinkage magnitude, such as incorporation of pozzolanic materials or using optimum sand to aggregate ratio, is very important for successful SCC applications. In this study, the effect of total cementitious material was investigated through group 1 mixes, whereas the effect of fly ash and silica fume was investigated through group 2 and 3 mixes, respectively.

The free shrinkage results of group 1 mixes are illustrated in Table 4-11 and plotted in Figure 4-11 as well. The lowest amount of total cementitious is used for G1M1 with 800lbs, while the maximum amount of total cementitious material was used for G1M3 with 900 pounds.

Table 4-11 Free Shrinkage Strain of Group 1 Mixes

Testing Day	5SF20FA-800lbs	5SF20FA-850lbs	5SF20FA-900lbs
14	0	0	0
16	-92	-148	-183
18	-132	-245	-297
21	-230	-315	-383
28	-330	-425	-537
35	-392	-	-620
42	-	-560	-717
49	-465	-603	-783
56	-495	-625	-830
91	-575	-	-957

G1M2 and G1M3 were found out to exhibit very high levels of free shrinkage compared to G1M1. The difference between the G1M1 and G1M3 is found to be 68% at

day 56. This significant difference is partially attributed to the weak mechanical properties of G1M3, but mainly the effect of additional 100 pounds of cementitious material used. G1M2 also exhibited higher free shrinkage compared to G1M1 since it had 50 pounds more cementitious material content.

Comparing the group 1 free shrinkage results to the 450 micro strain level recommended by Aktas (2007) and Montemerano (2008), even the SCC mix with 800 pounds of cementitious material is above this recommended level by 10%.

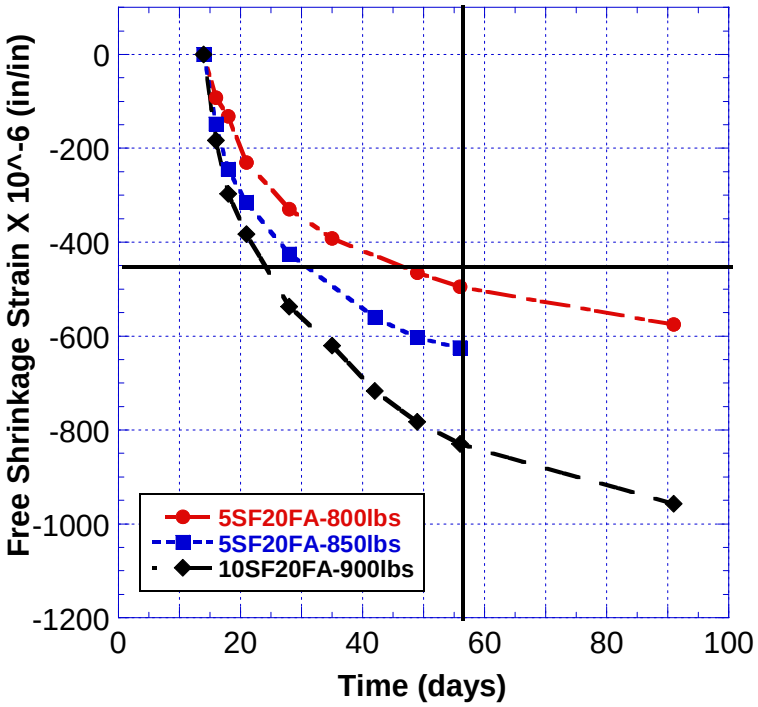

Figure 4-11 Free Shrinkage Strain of Group 1 Mixes

The measured free shrinkage strains for group 2 mixes are shown in Table 4-12 and Figure 4-12. This group consists of 3 mixes where 900 lbs of total cementitious material was used at each time but different percent of fly ash replacement was applied. As expected all the mixes had very high levels of free shrinkage strain even compared to the G1M1 where only 800 lbs of cementitious material was used.

Moreover, at this level of high total cementitious material, increasing the percentage of fly ash replacement did not help reducing the severity of free shrinkage. Such interpretation can be made by looking at Figure 4-12 where there is almost no difference in the free shrinkage strain between G2M1 and G2M3. This type of behavior was also supported by the research findings of Khayat and Mitchell (2009), where the effect of binder type was found to have no significant effect on the drying shrinkage of SCC.

Although G2M2 exhibited more shrinkage than the other 2 mixes, this was attributed to the mechanical properties and the high entrained air percentage, as discussed previously. In general, free shrinkage of SCC evaluated at 900 pounds of cementitious material usage is not sensitive to the change in fly ash replacement percentage for the given group 2 mixes.

Table 4-12 Free Shrinkage Strain of Group 2 Mixes

Testing Day	5SF10FA	5SF20FA	5SF30FA
14	0	0	0
16	-167	-183	-160
18	-247	-297	-
21	-320	-383	-
28	-433	-537	-410
35	-473	-620	-485
42	-530	-717	-545
49	-570	-783	-585
56	-603	-830	-615
91	-693	-957	-

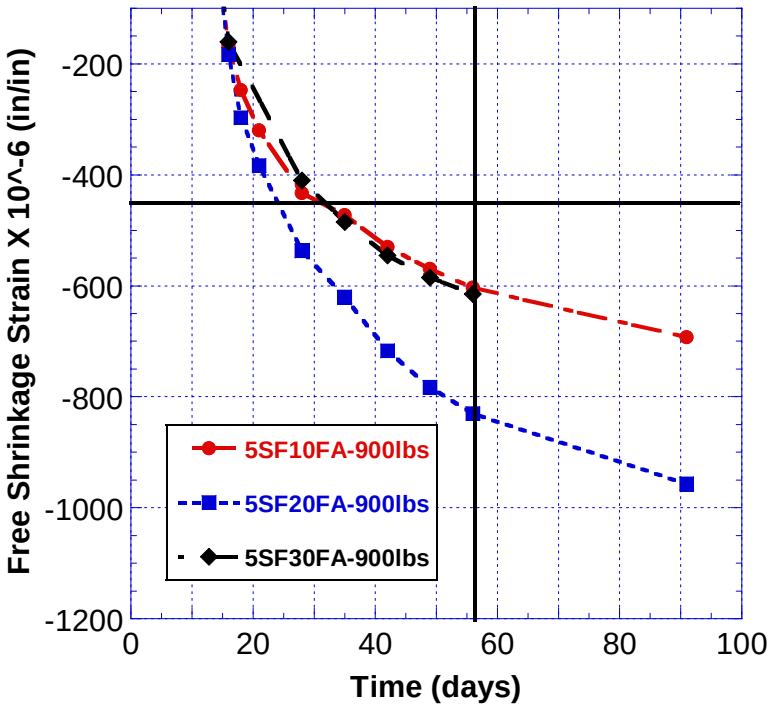

Figure 4-12 Free Shrinkage Strain of Group 2 Mixes

Table 4-13 and Figure 4-13 shows the free shrinkage testing results for group 3 mixes. The effect of silica fume replacement is investigated with the group 3 mixes. To provide a better comparison, only the G3M3 and G3M1 mixes are plotted in Figure 4-13, since these 2 mixes are similar in terms of mechanical and fresh concrete properties. Moreover, G3M1 is the lower threshold of this group with 0% silica fume replacement whereas the G3M3 is the upper threshold with 10% silica fume replacement. Since silica fume is a finer and more reactive material compared to Portland cement, thus the increase in the silica fume replacement percentage is expected to induce more shrinkage to SCC.

Table 4-13 Free Shrinkage Strain of Group 3 Mixes

Testing Day	20FA	5SF20FA	10SF20FA
14	0	0	0
16	-	-148	-
18	-190	-245	-253
21	-273	-315	-310
28	-360	-425	-407
35	-427	-	-
42	-473	-560	-520
49	-513	-603	-563
56	-543	-625	-597
91	-640	-	-713

At day 56, the free shrinkage strain of G3M3 which had 10 % silica fume was 563 micro strains, while G3M1 with 0% silica fume had 513 micro strains. At day 18, the difference of free shrinkage strain between these 2 mixes was 33%, whereas the difference reduced to 10% at day 56. This is due to the high reactivity of silica fume at the early ages. On the other hand, although the difference at early ages seems to be high, the effect of silica fume at later ages is not as significant as the effect of changing the cementitious material as discussed for group 1 mixes. It should be noted that the group 3 mixes had 850 pounds of total cementitious material, so, given that the amount of total cementitious material is increased, the effect of silica fume replacement ,may be less significant similar to the effect of fly ash replacement at 900-pound level.

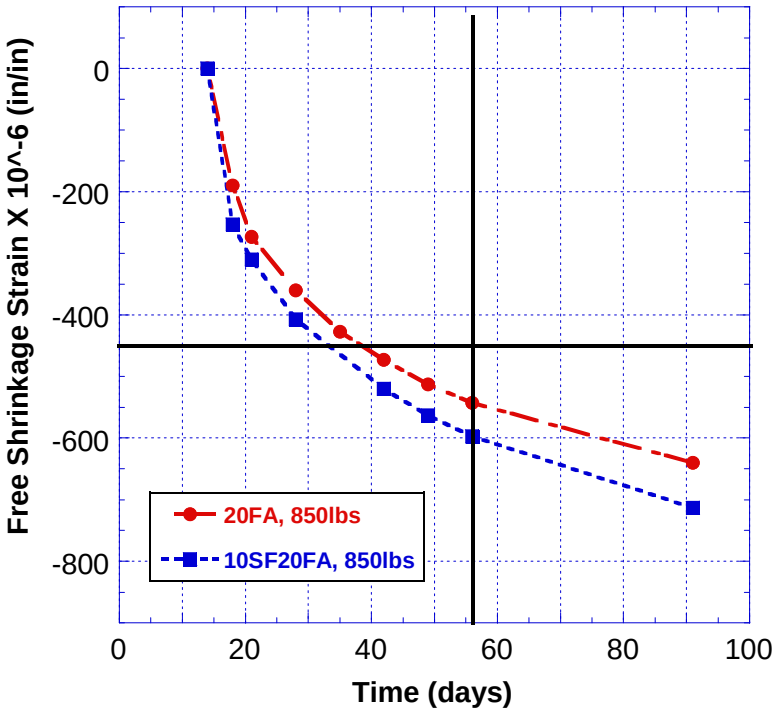

Figure 4-13 Free Shrinkage Strain of Group 3 Mixes

4.5 RESTRAINED SHRINKAGE

This section provides the restrained shrinkage testing results for the produced SCC mixes. As mentioned in the previous chapters, a modified ring test was used to provide restrained conditions for concrete shrinkage. This modified method was found to be very helpful in not only capturing shrinkage strains directly from concrete, but also providing more redundancy to the experimental setup. Since SCC is still considered to be a relatively new type of concrete with many non-established standards, the inclusion of additional testing tools becomes more important.

The restrained condition behavior of concrete mixes were interpreted and correlated by using steel ring sensor data, concrete sensor data, visual crack observations, and correlation with free shrinkage behavior. This multiple observation spectrum allows

elimination of uncertainties and unexpected experimental errors; hence the restrained shrinkage behavior of the SCC mixes can be extracted in a reliable manner.

The following sections of this chapter provide the findings along with associated discussions related to how the selected parameters affect the performance of SCC mixes under restrained conditions.

4.5.1 Early Age Behavior under Restrained Conditions

All the SCC ring specimens in this study were wet burlap cured for the first 14 days after casting. Since 14 days is a relatively long curing period, it was important to monitor the strain profile during the curing period. Steel ring foil gages were preferred to monitor the strain profile during the curing period. Since the wet burlap cover is replaced at least once on every curing day, the VWSG sensors were not suitable during this period because of their sensitivity to any disturbance.

The steel ring strain profiles for 2 of the SCC mixes are illustrated in Figure 4-14 and Figure 4-15 for G1M3 and G1M2, respectively. G1M3 has 900 pounds of cementitious material, whereas G1M2 has 850 pounds, and both of the mixes have 5% silica fume along with 20% fly ash replacement in their mix design.

During the very early stage of curing, the steel ring tends to expand due to the heat generated by the hydration of cementitious material particles. This can be observed from the steel strain profiles in Figure 4-14 and Figure 4-15. The heat of hydration exerts an expansion of maximum 23 and 18.5 micro strains on the steel rings of G1M3 and G1M2, respectively. Since the G1M3 has 50 pounds more cementitious material, this type of difference in hydration heat induced deformation is expected. In both cases, the measured strains peak at about 15 hours after casting of concrete.

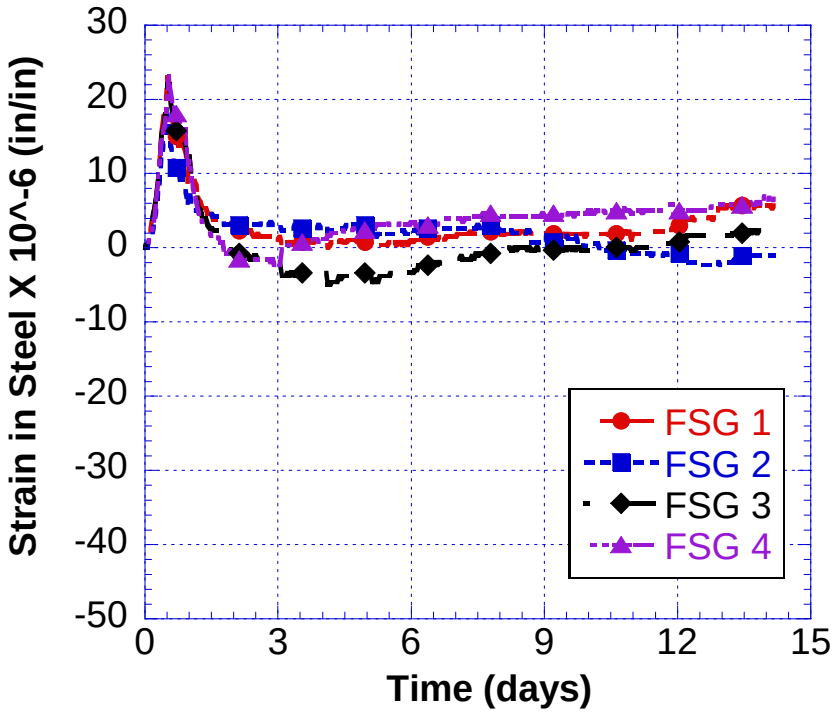

Figure 4-14 Early Age Behavior of 5SF20FA-900 lbs (G2M2)

After the peak is observed, the strain level tends to decrease and go back to almost zero strain level at around 1.5 to 2 days after casting. In between the peak strain and the 2 day strain levels, the ring specimens are demolded approximately at 24 hours and the burlap is replaced. After this point, the strain level still decreases and either stop at the zero level or show a low level of compression. Given that the concrete specimens are wet cured twice a day for the first 3 days of curing period, even the low levels of compression experienced is removed as the concrete surface absorbs the curing water.

Although the strain profile shows negligible or no shrinkage strain for the rest of the curing period, the concrete, the shrinkage occurring between the peak expansion strain and the 2 day strain should be noted. During this period, one of the reasons for concrete shrinkage is the effect of decrease in the temperature. Another reason can be the

autogenous shrinkage of concrete due to the self desiccation of cementitious material particles. Many researchers in the literature [11, 15] had findings related to the high vulnerability of SCC mixes to autogenous shrinkage due to the low water to cement ratios. According to Khayat and Mitchell (2009), SCC mixes produced for precast, prestressed applications can exhibit autogenous shrinkage deformations as high as 100 to 350 micro strains in the first 28 days after casting. So the shrinkage observed towards the end of the first 2 days of curing can be resultant from autogenous shrinkage or thermal shrinkage.

Another possibility in the very early 2 days of curing is the reverse effect of autogenous shrinkage and expansion caused by the heat of hydration. SCC is expected to exhibit high levels of autogenous shrinkage, so the expansion can be cancelling out the autogenous shrinkage exerted on the opposite direction.

As a summary, the curing strain history of the above mentioned mixes shows that SCC mixes can be kept under control in terms of shrinkage deformation if very extensive curing is applied until the drying is initiated.

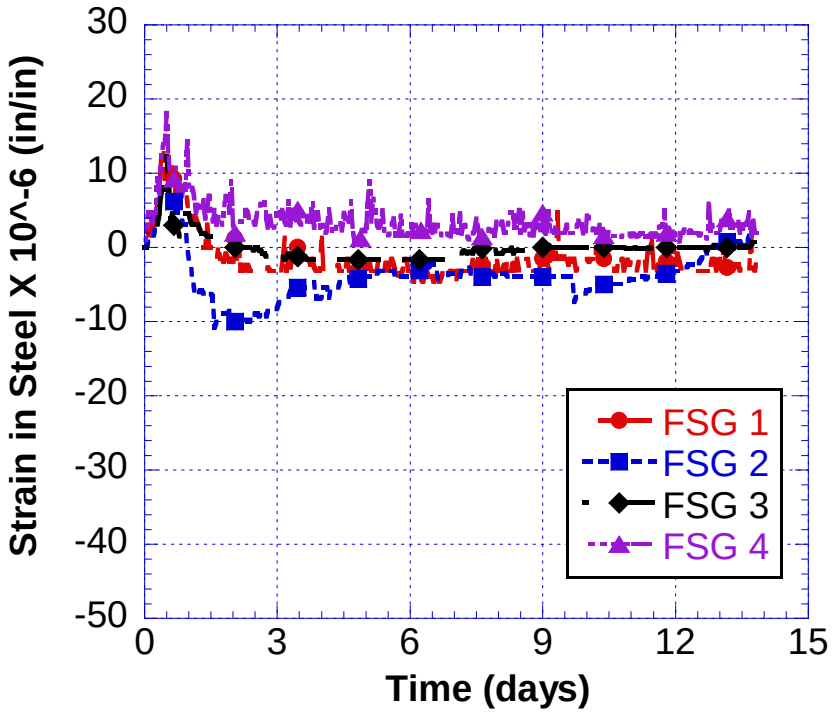

Figure 4-15 Early Age Behavior of 5SF20FA-850 lbs (G1M2)

4.5.2 Restrained Shrinkage Testing Results and Cracking Performance of SCC Mixes

The ring test results for G1M1 are presented in Figure 4-16 and in Figure 4-17 as well. G1M1 has 800 pounds of total cementitious and was proportioned with 5% silica fume along with 20% fly ash. From Figure 4-16, it can be seen that the strain data collected from VWSG 1 exceeds the cracking strain at day 26 after casting. The strain profile recorded by the VWSGs passing the cracking strain is considered as a signal of the initiation of drying shrinkage cracking around that specific region. The visual crack observations presented in Figure 4-18 confirms this behavior. From Figure 4-18, it can be seen that a drying shrinkage crack is initiated from the surface where the VWSG 1 is located. The cracked is observed 1 day after the cracking strain is exceeded. In general,

the visual crack observations coincide with the strain profile of the ring specimens within couple days.

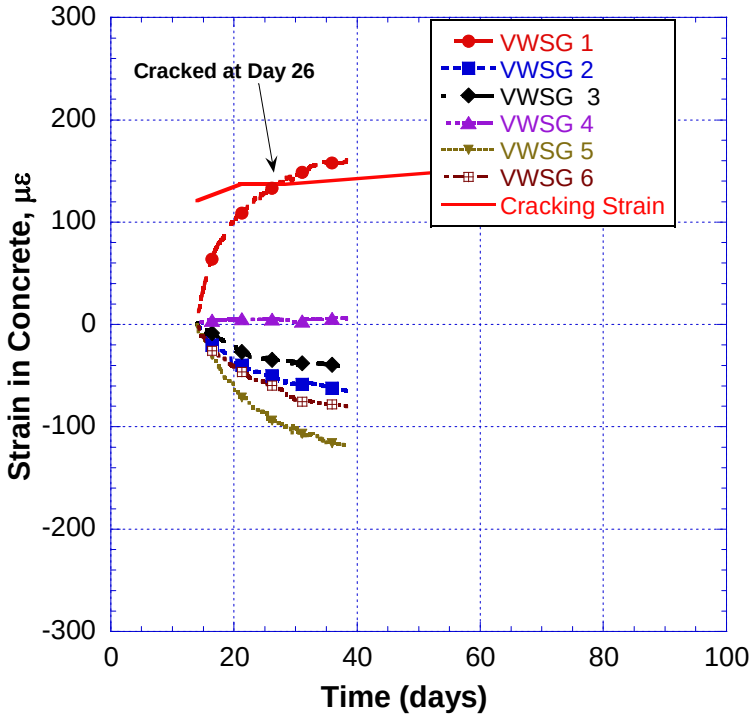

Figure 4-16 Concrete Strains for G1M1 Ring Specimen 1

The first ring specimen of G1M1 exhibits more drying shrinkage cracks after the first crack occurs on the surface of region 1. The visual crack observations presented shows indicates many other cracks at different regions. Also, the steel ring profile of G1M1 ring 1 presented in Figure 4-17 shows that the compressive strains exerted on the steel ring tends to slow down after day 30. This can be interpreted as the concrete ring had exhibited several tensile cracks, thus started to release the compressive forces exerted on the steel ring.

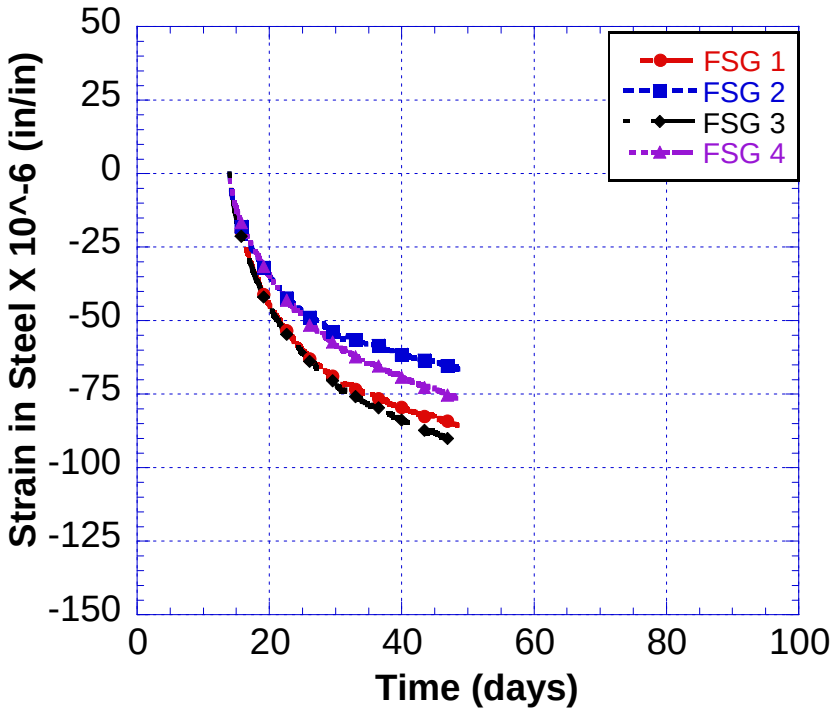

Figure 4-17 Steel Strains for G1M1 Ring Specimen 1

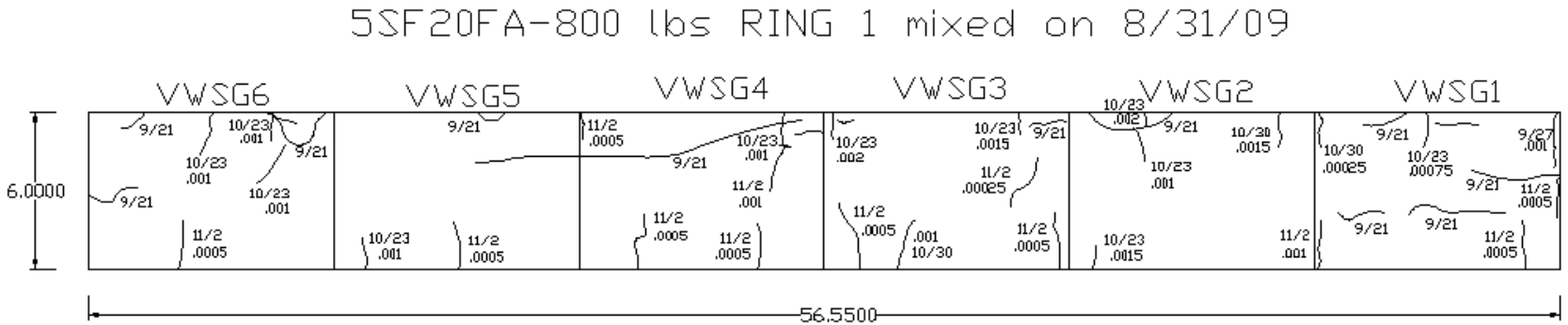

Figure 4-18 G1-M1 Crack Drawings for Ring Specimen 1, Side View (Top Figure) and Top-Bottom Views (Bottom Figure)

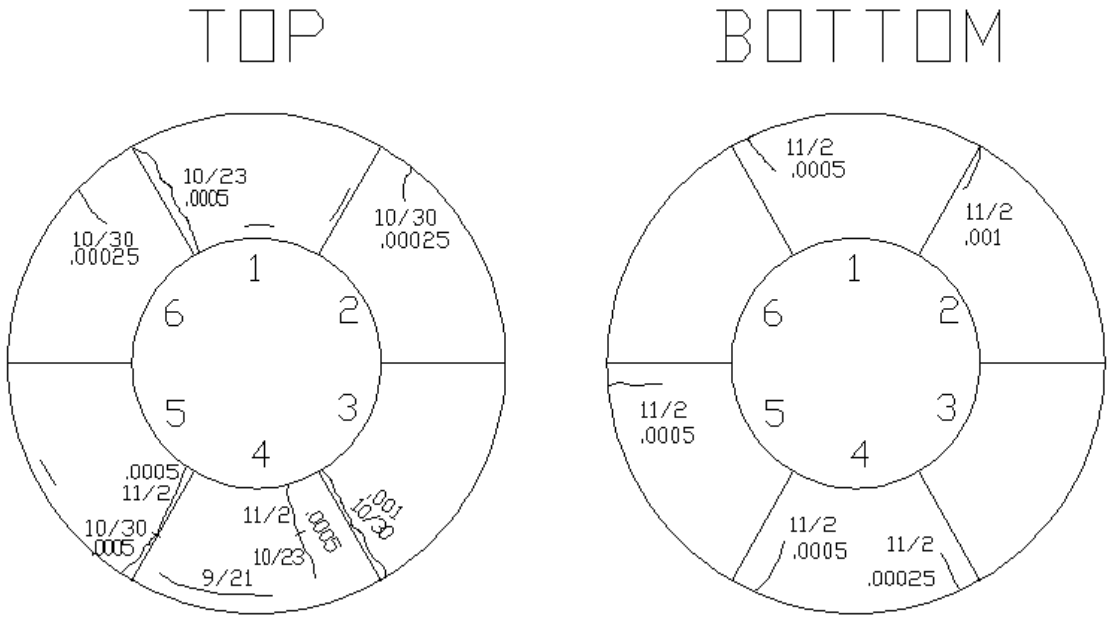

The strain records from the steel ring and the visual crack observations were used to evaluate the behavior of G1M1 ring specimen 2. The maximum steel ring compression strain level from Figure 4-19 is lower than that of the measured from ring specimen 1. The first drying shrinkage crack observed was at the age of 30 after curing. Figure 4-20 shows the cracking pattern of the G1M1 ring specimen 2. Although cracked slightly later than the first ring specimen, this ring also developed several drying shrinkage cracks both on the sides and top surface.

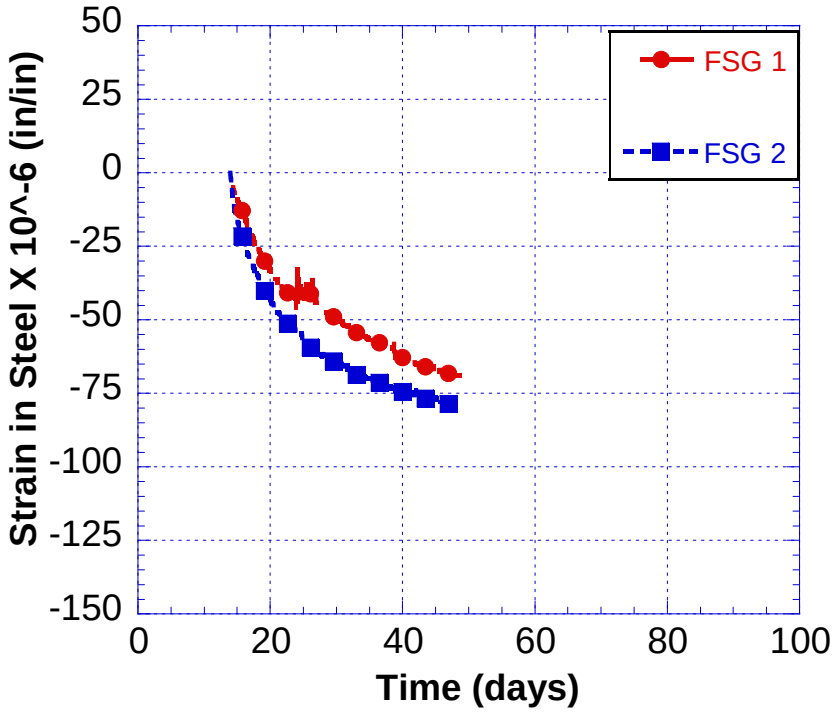

Figure 4-19 Steel Strains for G1M1 Ring Specimen 2

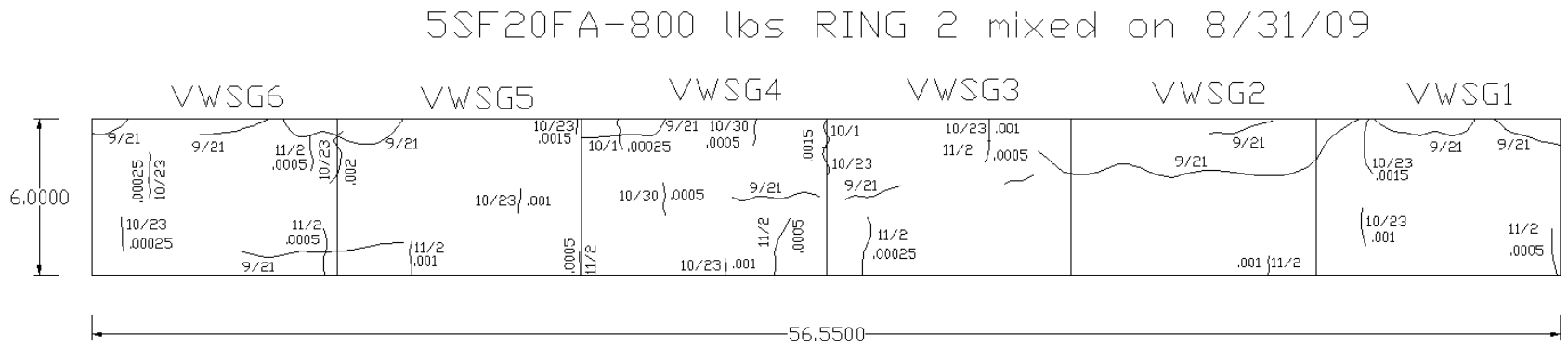

Figure 4-20 G1-M1 Crack Drawings for Ring Specimen 2, Side View (Top Figure) and Top-Bottom Views (Bottom Figure)

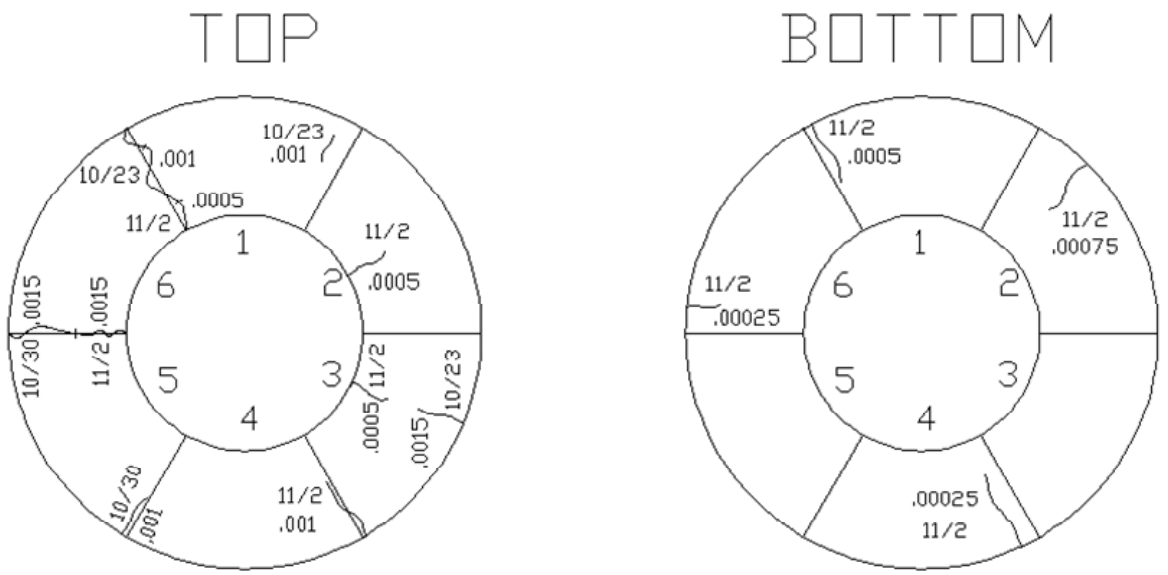

The strain profile recorded from the first ring specimen of G1M2 is shown in Figure 4-21. Similar to the second specimen of G1M2, the first observed shrinkage cracking was observed on day 20 for this ring specimen. From Figure 4-22, we can see that a drying shrinkage crack initiates and propagates on the region where VWSG 3 and VWSG 4 are connected. On this ring, FSG strain records indicate a similar trend for FSG 1 and FSG 3 whereas a slightly higher magnitude for FSG 4. Looking at Figure 4-22, we can see that there is more number of drying shrinkage cracks on the VWSG regions 1 through 4 both on the surface, top and bottom ring sections. Since there is relatively more cracking concentrated on these regions, the compressive strain trends recorded by FSG 1 and FSG 3 tend to slow down earlier than the FSG 4 strain profile.

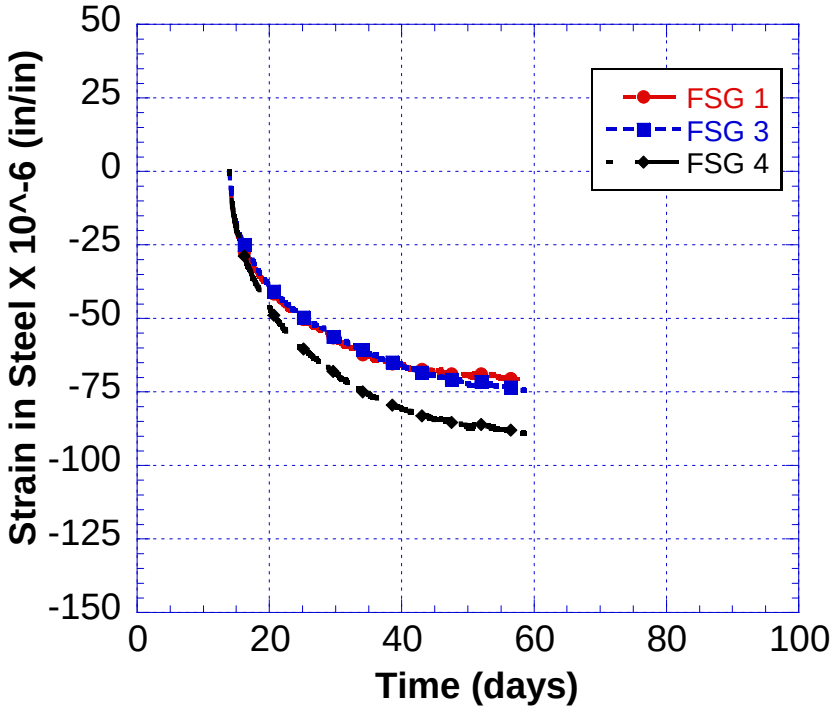

Figure 4-21 Steel Strains for G1M2 Ring Specimen 1

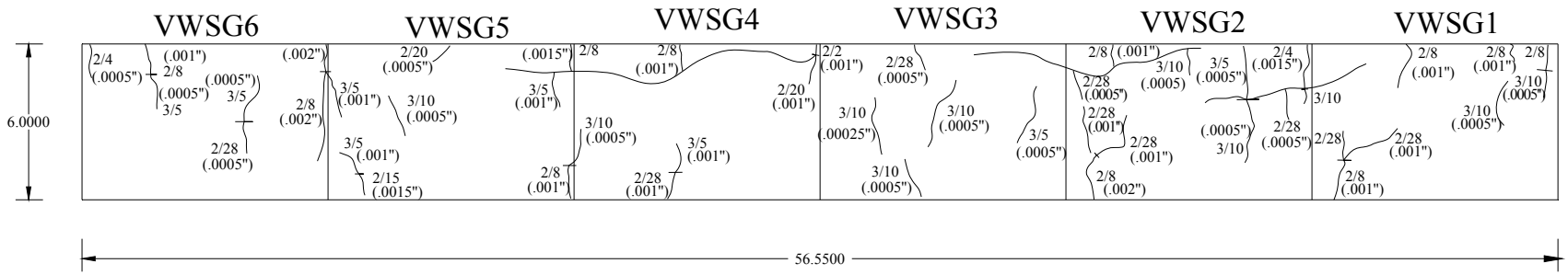

Figure 4-22 G1M2 Crack Drawings for Ring Specimen 1, Side View (Top Figure) and Top-Bottom Views (Bottom Figure)

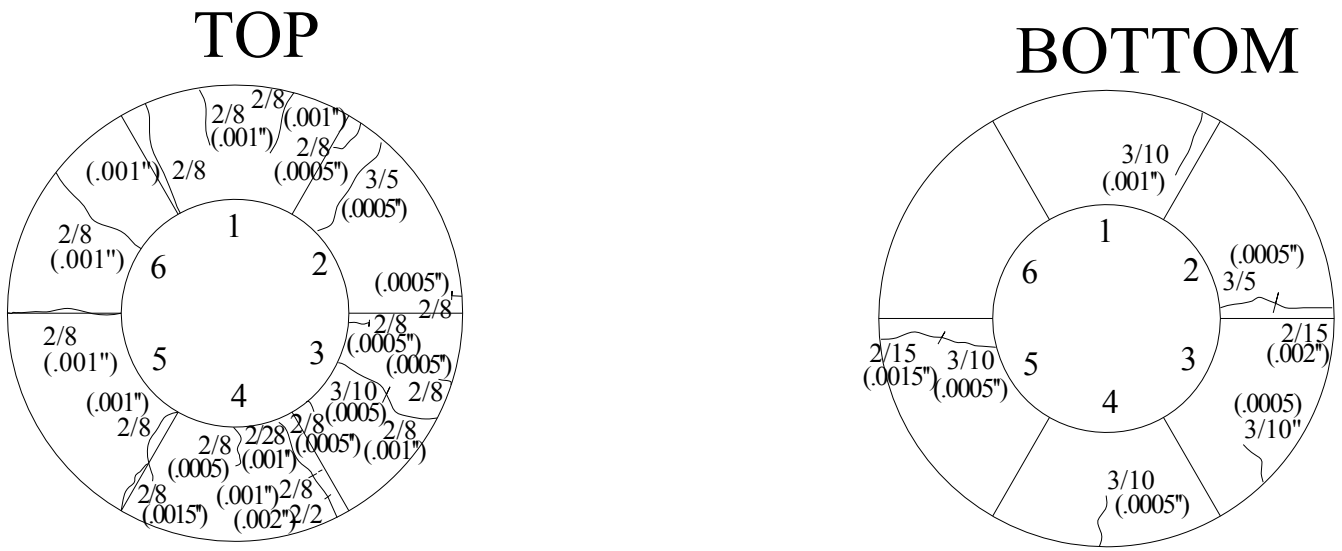

Figure 4-23 and Figure 4-24 illustrates the strain profile of the steel ring and concrete for the second ring specimen of G1M2. This mix has 850 pounds of cementitious material content of which 5% is silica fume and 20% is fly ash. As shown in Figure 4-23, the concrete strain profile indicates that VWSG 4 exceeds the cracking strain at day 18 after curing. Looking at the observed crack drawings of this ring specimen from Figure 4-25, it can be seen that a drying shrinkage crack formed at day 21 on the region where VWSG 4 and 5 is connected. Thus, it can be seen that the location and approximate time of the initial drying shrinkage crack was signaled by the VWSG sensors.

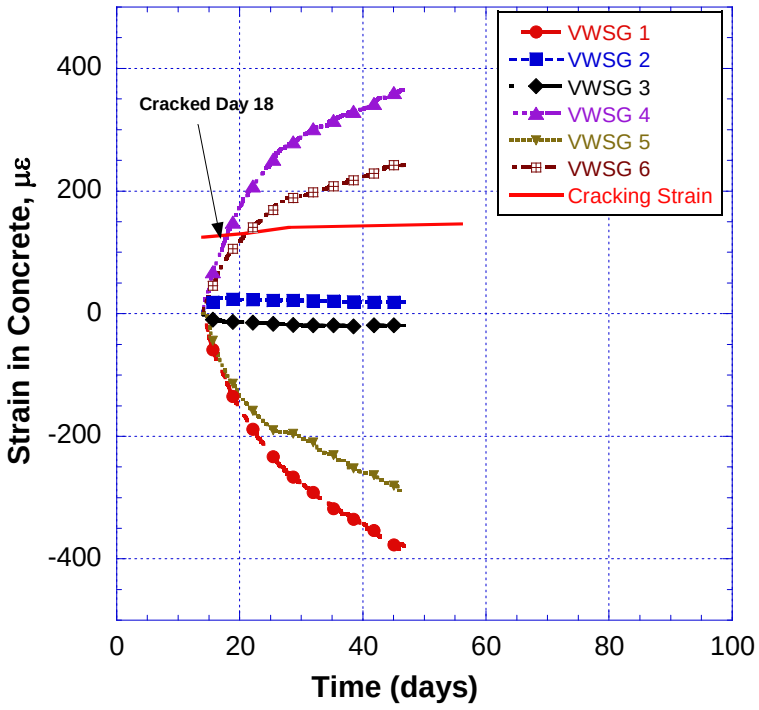

Figure 4-23 Concrete Strains for G1M2 Ring Specimen 2

From Figure 4-24, it can be seen that the compressive strain recorded by FSG's tend to increase in parallel to each other in magnitude. After day 20, drying shrinkage

crack occurs on different regions of the steel ring thus the rate of strain recorded starts to slow down. Also the measured compressive strain profile recorded by FSG3 tends to slow down faster than FSG 1 and FSG 2 strain profiles since the initial cracks on this ring occurred around the adjacent VWSG 4 region. Similar to this trend, the compressive strain rates recorded by FSG 1 and FSG 2 also tend to slow down as more cracking takes place on the ring specimen.

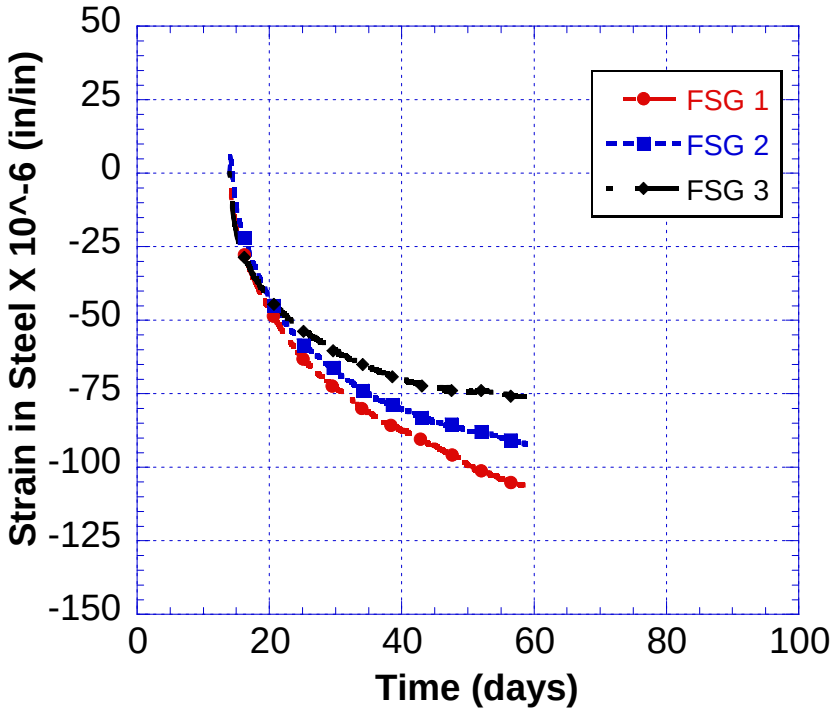

Figure 4-24 Steel Strains for G1M2 Ring Specimen 2

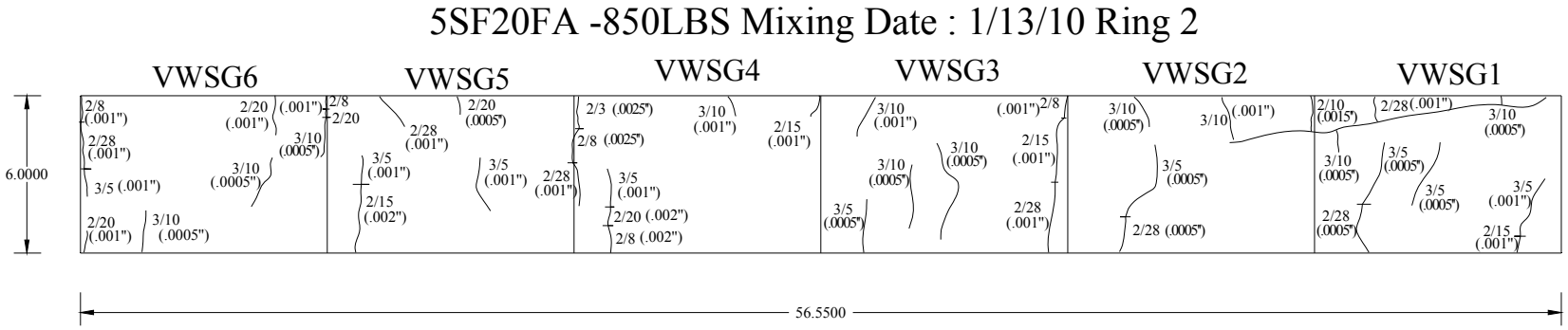

Figure 4-25 G1M2 Crack Drawings for Ring Specimen 2, Side View (Top Figure) and Top-Bottom Views (Bottom Figure)

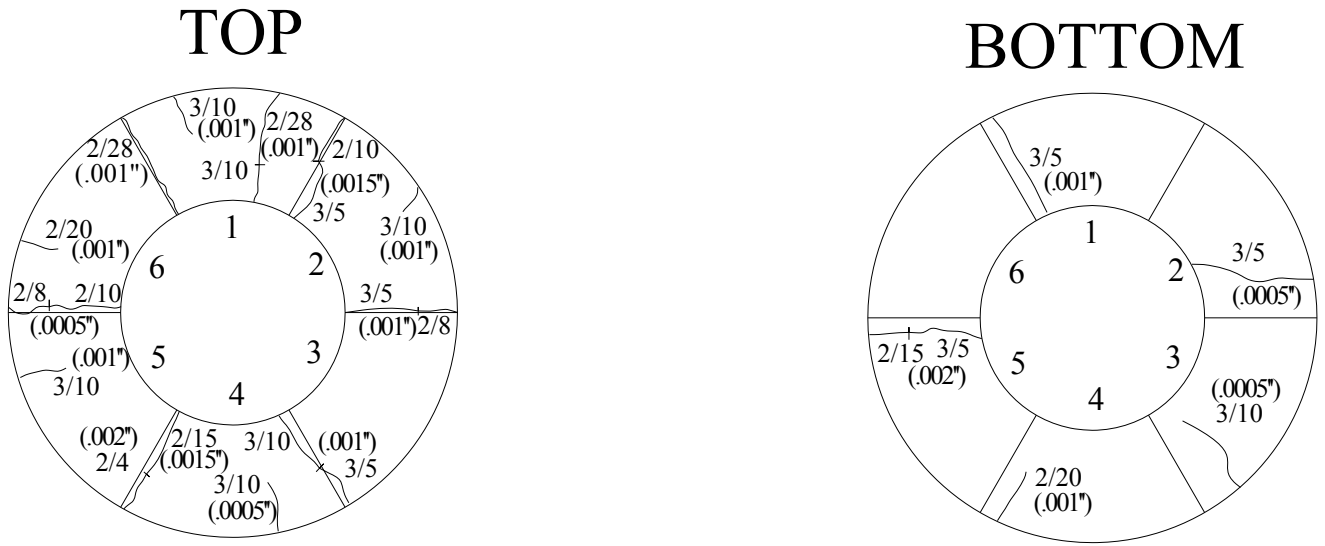

Figure 4-26 shows the steel ring strain profile of 5SF20FA with 900 pounds of total cementitious material. This mix has the highest total cementitious material among group 1 mixes and is also used as one of the three mixes for the second group of mixes.

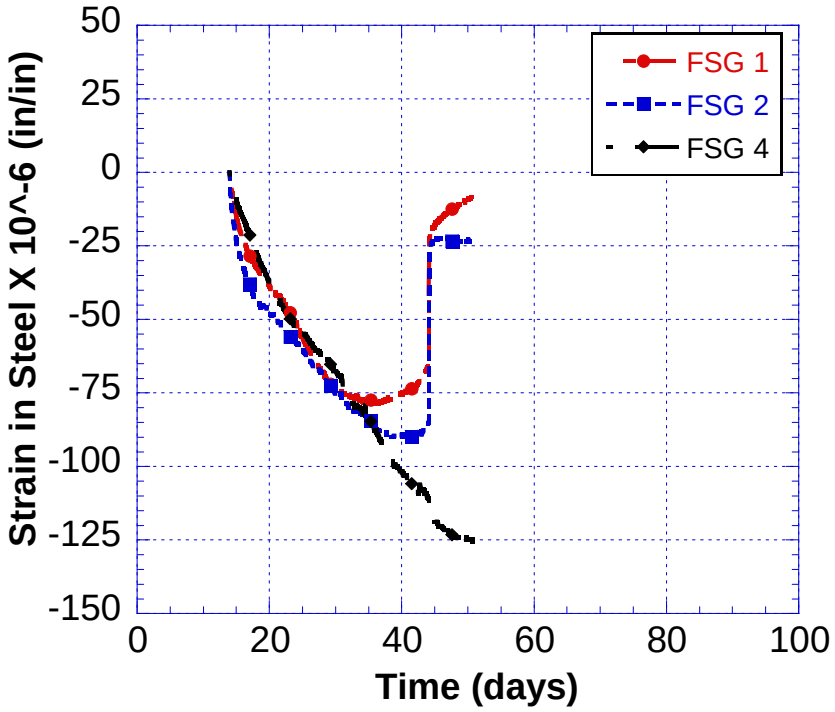

Figure 4-26 Steel Strains for G1M3 Ring Specimen 1

The strain gage data profile presented in Figure 4-26 shows almost an even distribution of strains exerted on the steel ring with the initiation of drying shrinkage at day 14 and until day 30. After the age of 22, Figure 4-27 indicates that several drying shrinkage cracks were observed at different locations of the ring specimen. At this point, 3 of the steel ring foil gages show a strain magnitude of approximately 75 micro strains. The strain profile of the ring at different locations being very close to each other in terms of magnitude and the visual observations showing cracks at different locations of the specimens at the same time confirms each other.

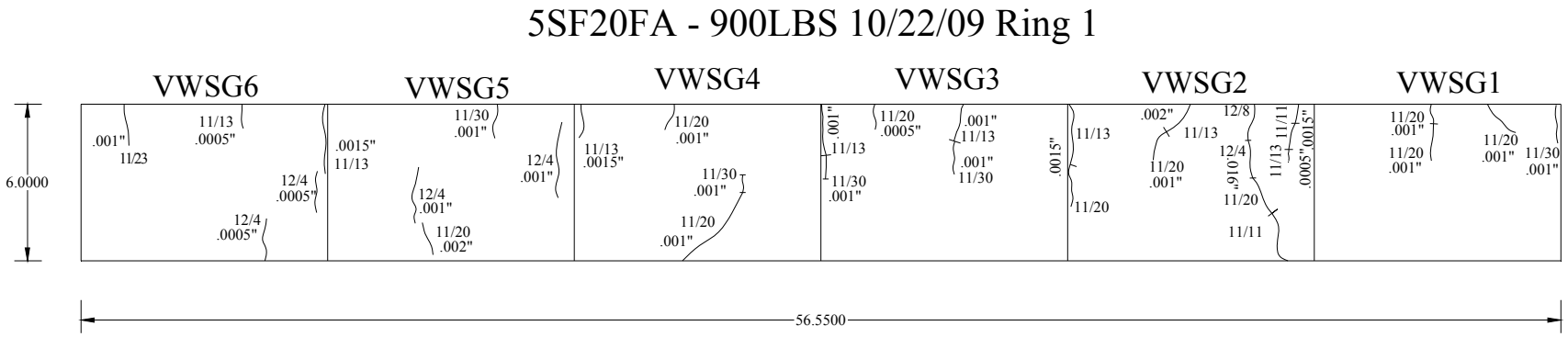

Figure 4-27 G1-M3 Crack Drawings for Ring Specimen 1, Side View (Top Figure) and Top-Bottom Views (Bottom Figure)

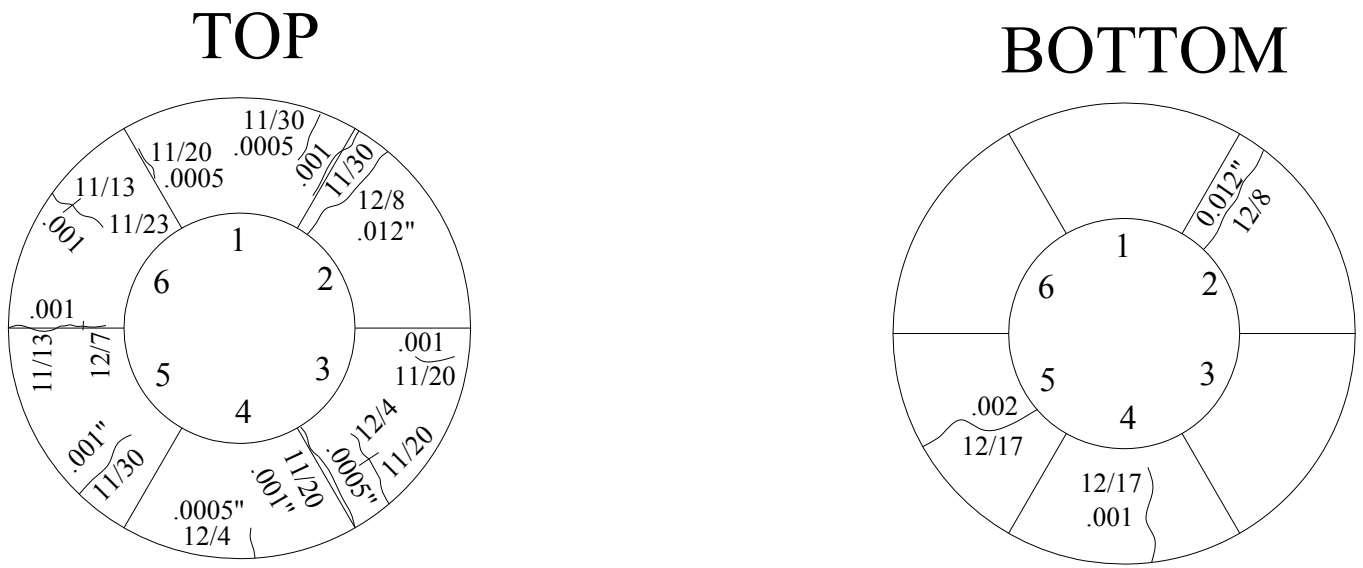

Later at around day 45 after casting, the first ring specimen of G1M3 exhibits a very wide shrinkage crack on VWSG 2 region. This crack was 0.16”wide on the average along the side of the ring, and propagated towards the steel ring both on the top and bottom of the ring. Since the propagation of the crack was abrupt and sudden, this was reflected as a sharp decrease in the FSG strain records. From Figure 4-26, we can see that there was a sudden decrease in strain recorded by FSG 1 and FSG 2 both of which are located very close to the large crack opening. A view from the large crack opening on this ring is shown in Figure 4-28.

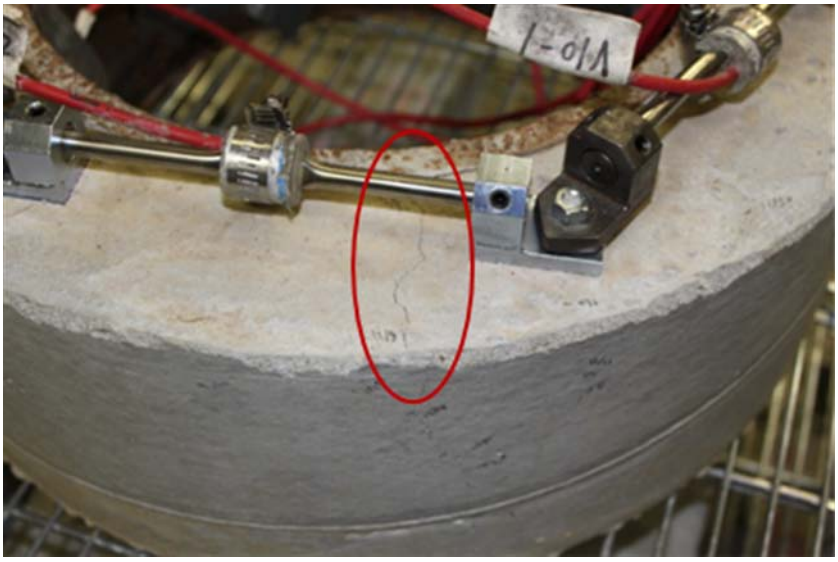

Figure 4-28 Full Depth Shrinkage Crack Observed on G1M3 Ring Specimen 1

Figure 4-29 and Figure 4-30 shows the recorded concrete and steel strains of 5SF20FA second specimen with 900 pounds of cementitious material, respectively. The concrete strain shown in Figure 4-29 indicates that the VWSG 4 exceeds the cracking strain at day 20 after casting.

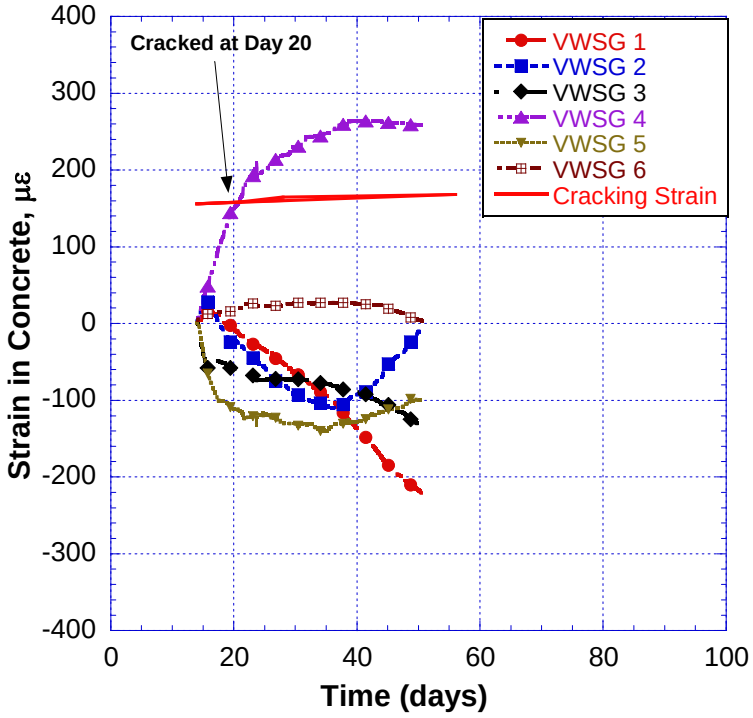

Figure 4-29 Concrete Strains for G1M3 Ring Specimen 2

The cracking shown by the concrete strain gages 4 was also confirmed by the visual crack observations. It can be seen from Figure 4-31 that there was a crack observed at location 4 at day 19 after casting. The age of observed cracking on the second specimen of this mix is very similar to the first specimen, 19 days and 20 days, respectively. Following the first cracking at day 19, other drying shrinkage cracks were also observed on ring specimen 2 and this behavior also corresponds with the first specimen of this mix.

Looking at Figure 4-29, we can see that VWSG 2 tends to decrease in compressive strain very rapidly after day 35. In other words, between day 35 and 45, VWSG 2 tends to record 100 micro strains of tensile strain. This behavior can be explained by the large crack opening on region 2 of the ring specimen. From Figure 4-31, we can see that a large crack has formed on region 2 and reached to the steel ring on the top surface at day 39 and on the bottom surface at day 47.

The steel ring strain recorded from G1M2 indicates the shrinkage cracking as well. Similar to the first specimen of this ring, an abrupt change in FSG strain was recorded around day 47. This was due to wide crack on region 2 propagating towards the steel ring on all 3 surfaces of the concrete ring. Once the crack reached the steel ring along the entire section, the compressive strain is released on the steel ring, and thus an abrupt change in the strain profile is recorded by the FSG's, as illustrated in Figure 4-30.

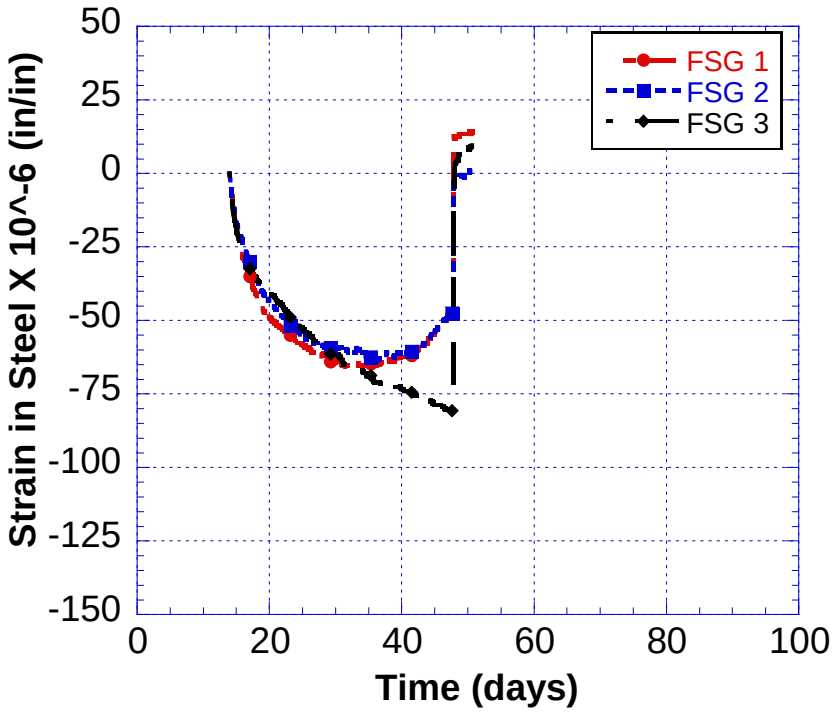

Figure 4-30 Steel Strains for G1M3 Ring Specimen 2

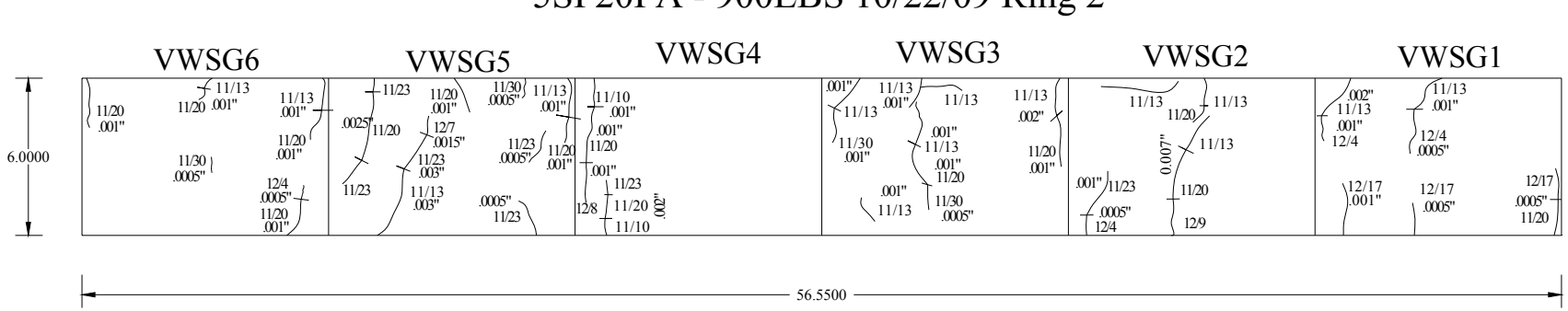

Figure 4-31 G1-M3 Crack Drawings for Ring Specimen 2, Side View (Top Figure) and Top-Bottom Views (Bottom Figure)

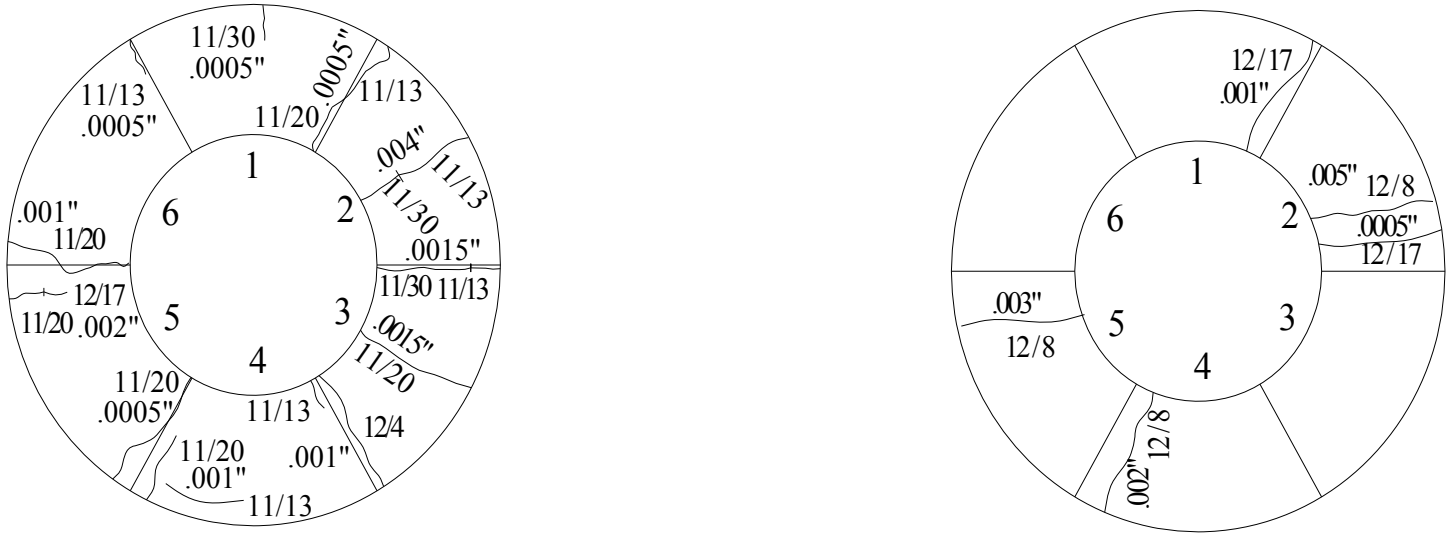

The concrete strain measured with the VWSG's and the steel ring strain measured by the FSG's for 5SF10FA are shown in Figure 4-32 and Figure 4-33, respectively. This mix was batched with 900 pounds of cementitious material and %10 fly ash as a replacement of Portland cement.

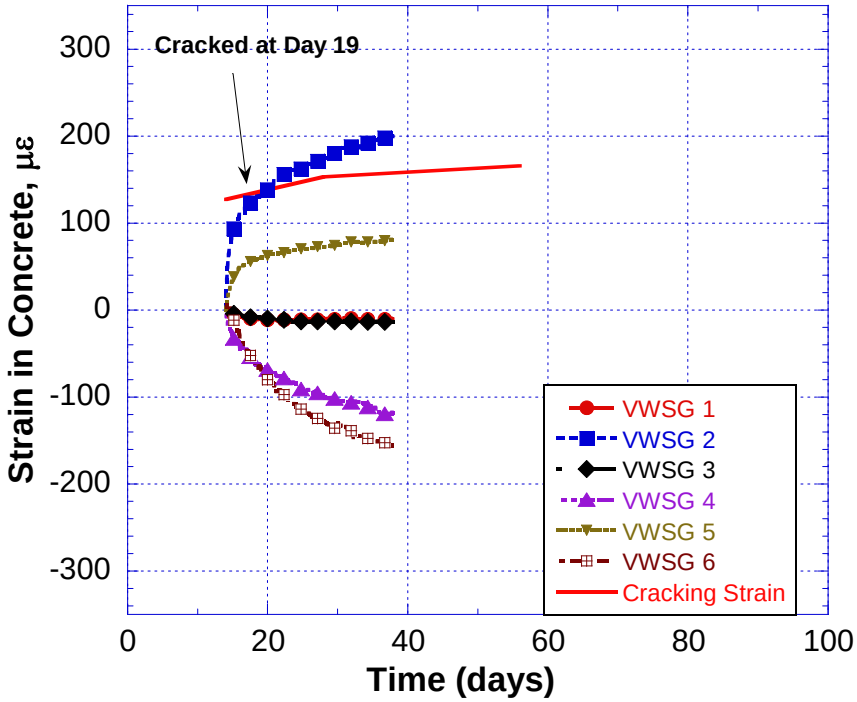

Figure 4-32 Concrete Strains for G2M1 Ring Specimen 1

At day 19 after casting, the shrinkage strain measured from VWSG 2 exceeds the cracking as shown in Figure 4-32. Meanwhile, foil gage 2 strain records displayed in Figure 4-33 shows a decrease in the compressive strain rate at day 20 after casting. In other words, the response of the rapid tensile strain rate and the crack formation at VWSG 2 region leads to a release in compressive strain recorded by FSG 2.

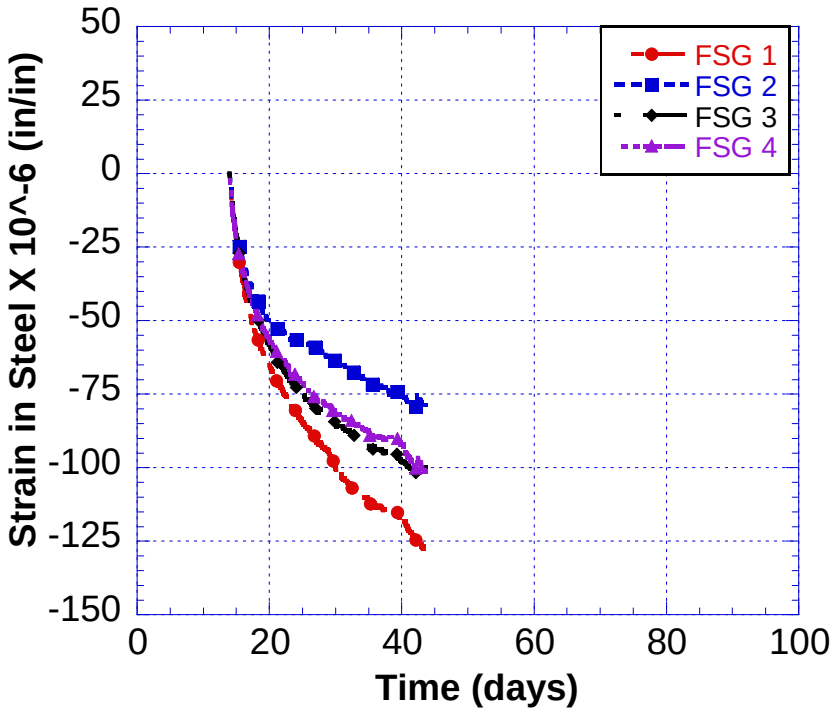

Figure 4-33 Steel Strains for G2M1 Ring Specimen 1

The first drying shrinkage crack observed on the ring specimen 1 of G1M2 at day 23 can be seen in Figure 4-34 at the region 2. This very first shrinkage crack at the top of region 2 is very short in length relative to the cracks formed at later ages or to the cracks at the other regions. Since this mix exhibited very extensive amount of cracking between the ages of 20 and 30, the VWSG's are not able to pick up this type of rapid crack formation at all the regions. This assumption is very likely to happen once the complexity of restrained shrinkage cracking is considered especially on a ring specimen where severe and rapid cracking occurs. Even so, the VWSG strain records point out the region where the first crack opening will occur, and thus provides insightful information along with the FSG sensors.

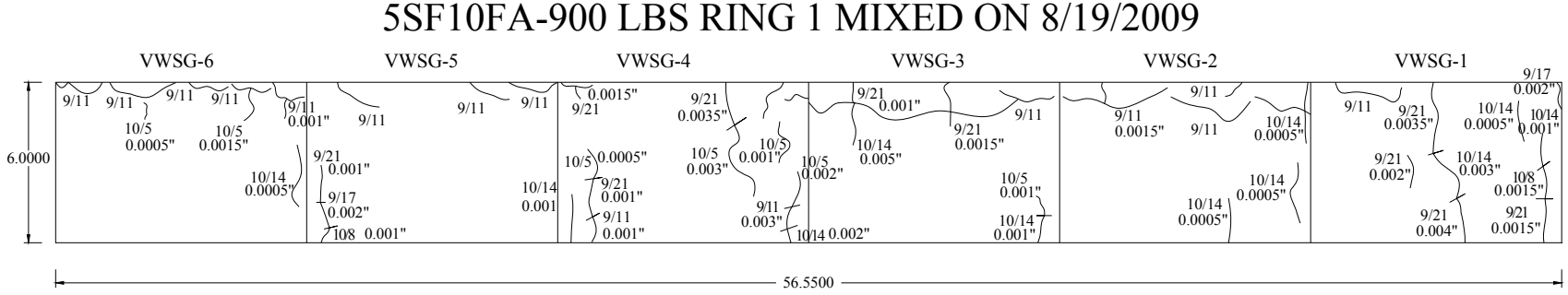

Figure 4-34 G2-M1 Crack Drawings for Ring Specimen 1, Side View (Top Figure) and Top-Bottom Views (Bottom Figure)

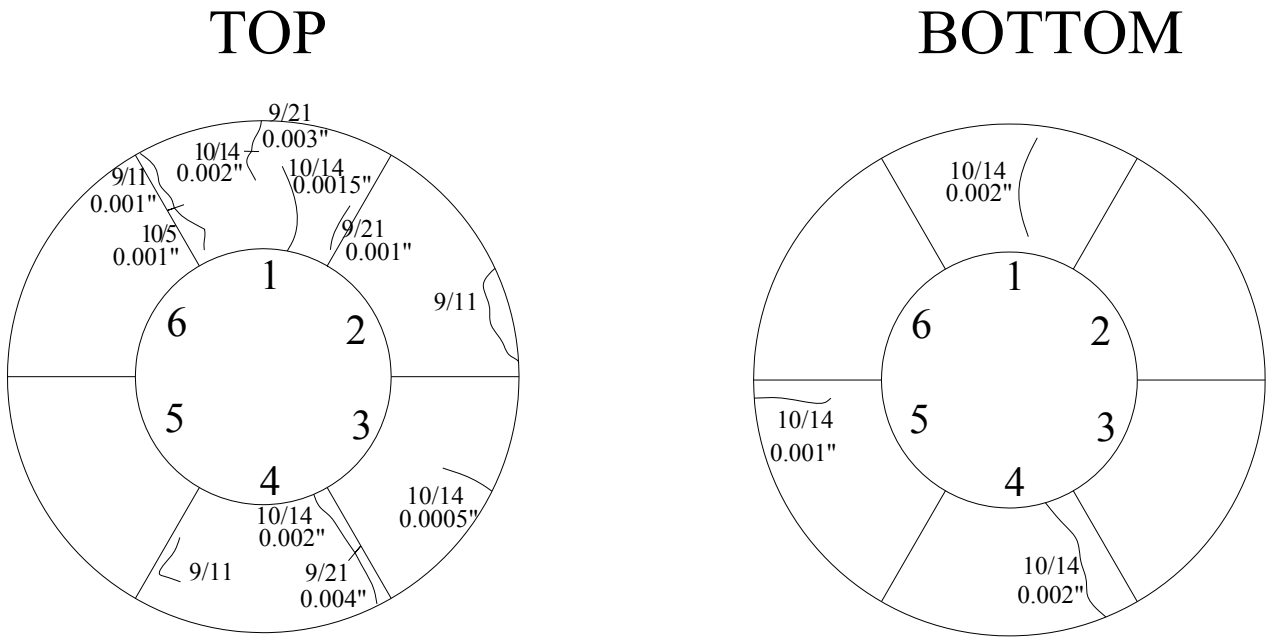

Figure 4-35 and Figure 4-36 illustrates the steel ring strain and restrained shrinkage cracking observations from the second ring specimen of G2M2. Similar to the first specimen of this mix, severe restrained shrinkage cracking was observed at all the regions of the specimen. The first crack on this specimen was observed at day 23 after cracking. This point of time corresponds to the decrease in the rate of compressive strain recorded by the foil gages. From Figure 4-35, it can be seen that all the foil gages started to record a lower rate of strain after passing day 25. There is a more clear strain rate decrease especially at foil gage 4. FSG 4 is located at the intersection of region 4 and 5 at where one of the severe shrinkage cracks formed.

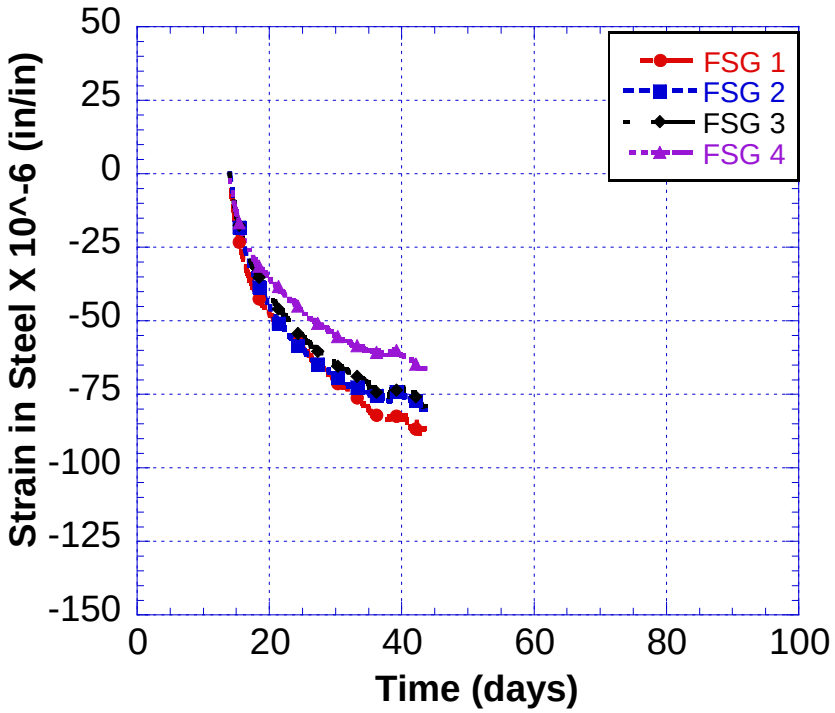

Figure 4-35 Steel Strains for G2M1 Ring Specimen 2

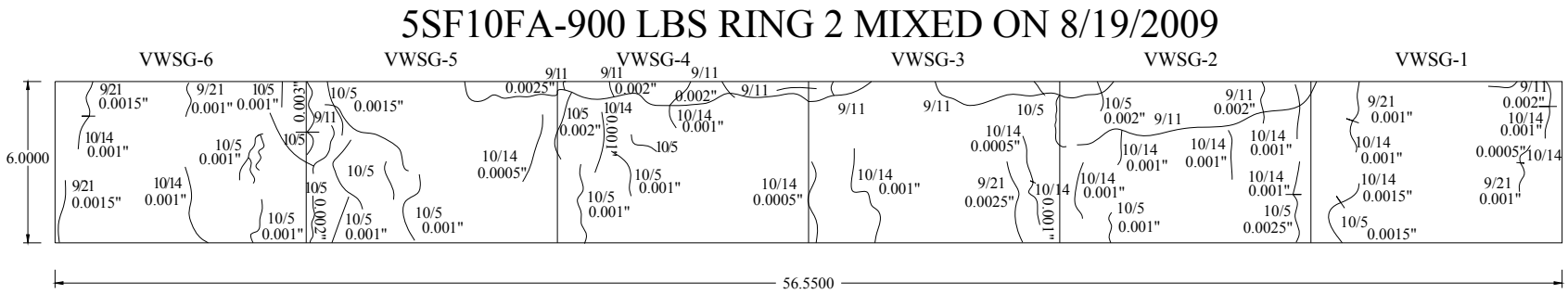

Figure 4-36 G2-M1 Crack Drawings for Ring Specimen 2, Side View (Top Figure) and Top-Bottom Views (Bottom Figure)

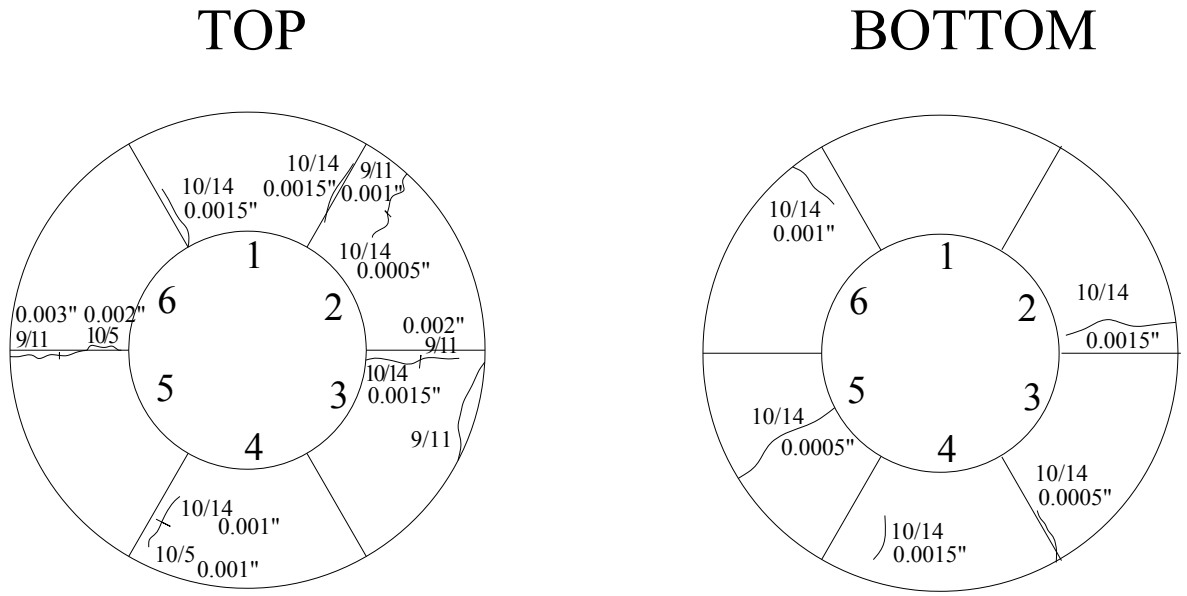

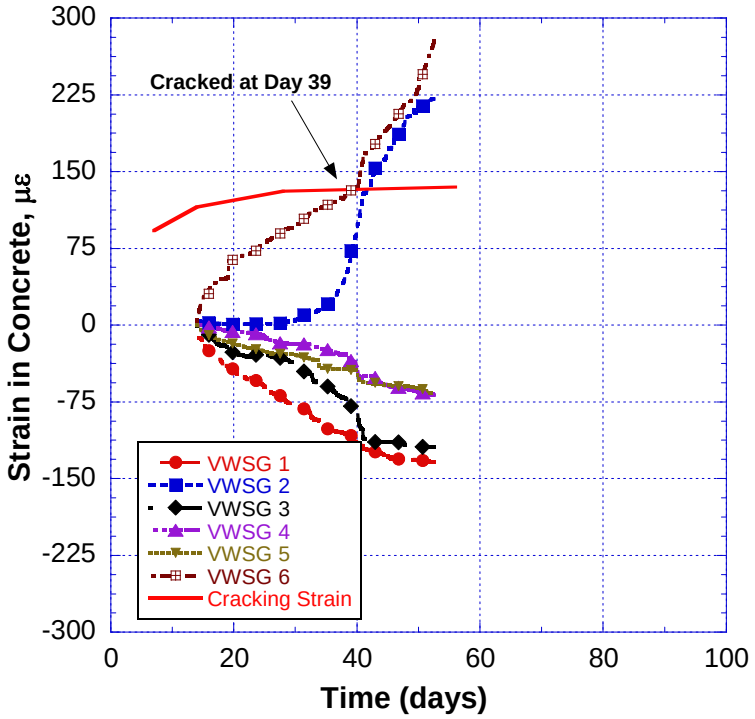

Figure 4-37 Concrete Strains for G2M3 Ring Specimen 1

Figure 4-37 shows the strain gage data measured from the concrete ring of G2M3 ring specimen 1. This mix is proportioned such that the 900lbs of total cementitious material consists %5SF, %30FA and %65 PC by weight. The concrete strain results show that the cracking strain level was reached by VWSG 6 at the age of 39 after casting. On the other hand, VWSG 2 data shows a very small rate of shrinkage in the first 25 days, and then very rapidly increases in tension and eventually exceeds the cracking strain of around day 40 after casting. The visual crack observations shown in Figure 4-38 confirms the drying shrinkage cracks recorded by WVSG 2 and VWSG 6. From Figure 4-38, we can see that drying shrinkage cracks were observed on day 41 and 36 days after casting at regions VWSG 6 and VWSG 2.

Figure 4-39 illustrates the drying shrinkage cracking pattern observed from the second ring specimen of G2M3.

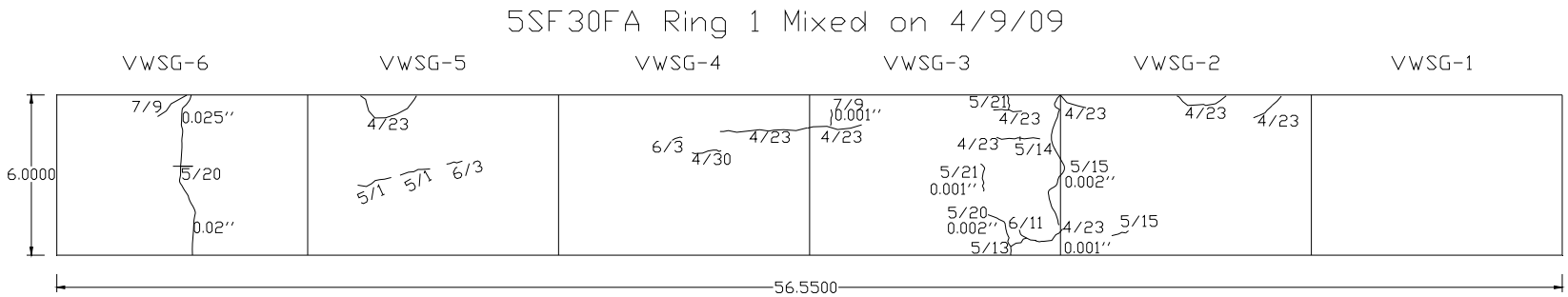

Figure 4-38 G2-M3 Crack Drawings for Ring Specimen 1, Side View (Top Figure) and Top-Bottom Views (Bottom Figure)

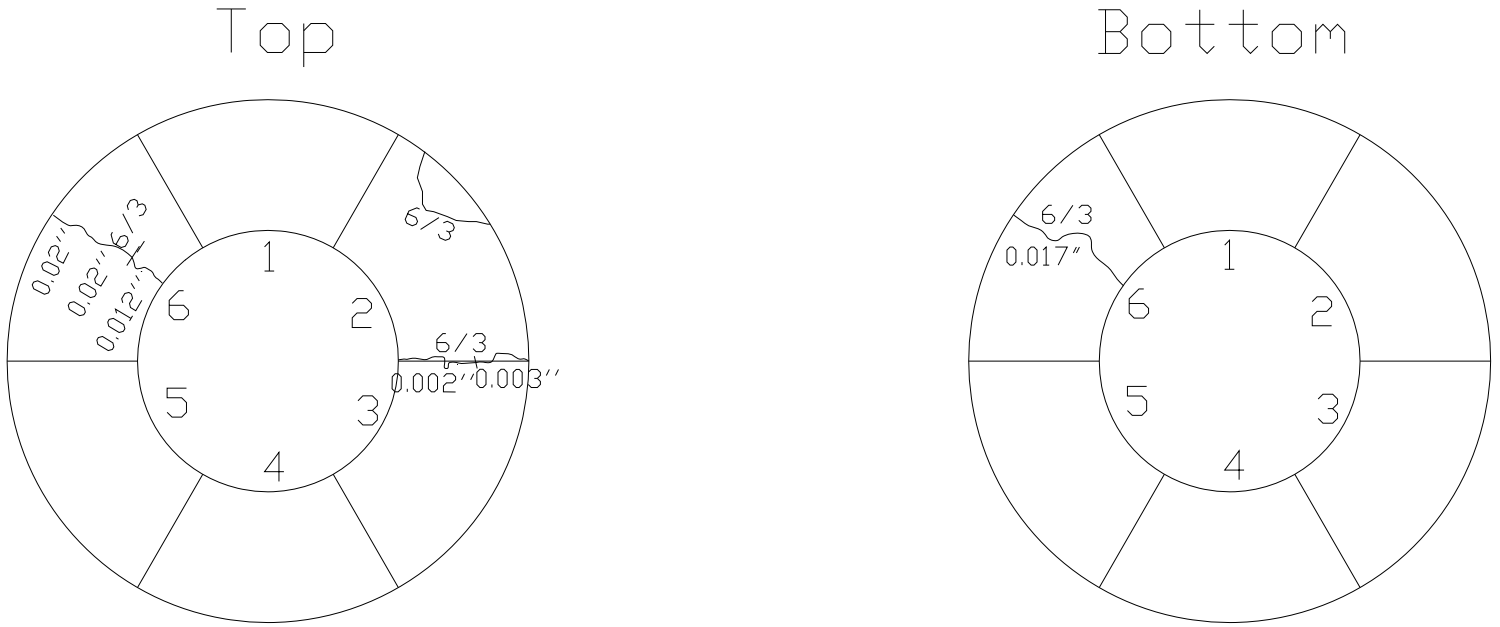

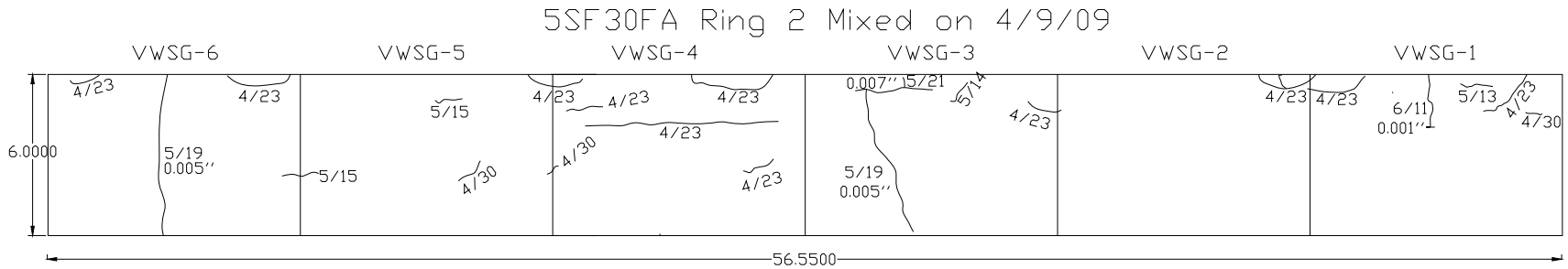

Figure 4-39 G2-M3 Crack Drawings for Ring Specimen 2, Side View (Top Figure) and Top-Bottom Views (Bottom Figure)

Figure 4-40 and Figure 4-41 shows the strain profile of 20FA with 850 pounds of cementitious material for both the concrete and the steel ring, respectively. VWSG data records in Figure 4-40 show that the cracking strain was exceeded at day 25 after cracking. The visual crack observations plotted in Figure 4-42 also follow this finding since there was an observed drying shrinkage crack at day 26 after casting where the VWSG 3 and VWSG 2 are connected.

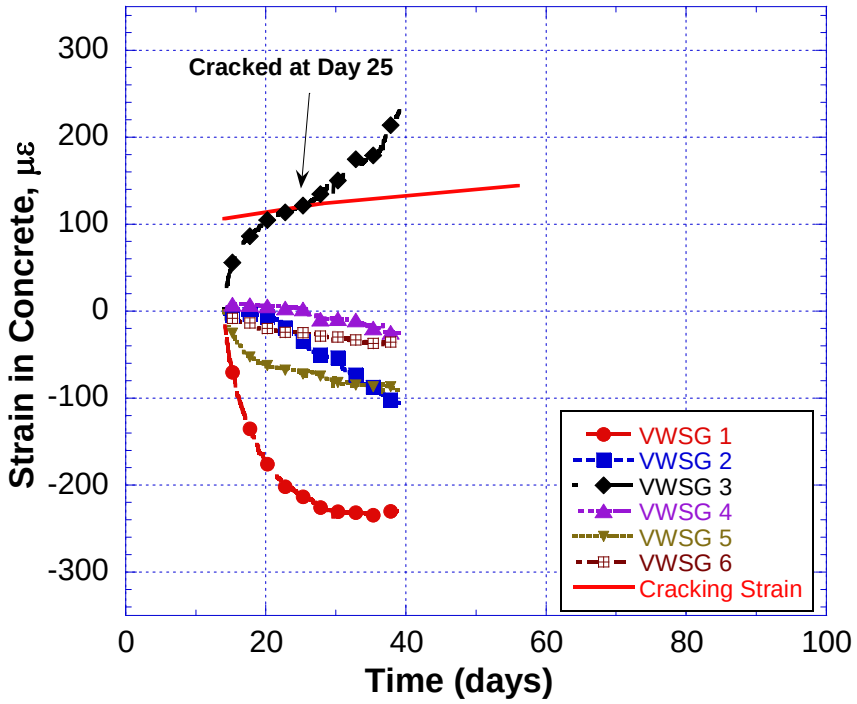

Figure 4-40 Concrete Strains for G3M1 Ring Specimen 1

From Figure 4-41, it can be seen that the FSG 2 starts to slow down in taking compression strain after day 25. Since the concrete at this region exerted tensile stresses, the compression captured by the foil gage 2 is relatively lower than the other foil gages. The bottom drawing in Figure 4-42 also confirms this since we can see cracks through the entire thickness off the casted concrete at region 2 and 3 intersection.

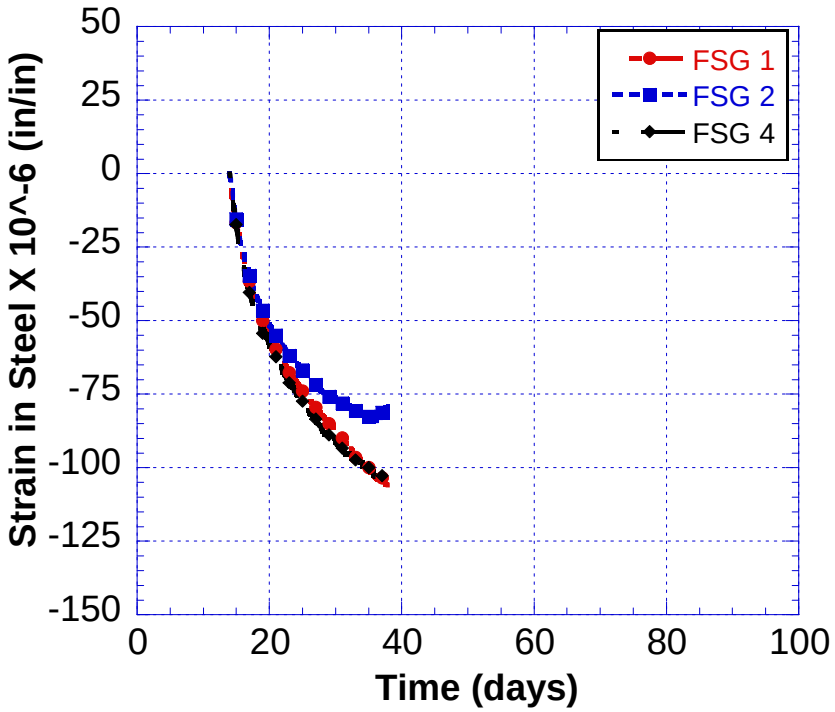

Figure 4-41 Steel Strains for G3M1 Ring Specimen 1

Figure 4-42 top drawing shows another crack where region 3 and 4 intersects. This drying shrinkage crack is at the region where the VWSG 3 and 4 is connected, and is also relatively wider than the other observations on the same ring specimen. Evaluating the concrete strain profile of this ring at VWSG 3, it can seen that this region is locally tensioned at both ends, thus has high a concrete strain level up to 230 micro strains at day 40 after casting. Moreover, the rate of shrinkage recorded by VWSG after the initial crack is relatively higher that the rate recorded before the initial crack. This can be resultant from wider crack openings occurring at the later ages of concrete ring specimen drying.

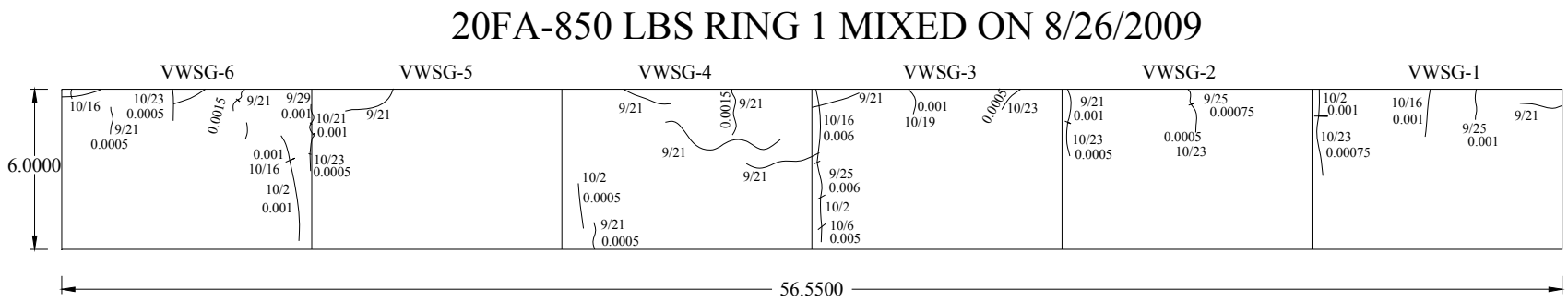

Figure 4-42 G3M1 Crack Drawings for Ring Specimen 1, Side View (Top Figure) and Top-Bottom Views (Bottom Figure)

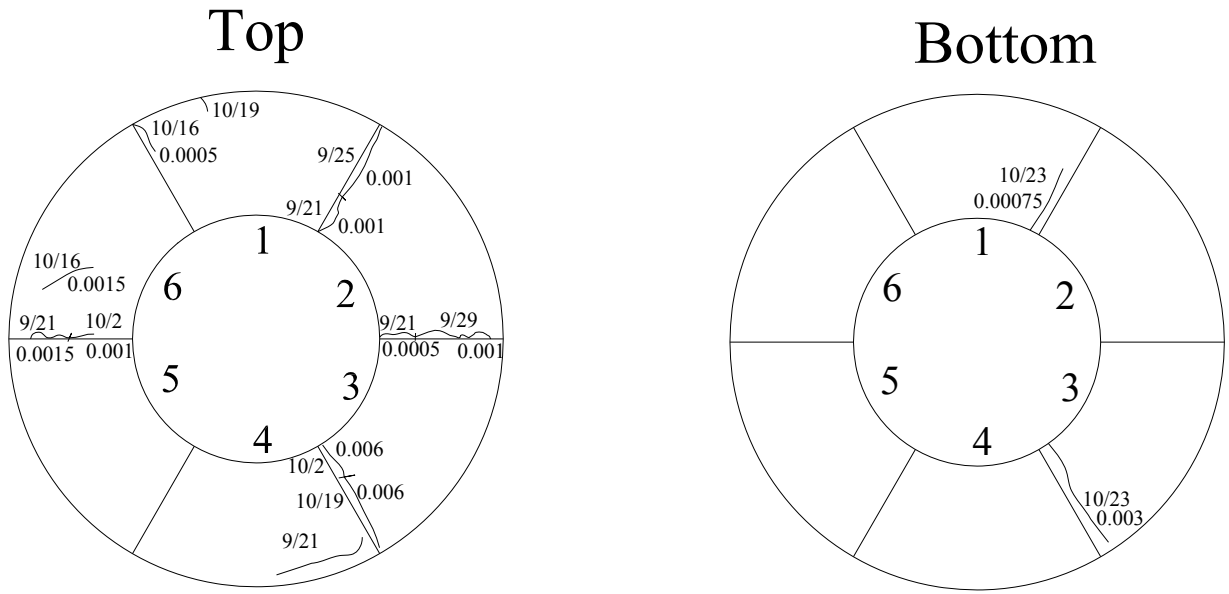

Figure 4-43 shows the steel ring strain profile recorded from the second specimen of 20FA with 850 pounds of cementitious material. This ring specimen experienced drying shrinkage cracking at day 30 after casting. Figure 4-44 shows the cracking pattern observed on this ring specimen. Steel ring strain profile in Figure 4-43 shows the starting of strain release in foil gages is approximately 3-5 days after the cracking is observed on day 30.

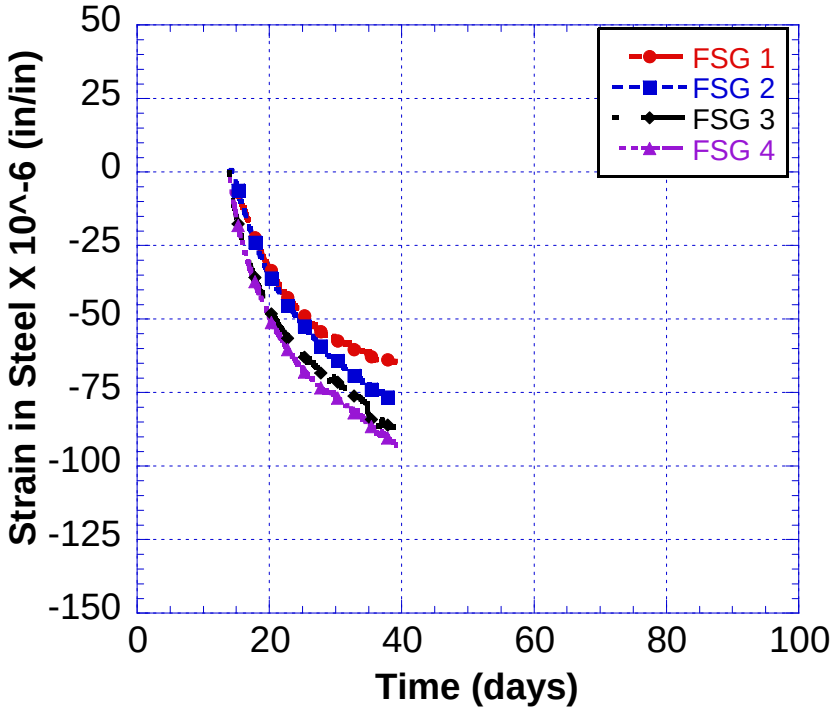

Figure 4-43 Steel Strains for G3M1 Ring Specimen 2

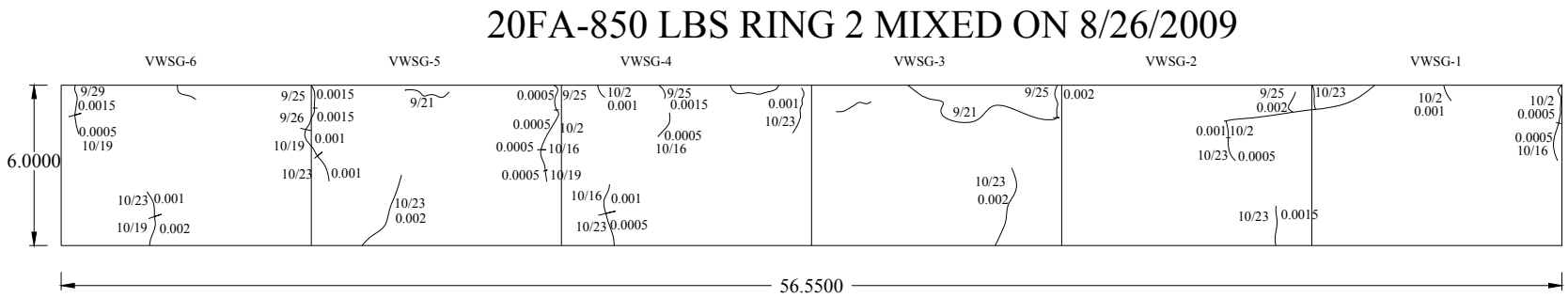

Figure 4-44 G3M1 Crack Drawings for Ring Specimen 1, Side View (Top Figure) and Top-Bottom Views (Bottom Figure)

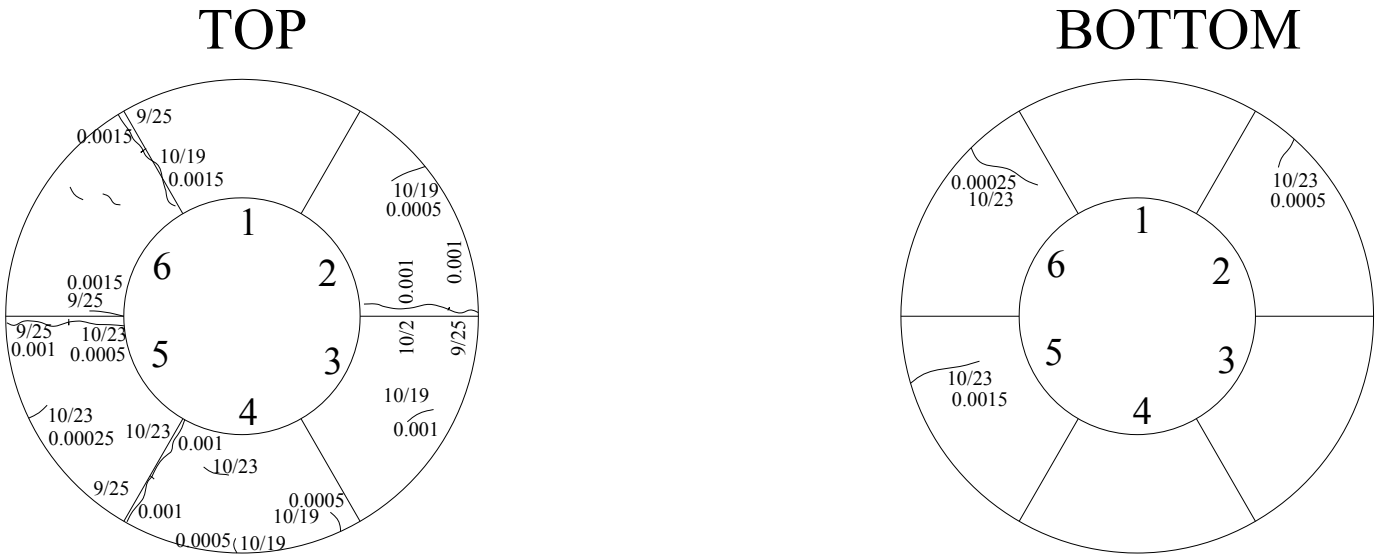

Figure 4-45 shows the concrete strain whereas Figure 4-46 shows the steel ring strain for G3M3 with 850 pounds of cementitious material. This mix has %10 silica fume by weight as a replacement of Portland cement. Although the maximum tensile strain observed on the Figure 4-45 is not exceeding the cracking strain, drying shrinkage cracks were observed on this ring specimen at day 27 after casting. Figure 4-47 represents the cracking pattern observed on this ring specimen.

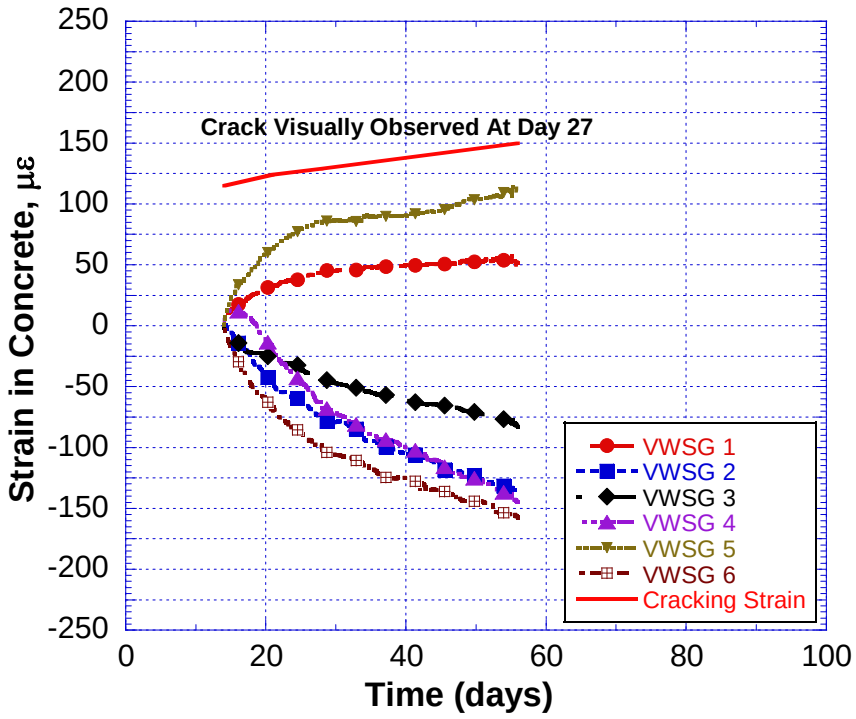

Figure 4-45 Concrete Strains for G3M3 Ring Specimen 1

While the VWSG concrete strain data is not showing the level of strain to initiate a crack, it is in fact pointing out the region of first cracking that occurs on this ring specimen. It can be seen from Figure 4-47 that this ring specimen started to crack at day 27 after casting at the region where the VWSG 5 is located. The initial cracks on this

region is relatively short in length on the side and on the top surface of the ring, though, there are very long and clear horizontal cracks on the following days at the same region.

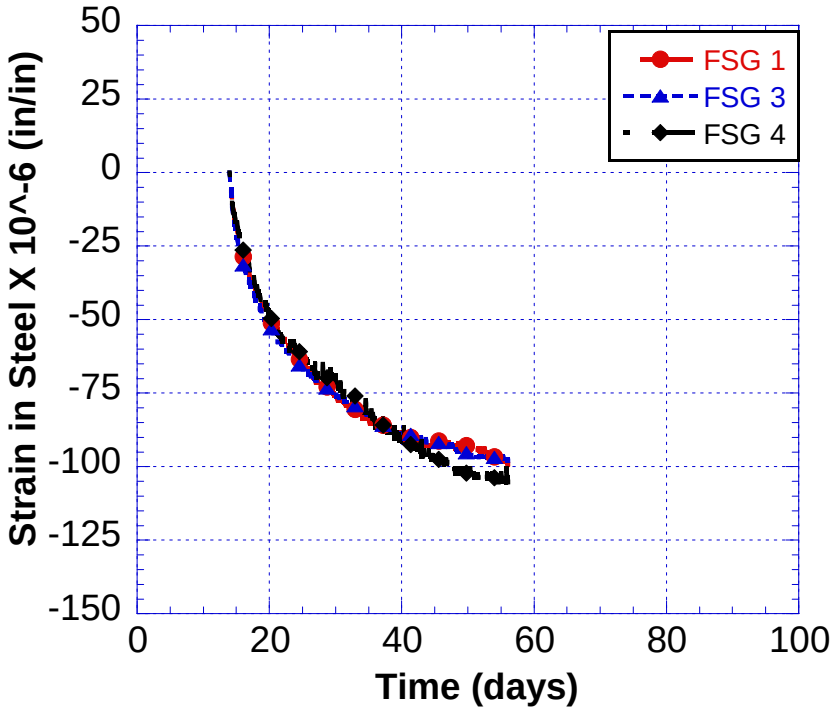

Figure 4-46 Steel Strains for G3M3 Ring Specimen 1

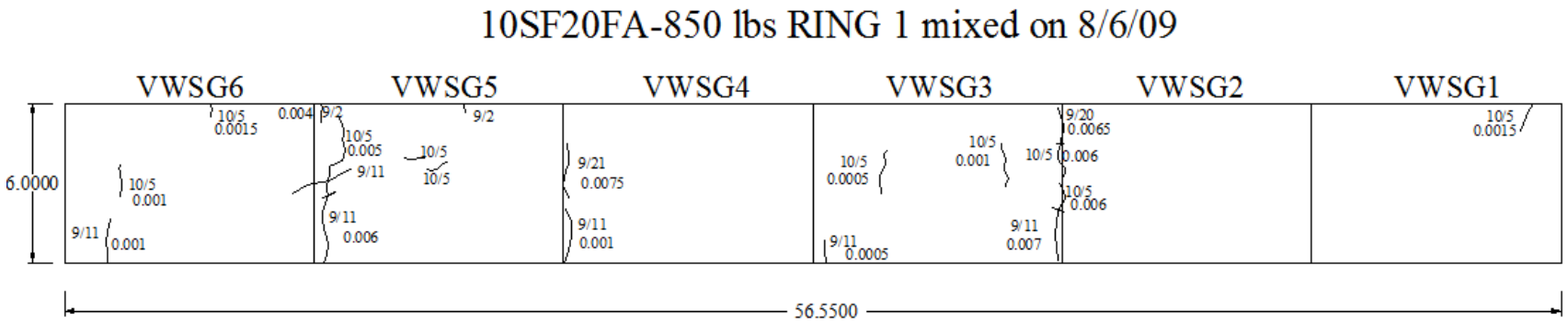

Figure 4-47 G3-M3 Crack Drawings for Ring Specimen 1, Side View (Top Figure) and Top-Bottom Views (Bottom Figure)

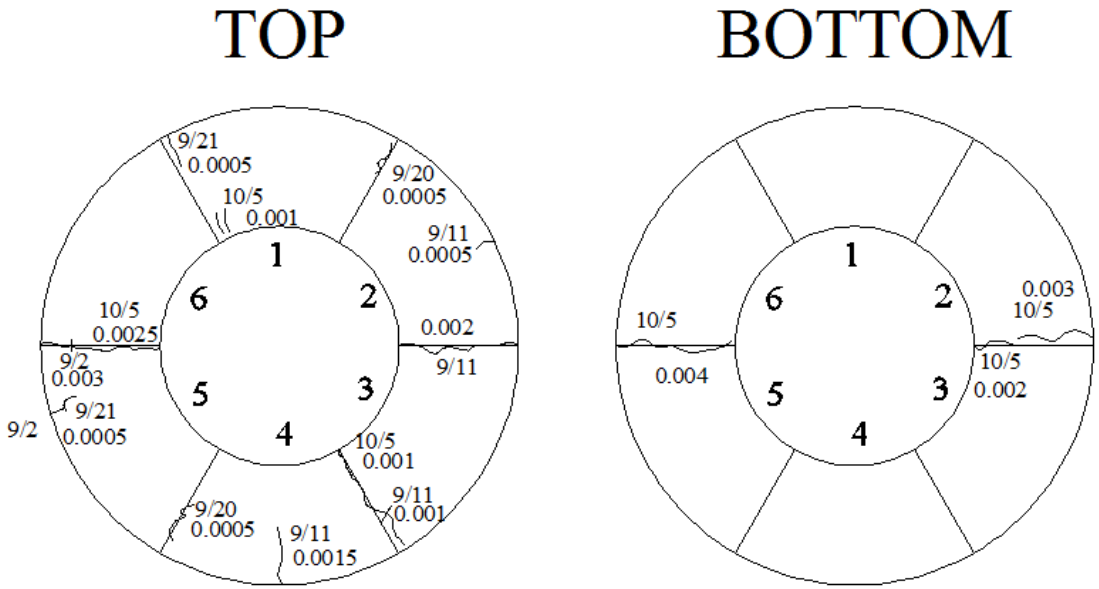

G3M3 second ring specimen strain profiles are presented in Figure 4-48 and Figure 4-49 for the concrete and the steel ring, respectively. Similar behavior of VWSG gages are observed at this specimen, where the maximum tensile being almost at the level of cracking strain but not exceeding the limit at the age when the initial cracking was visually observed. The area of initial crack observation was again confirmed by the VWSG strain data. After the earlier cracks at region 2, many other drying shrinkage cracks were observed on this ring specimen. It can be seen from Figure 4-48 that the VWSG 6 reaches the strain magnitude level of VWSG 2 approximately at day 40. At this point, where VWSG 2 tensile strain overtakes the VWSG 6 tensile strain, drying shrinkage cracks are observed at region 6. The VWSG 6 strain profile plotted in Figure 4-48 indicates that the tensile strain record exceeds the cracking strain at later at day 51.

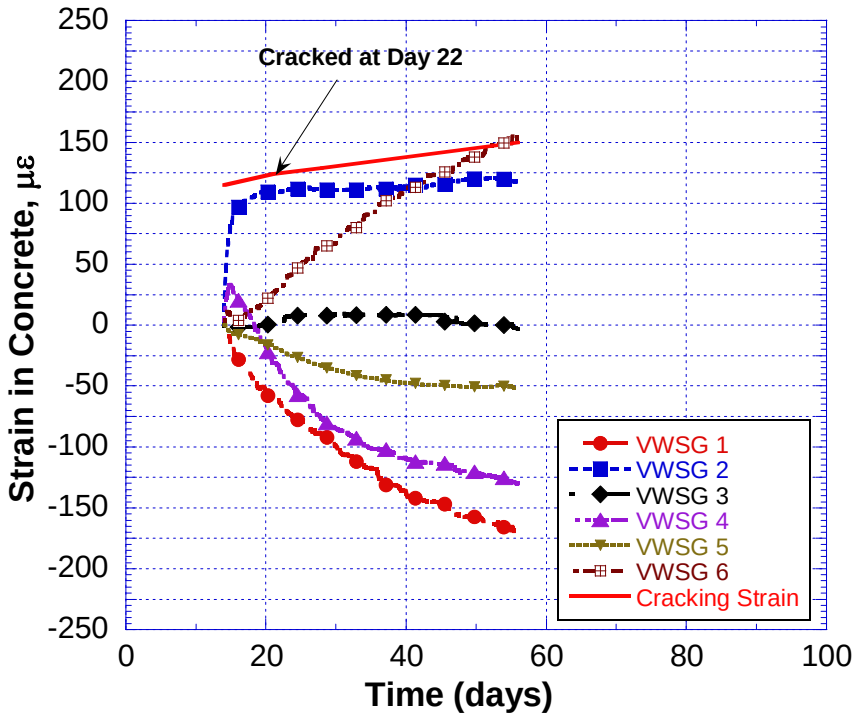

Figure 4-48 Concrete Strains for G3M3 Ring Specimen 2

The reason for the mixture G3M3 exhibiting drying shrinkage cracking, yet the concrete strain gages not exceeding the cracking strain can be due to the residual strains left-over from the curing period. Since this mix has %10 silica fume as a part of total cementitious material in its design, and also has high amount of total cementitious material, it is likely to go under high levels of autogenous shrinkage.

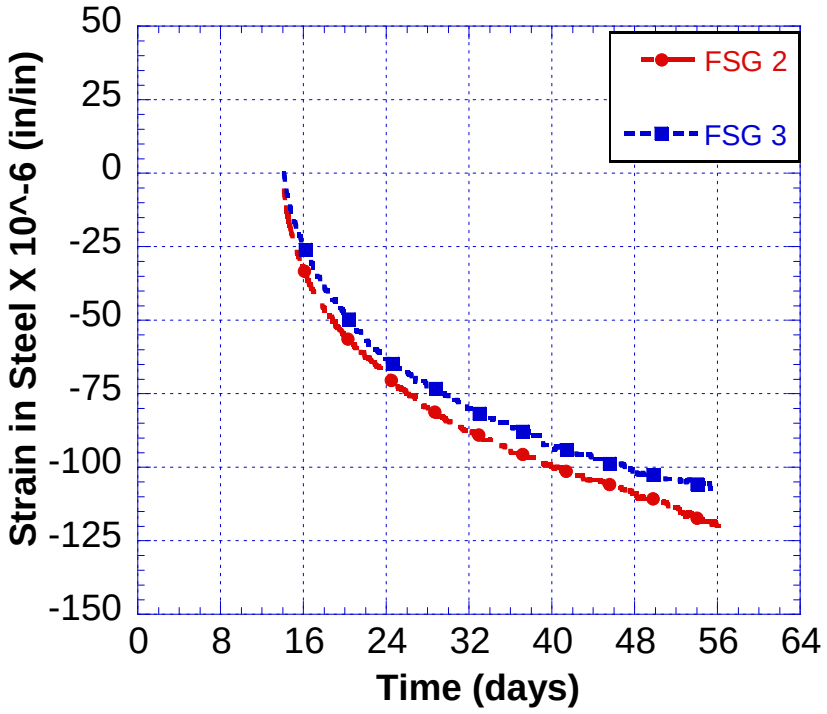

Figure 4-49 Steel Strains for G3M3 Ring Specimen 2

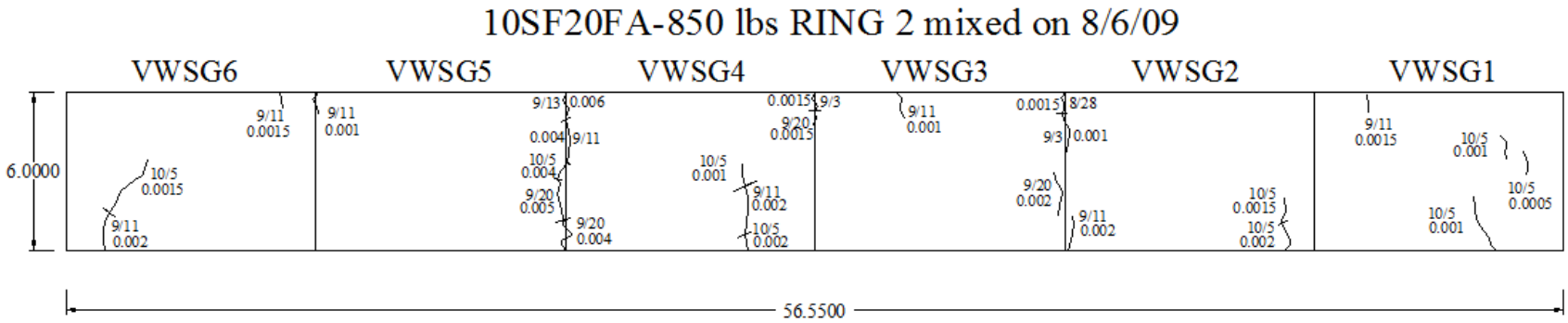

Figure 4-50 G3-M3 Crack Drawings for Ring Specimen 2, Side View (Top Figure) and Top-Bottom Views (Bottom Figure)

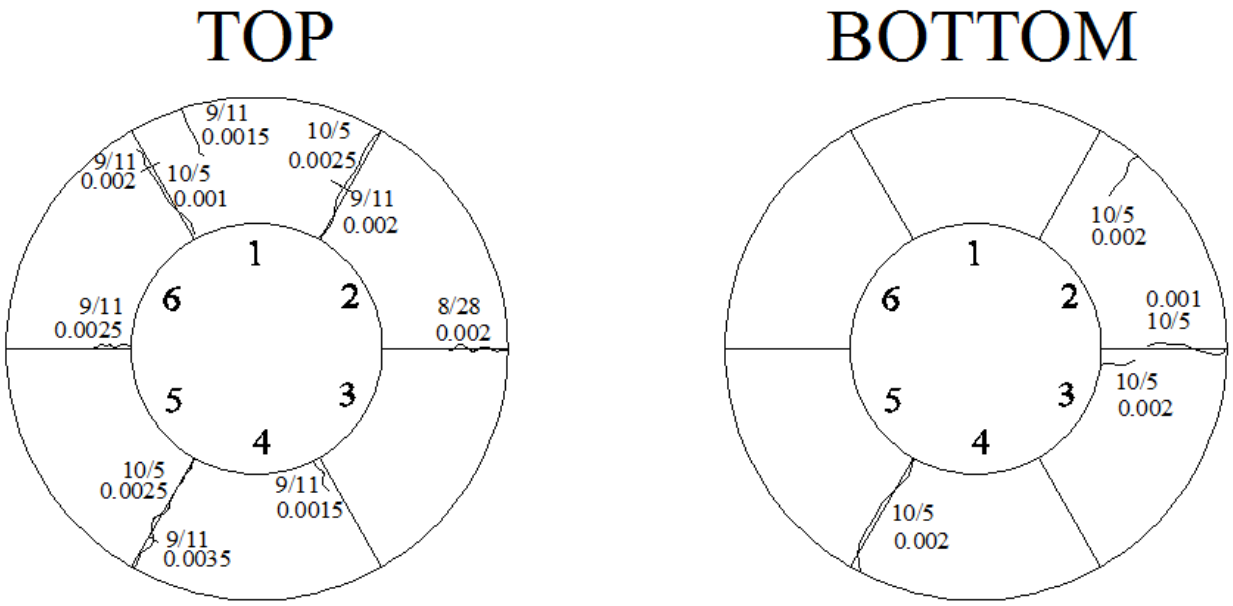

Table 4-14 includes the calculated restrained shrinkage cracking areas from the ring specimens of all casted SCC mixes. The total cracked area calculations were performed within the first week after day 56 to provide comparable levels cracking areas for all the mixes. The average crack width measured with microscope was multiplied with the length for each individual restrained shrinkage crack. After the total cracked area on each ring specimen was found out, the cracked area of each mix was calculated by averaging the 2 specimen of each mix.

Table 4-14 Summary of Restrained Shrinkage Cracking Areas for All Mixes

Mix	Restraint Shrinkage Cracking Area (in^2)			Total Cemt. (lbs/cu yd)	% FA Repl.	% SF Repl.
	Ring 1	Ring 2	Average			
G1-M1	0.047	0.039	0.043	800	20%	5%
G1-M2	0.095	0.102	0.106	850	20%	5%
G1-M3	0.252	0.196	0.224	900	20%	5%
G2-M1	0.125	0.141	0.133	900	10%	5%
G2-M3	-	0.096	0.096	900	30%	5%
G3-M1	0.093	0.060	0.077	850	20%	0%
G3-M3	0.143	0.108	0.126	850	20%	10%

From Table 4-14, we can see that the largest cracking area on the average of 2 ring specimen was observed at G1M3. This mix has 900 pounds of cementitious material and has only 20 % fly ash replacement. G1M3 performed considerably worse than the rest of the SCC mixes, since it exhibited very early cracking along with the highest free shrinkage. Also, both of the rings from this mix exhibited cracks that propagated towards the steel ring along the entire height of the specimen. The second largest cracking area was observed at G2M1 which had 900 pounds of cementitious material with only 10% fly

ash replacement. The lowest cracking area was calculated on the G1M1 ring specimens, where only 800 pounds of total cementitious material was used.

Table 4-15 lists the restrained shrinkage cracking ages for all the SCC mixes. For each mix, the age of the observed cracking for each specimen is listed, and then the 2 ring specimens are averaged to provide a single cracking age for each mix.

Table 4-15 Comparison of Observed Cracking Ages for SCC Mixes

MIX	Cracking Day			Total Cemt. (lbs/cu yd)	% FA Repl.	% SF Repl.
	Ring 1	Ring 2	Average			
G1-M1	27	31	29	800	20%	5%
G1-M2	20	21	20.5	850	20%	5%
G1-M3	20	19	19.5	900	20%	5%
G2-M1	23	23	23	900	10%	5%
G2-M3	36	40	38	900	30%	5%
G3-M1	26	30	28	850	20%	0%
G3-M3	27	22	24.5	850	20%	10%

All the SCC mixes in this study cracked before day 56, all the cracks were observed between day 19.5 and 29 with the exception of G2M3. The changes in the pozzolanic replacement materials influenced the cracking time up to a certain limit. Since all the SCC mixes had very high amounts of cementitious material, they all eventually experienced cracking. The difference between the 0% silica fume mix and 10% silica fume mix in terms of initial cracking was found to be 3.5 days on the average of 2 rings. This slight difference corresponds with the slight difference in the free shrinkage of these 2 mixes. The comparison of G1M1 versus G1M3 in terms of initial cracking age yielded a difference of 9.5 days. Although the shrinkage rate of G1M3 is affected by the adverse effect of low modulus of elasticity, the effect of increased cementitious material is still

substantial since the cracking age is decreases by 9.5 days with the additional 100 pounds of cementitious material.

G2M1 with 10% fly ash exhibited cracking at day 23 while G1M3 with 30% exhibited cracking at day 38. The large difference between the cracking ages of these mixes can be attributed to the fly ash replacement percentage. On the other hand, shrinkage performances of these 2 mixes were very similar. G2M1 had slightly higher shrinkage at day 28, whereas the free shrinkage level was almost the same by day 56. So the effect of fly ash replacement was found to be significant under restrained conditions, whereas almost no difference was found for free shrinkage.

4.6 COMPARASION OF FREE AND RESTRAINED SHRINKAGE RATES OF SCC MIXES

In this section, the shrinkage cracking of the SCC mixes under restrained conditions is evaluated along with their free shrinkage performance. Although the mechanical properties of the concrete and the test specimen geometry are very important in restrained shrinkage, free shrinkage can be used as a good indicator to assess the cracking potential. In this sense, the approach that Aktas (2007) and Montemerano (2008) used was adopted to evaluate how far the 2 different shrinkage types correlate to each other. According to this approach, the AASHTO ring test results, and the free shrinkage measurements are proportional to the logarithm of time. Thus, if the restrained and free shrinkage strains of the mixes are evaluated on a logarithmic time scale, a slope for each equation can be derived and used to asses a relationship between the two shrinkage types.

To understand this relationship, the restrained and free shrinkage rate of each SCC mix was derived as illustrated in Figure 4-51a, and then the relationship between the shrinkage types was illustrated on the same graph shown in Figure 4-51b.

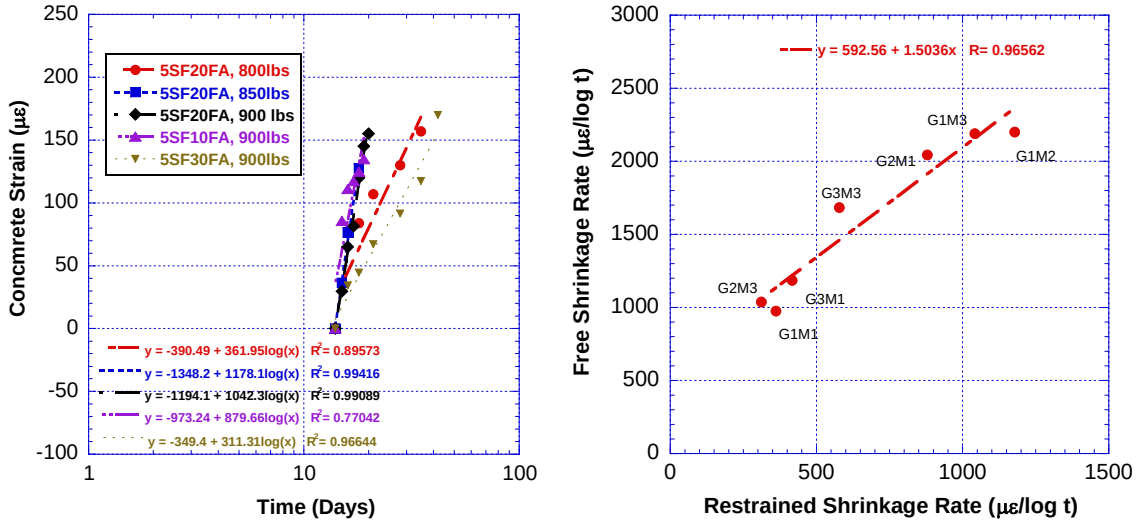

(a) (b)

Figure 4-51 a) Derivation of Shrinkage Rate vs. Logarithm of Time b) Comparison of Free and Restrained Shrinkage Rates

Once the slope of each SCC mix in free and restrained shrinkage, which is derived from the shrinkage rates on the logarithm of time scale, is plotted on the same graph, the free and restrained shrinkage rates of the mixes can be compared to each other. From Figure 4-51b, we can see that G1M2 and G1M3 have the highest potential to exhibit both restrained and free shrinkage since they had the highest rates. Following these mixes, G2M1 had the highest potential to exhibit high shrinkage since it has the lowest amount of fly ash replacement percentage along with 900 pounds of total cementitious material content.

Since all the SCC mixes cracked under restrained conditions, it is not possible to relate to free shrinkage rate to cracking occurrence or non-occurrence. But even with all the mixes cracked, the correlation in Figure 4-51b is found out to be suitable while interpreting restrained shrinkage behavior from the free shrinkage performance.

Another comparison between the free and restrained shrinkage was done by plotting the measured free shrinkage strain until the cracking day for each mix versus the measured restrained shrinkage ring strains on a linear scale. This type of relationship is illustrated in Figure 4-52 for all the SCC mixes together.

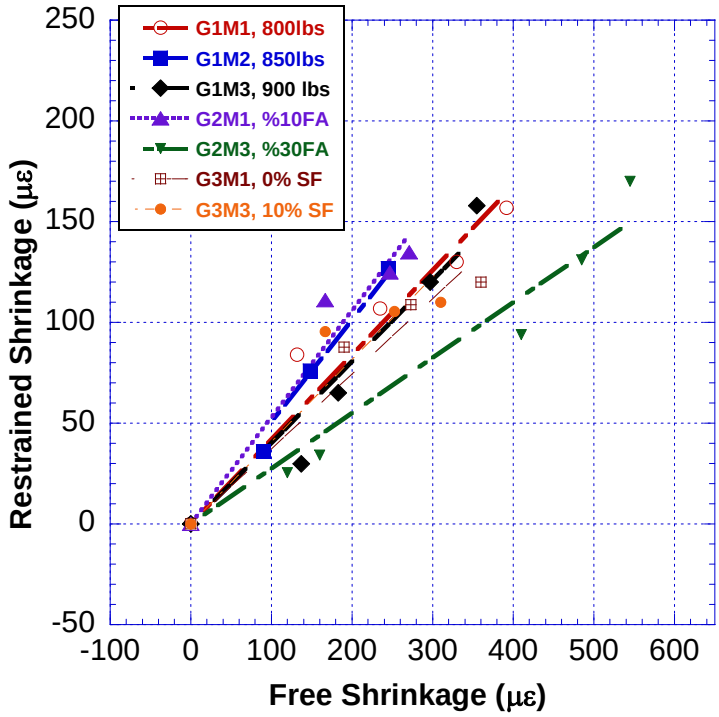

Figure 4-52 Restrained Shrinkage Strain vs. Free Shrinkage

As the free and restrained shrinkage is plotted versus each other, the slope of the function for each fit can be assumed as a correlation factor between restrained and free shrinkage. The correlation value can be used as a measure of the cracking performance for the SCC mixes, moreover, it can be used to relate the cracking performance to other

mechanical properties. In this sense, the correlation factor, denoted as α, is plotted versus the average daily free shrinkage strain of each in Figure 4-53.

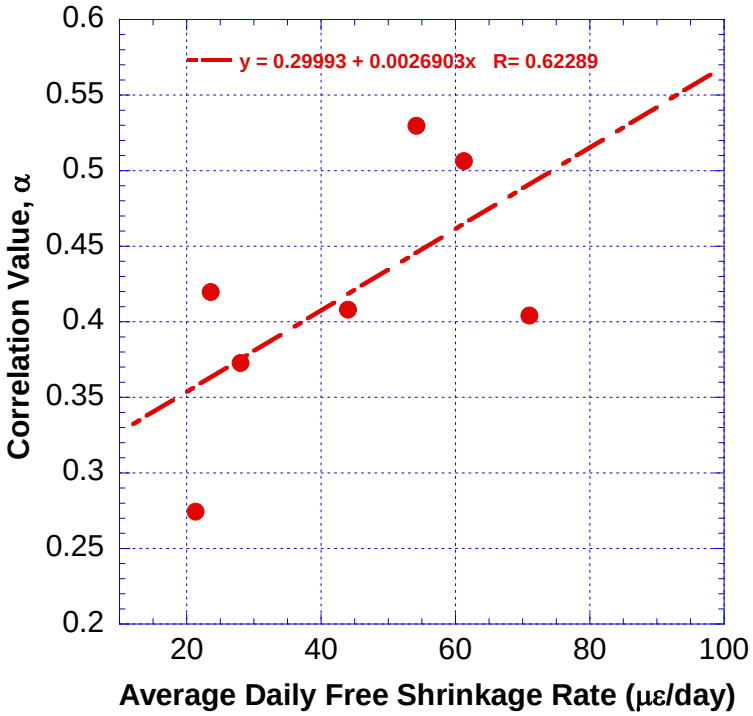

Figure 4-53 Correlation Parameter vs. Average Daily Free Shrinkage Strain

4.7 CORRELATION OF RESTRAINED SHRINKAGE CRACKING WITH POZZOLANIC MATERIAL REPLACEMENT AMOUNT

The effect of pozzolanic material use in the SCC batches is evaluated by comparing the correlation factors that are already derived in the previous sections. Fly ash and silica fume were used as pozzolans for the SCC mixes produced in this study. While evaluating the effect of pozzolanic materials, the replacement percentage with respect to the total cementitious material content is used. In other words, a replacement of 20% means substituting 20% of the total cementitious material content by the pozzolanic material in terms of weight.

Since different ranges of fly ash replacement are used throughout the concrete industry, a correlation with a wider range of fly ash replacement is important. For silica fume, on the other side, the commonly used replacement percentage varies only between 0% and 10%.

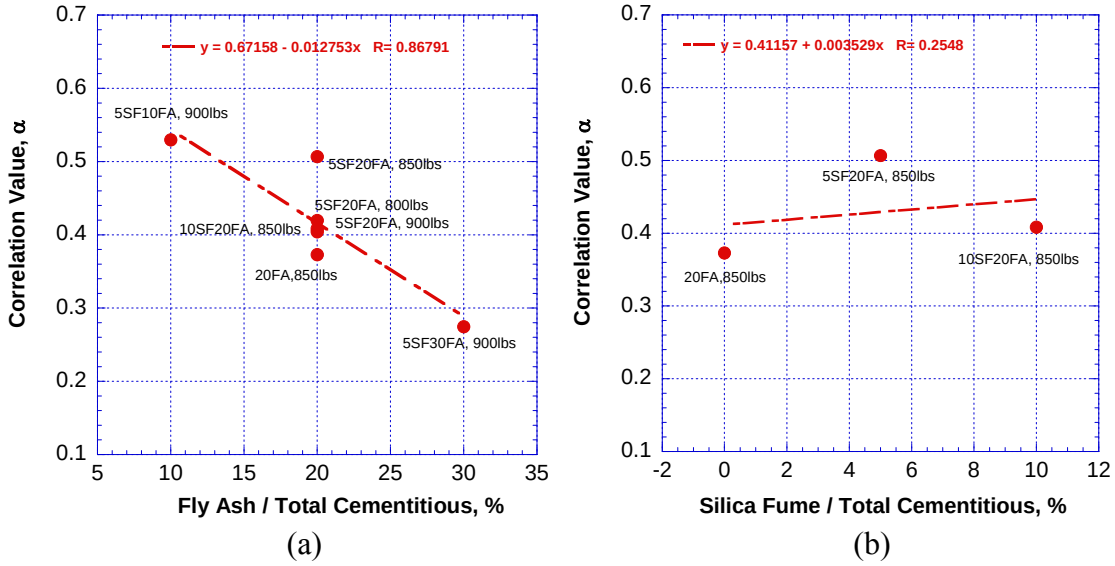

Figure 4-54 Pozzolanic Material Replacement Percents vs. Correlation Factor

Figure 4-54a and Figure 4-54b shows the change in the correlation value with both fly ash and silica fume replacement, respectively. Three dominant regions can be observed by looking at Figure 4-54a while evaluating the effect of fly ash replacement. The mixes with the highest and lowest fly ash replacements, 5SF30FA and 5SF10FA, distinct from the other mixes clearly. These mixes had 15 days of difference in the elapsed time until cracking. On the other side, all the other mixes having 20% fly ash replacement had slight to moderate variations for the correlation value and cracking time. The range of cracking age among all the 20% fly ash mixes was found to be between 19.5 and 29, with an average of 24. At this region where the replacement is 20%, the variations between the mixes are also influenced by the effect of silica fume replacement

percentage, cementitious material content, and even more significantly by the modulus of elasticity. In spite of the additional influencing factors, the observed trend shows that using high percents fly ash replacement has potential in increasing the elapsed time until cracking under restrained conditions.

Figure 4-54b illustrates the effect of silica fume replacement in changing the correlation factor, thus the cracking performance. The evaluation of silica fume influence was done within the group 3 mixes only, where the total cementitious material content is kept at 850 pounds and replacement percentage varies between 0 and 10. This range is widely used in the industry and the concrete research area. As shown in Figure 4-54b, 5SF20FA with 5% SF replacement has the highest correlation value among the 3 group mixes. Although there is an increasing trend between 0% and 10% SF replacement in terms of cracking age, the 5% SF mix does not follow the trend, thus results an insignificant correlation as shown in Figure 4-54b. This can be due to differences in the aggregate source at the time of mixing, as well as the differences in the fluidity levels in the group mixes. Since this mix was included at the later ages of the research, a different source of aggregate was used with slightly different properties. Thus, this mix is considered to be an outlier in group 3 where the effect of silica fume amount on cracking is evaluated. If the other 2 group 3 mixes are compared, we can see that 20FA had a slightly better cracking performance compared to 10SF20FA. When the earliest shrinkage cracks from 20FA and 10SF20FA is compared, the elapsed time until cracking is found to be decreasing by 3.5 days with the incorporation of 10% silica fume. Meantime, the differences in the free shrinkage strain between these 2 mixes are found to be 10% at day 56. So, by comparing 0% and 10% SF replacement, it can be concluded

that increasing the silica fume replacement in the mix design mitigated both free and restrained shrinkage performance, but not very significantly.

4.8 FREE SHRINKAGE PERFORMANCE OF SCC RELATIVE TO SELECTED HPC MIXES

For the sake of providing a basic evaluation between the free shrinkage performance of SCC and HPC, representative mixes were selected from Aktas (2007) and Montemerano (2008), and compared to the casted SCC mixes. The characteristic mix design parameters of the selected HPC mixes are summarized in Table 4-16. Among the selected HPC mixes, the main parameters that were investigated by Aktas (2007) and Montemerano (2008) were course aggregate to fine aggregate ratio (CA\FA), the amount of slag replacement, and the amount of total cementitious material. These parameters are briefly summarized in Table 4-16.

Figure 4-55 illustrates all the free shrinkage measurements from the selected HPC mixes and the SCC mixes from this study as well. From this figure, we can see that SCC and HPC mixes distinguish clearly in terms of free shrinkage strain. At day 56, free shrinkage measurements of HPC mixes fall in a range of 303 and 693 micro strains, whereas this range is between 495 and 830 micro strains for the SCC mixes. In other words, the lower bound of SCC free shrinkage strain measurements are 63% higher than that of HPC mixes, where as the upper bound is 20% higher.

The main reason for SCC mixes exhibiting higher shrinkage values than the HPC mixes can be attributed to the high cementitious content. The selected HPC mixes had a maximum of 707 pounds cementitious material, whereas 6 of 7 SCC mixes presented in this study had 850 or 900 pounds of cementitious material. Two other dominant factors

creating the poor free shrinkage performance of SCC can be shown as the size of the coarse aggregate and the sand to total aggregate ratio. SCC mixes were produced using 3/8" crushed stone whereas larger aggregate sizes such as ¾" were used for HPC mixes. Also, due to the workability demand on SCC, an increased sand volume was used in the SCC mix designs. Same amount of coarse and fine aggregate was used for the SCC mix proportions presented in this thesis. On the other hand, HPC mixes were proportioned using higher volumes of coarse aggregate than fine aggregate. The contributory effect of increasing the CA/FA ratio was found out by Aktas (2007) and Montemerano (2008).

The comparison of SCC and HPC in terms of free shrinkage performance clearly points out the need for more SCC research for refining the SCC mix designs. The lower bound of HPC free shrinkage strain being significantly less than that of SCC shows that HPC mixes have been well designed such that they either did not crack or cracked at very later ages under restrained conditions. In the case of SCC, all the mixes presented here cracked, thus the lower bound has a larger difference than the upper bound when HPC and SCC free shrinkage strain is compared.

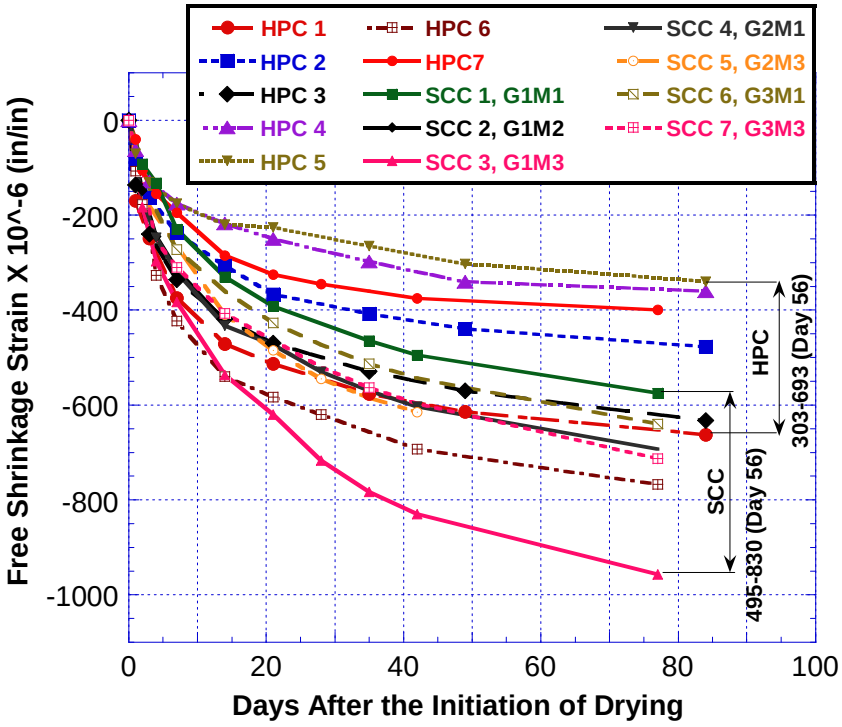

Figure 4-55 Free Shrinkage Strain of SCC and Selected HPC Mixes

Table 4-16 Selected HPC Mixes from Aktas (2007) and Montemerano (2008)

DESIGN PARAMETER	HPC 1	HPC 2	HPC 3	HPC 4	HPC 5	HPC 6	HPC 8
SF Replacement, %	0	0	4%	4%	7%	4%	4%
Slag Replacement, %	40%	40%	30%	30%	37%	30%	30%
Total Cement. Amount, lbs	658	660	658	657	707	700	600
CA/FA	1.42	1.57	31.1	31.5	1.48	1.32	1.6
W/C	0.4	0.4	0.4	0.4	0.37	0.4	0.4
Free Shrinkage, Day 56, μ	-614	-440	-570	-340	-303	-693	-375

Since all the SCC mixes presented herein exhibited cracking, it is not possible to define a limit of free shrinkage strain to control cracking. For instance, Aktas (2007) had found out that if the free shrinkage strain is less day 450 micro strains, the mix will not crack under restrained conditions. Such findings from Aktas (2007) are shown in Table 4-17.

Table 4-17 Comparison of Free Shrinkage and Cracking Ages, Aktas (2007)

	G1M3	**G2M3**	**G3M2**	**G4M1**	**G4M3**	**G4M4**
Cracking Day	N/A	N/A	N/A	N/A	N/A	60
56 day Free Shrinkage (με)	-440	-340	-383	-365	-303	-336

Since the mixes exhibiting free shrinkage strain under 450 micro strains did not crack, Aktas (2007) correlates this limit with the restrained shrinkage cracking potential. Table 4-18 shows a similar approach for the SCC mixes studied in this research.

Table 4-18 Comparison of Free Shrinkage and Cracking Ages for SCC Mixes

	G1M1	**G1M2**	**G1M3**	**G2M1**	**G2M3**	**G3M1**	**G3M3**
Cracking Day	26	18	20	19	38	25	22
28 day Free Shrinkage (με)	-330	-425	-537	-433	-410	-360	-407

From Table 4-18, we can see that the lowest free shrinkage at day 28 was measured from G1M1 which had the lowest amount of total cementitious material content among all mixes. On the other side, the latest cracking was observed from G1M3 which had the highest amount of fly ash replacement by 30%. As discussed in the earlier sections, the restrained and free shrinkage performance of G1M3 did not correlate as well

as the other SCC mixes. This is mainly attributed to the mechanism of restrained shrinkage test, and as well as the very high amount of total cementitious material content (900 pounds). Nonetheless, the free shrinkage strain of G2M3 (30% FA) was slightly lower than that of G2M1 (10% FA) at day 28.

For future research purposes, we can consider the lowest amount of free shrinkage measurement presented in Table 4-18, as the limit to even further decrease. So for an SCC mix to resist restrained shrinkage cracking, or to extend the elapsed time until cracking beyond day 26, the mix should be designed such that the free shrinkage strain will be less than 330 micro strains measured at day 28 after casting.

CHAPTER V

SUMMARY AND CONCLUSIONS

5.1 SUMMARY AND CONCLUSIONS

The primary purpose of this study is to compare the effect of different mix design parameters specifically on the restrained shrinkage behavior of SCC mixes. A total of 7 SCC mixes were designed and mixed at laboratory conditions. The restrained conditions of SCC mixes were simulated by using the AASHTO-T334 ring test with an additional data collection method. Four ASTM tests were performed in companion with the AASHTO-T334 to test the mechanical properties of the SCC mixes. The restrained condition behavior was evaluated with respect to the following mix design parameters: (1) Total cementitious material content (2) Percentage of fly ash replacement (3) Percentage of silica fume replacement.

The summary of the results from the testing results can be listed as follows:

1) SCC is very susceptible to tensile cracking under restrained conditions. All the studied SCC mixes exhibited cracking before day 56 under the restraint provided by the AASHTO-T334 ring. Moreover, 6 of the 7 SCC mixes cracked between day 19.5 and 29 after casting on the average of two ring specimens.

2) Free shrinkage behavior of the studied SCC mixes is also found to be very severe compared to the related HPC or OPC findings from previous research. The lowest free shrinkage strain measured was 10% higher than the 450 micro strains recommended strain level at 56 day recommended by Aktas (2007) and Montemerano (2008).
3) Since all the studied SCC mixes exhibited restrained shrinkage cracking, it was not possible to define a limit of free shrinkage strain for no cracking. On the other hand, based in the free shrinkage measurements, it can be concluded that the free shrinkage strain should be kept under 330 micro strains for SCC mixes not to crack, or to extend the cracking age beyond day 26.
4) The effect of total cementitious material content in the restrained and free shrinkage behavior of the studied SCC mixes was found to be significant. Based on the visual crack observations, an increase of 100 pounds in the total cementitious material content decreased the elapsed time until cracking by 9.5 days. In other words, after the curing is removed, additional 100 pounds of cementitious material decreased the crack-free lifetime almost 3 times. (15 days versus 5.5 days). Similarly, free shrinkage strain at day 56 aggravated by 24% to 68% with additional 100 pounds of cementitious material content. Although the shrinkage behavior was partially influenced by variations in the modulus of elasticity, and the pozzolanic material replacement amount, the effect of total cementitious material content was found to be significant since the range of percentile difference is very high.

5) Fly ash as a partial replacement of Portland cement was found to be not significantly influencing the free shrinkage performance of the SCC mixes. This was attributed to the high level cementitious material content at which the free shrinkage performances were compared. Since the free shrinkage performance of fly ash replacement was evaluated at 900 pounds, the free shrinkage magnitude was already very high, and thus not very sensitive to fly ash amount changes. On the other hand, the restrained shrinkage cracking performance of the SCC mixes was found to be improved with the increase of fly ash replacement percentage. Although, the cracking was inevitably observed, the cracking age was delayed 15 days with 30% fly ash replacement with respect to 10% replacement. (Cracking observed day 23 versus day 38). Also, if 20% fly ash replacement is used, the cracking age was found to be 24 on the average of 5 mixes. Although only one mix above the 20% exhibited a long crack-free lifetime, high percentages of fly ash replacement is found to be potentially contributory in reducing the shrinkage performance of SCC.
6) The influence of silica fume replacement percentage in changing the free and restrained shrinkage behavior of SCC mixes was found to be not significant. Between 0% and 10% replacement, a difference of 3.5 days was observed in the elapsed time until cracking (28 days versus 24.5 days). The free shrinkage performance was influenced moderately with the change in silica fume replacement amount. SCC with no silica fume had 10% less free shrinkage strain at day 56 compared to SCC with 10% silica fume replacement given that the cementitious material content is kept the same.

5.2 RECOMMENDATIONS FOR FUTURE RESEARCH

The total amount of cementitious material for the SCC mixes falls into a large scale. One of the primary reasons that create this large range is the advances in the concrete admixtures. Both in concrete research area and in the industry desired fresh concrete values are achieved with the utilization of appropriate concrete admixtures. Although these advanced materials contribute to the improvement of SCC in general, it indirectly creates this type of a large spectrum for the total amount of cementitious material. And as a result of this large spectrum, the effect of other parameters, such as the pozzolanic material effects becomes unidentifiable in some cases. Thus, a more refined range of total cementitious material content for SCC mix designs can be investigate in more detail.

Also, the contributory effect of coarse aggregate content and size has been well established in the case of HPC, and not as extensively in SCC. Since the water to cement ratio can't be increased to significantly due to the required flowability level, the possibility of any benefits from the aggregate proportioning could be investigated in more detail.

REFERENCES

1. Aktas, K., "Assessment of Cracking Potential of High-Performance Concrete due to Restrained Shrinkage", M.S. Thesis, Rutgers University, 2007.

2. ASTM C 1621/C 1621M – 06, "Standard Test Method for Passing Ability of Self Consolidating Concrete by J - -Ring".

3. Bonen, D., Shah, S., P., "Fresh and Hardened Properties of Self-Consolidating Concrete", Prog. Struct. Engng. Mater. 2005, pp 14-26.

4. Domone, P., L., "Self-Compacting Concrete: An Analysis of 11 Years of Case Studies", Cement & Concrete Composites 28, 2006, pp 197-208.

5. El-Chabib, H., Nehdi, M., "Effect of Mixture Design Parameters on Segregation of Self-Consolidating Concrete", ACI Materials Journal, Vol. 103, No.5, September-October 2006, pp 374-383.

6. Felekoglu, B., Turkel, S., Baradan, B., "Effect of Water/Cement Ratio on the Fresh and Hardened Properties of Self-Compacting Concrete", Building and Environment 42, 2007, pp 1795-1802.

7. Gomez, J., F., Landsberger, G., A., "Evaluation of Shrinkage Prediction Models for Self-Consolidating Concrete", ACI Materials Journal, Vol. 104, No.5, September-October 2007, pp 464-473

8. Gurjar, A., H., "Mix Design and Testing of Self-Consolidating Concrete Using Florida Materials", Florida Department of Transportation, Report No. BD 503, December 2004.

9. Hodgson III, D., Schindler, A., K., Brown, D., A., Stroup-Gardiner, M., "Self-Consolidating Concrete for Use in Drilled Shaft Applications", Journal of Materials in Civil Engineering, Vol. 17, No.3, May-June 2005, pp 363-369.

10. Hwang, S., D., Khayat, K., H., "Effect of Mixture Composition on Restrained Shrinkage Cracking of Self-Consolidating Concrete Used in Repair", ACI Materials Journal, V. 105, No. 5, September-October 2008, pp 499-509.

11. Hwang, S., D., Khayat, K., H., Bonneau, O., "Performance-Based Specifications of Self-Consolidating Concrete Used in Structural Applications", ACI Materials Journal, Vol. 103, No. 2, March-April 2006, pp 121-129.

12. Khayat, K., H., Mitchell, D., "Self-Consolidating Concrete for Precast, Prestressed Concrete Bridge Elements", Transportation Research Board of the National Academies, NCHRP Report 628, 2009.

13. Kim, J., K., Han, S., H., Park, Y., D., Noh, J., H., "Material Properties of Self-Flowing Concrete", Journal of Materials in Civil Engineering, Vol. 10, No. 4, November 1998, pp 244-249.

14. Kiousis, P., D., Whitcomb, B., L., Study on the Use of Self-Consolidating Concrete for the Repair of the Mead Bridges on I-25", Colorado Department of Transportation Research, Interim Report No. CDOT-2007-1, 2007.

15. Lachemi, M., Hossain, K., M., A., Lambros, V., Bouzoubaa, N., "Development of Cost-Effective Self-Consolidating Concrete Incorporating Fly Ash, Slag Cement, or Viscosity-Modifying Admixtures", ACI Materials Journal, Vol. 100, No.5, September-October 2003, pp 419-425.

16. Lange, D., A., Struble, L., J., Dambrosia, M., D., Shen, L., Dominguez, F., T., Birch, B., F., Brinks, A., J., "Performance and Acceptance of Self-Consolidating Concrete: Final Report", Illinois Department of Transportation, Report No. FHWA-ICT-08-020, July 2008.

17. Larson, K., H., Peterman, R., J., Esmaeily, A., "Evaluating the Time-Dependent Deformations and Bond Characteristics of a Self-Consolidating Concrete Mix and The Implications for Pretensioned Bridge Applications", Kansas Department of Transportation, Report No. K-Tran-KS-07-1, April 2007.

18. Loser, R., Leemann, A., "Shrinkage and Restrained Shrinkage Cracking of Self-Compacting Concrete Compared to Conventionally Vibrated Concrete", Materials and Structures 42, 2009, pp 71-82.

19. Montemerano, J., "Restrained Shrinkage and Cracking Behavior of High-Performance Concrete Containing Slag", M.S. Thesis, Rutgers University, December 2008.

20. Naito, C., Brunn, G., Parent, G., Tate, T., "Comparative Performance of High Early Strength and Self Consolidating Concrete for Use in Precast Bridge Beam Construction", National Center for Engineering Research on Advanced Technology or Large Structural Systems, ATLSS Report No. 05.03, May 2005.

21. Nassif, H., Aktas, K., Suksawang, N., Najm, H., "Assessment of Cracking Potential in High-Performance Concrete under Restrained Conditions", Transportation Research Board Annual Meeting, Paper No. 08-3042, 2008.

22. NG, P., L., Wong, H., H., C., Ng, I., Y., T., Kwan, A., K., H., "Measuring Shrinkage of Self-Consolidating Concrete Incorporating Fly Ash and Silica Fume Using Fiber-Optic Sensor", ACI Special Publication 242-17, April 2007, pp 211-226.

23. Nowak, A., S., Laumet, P., C., Kaszynska, M., Szerszen, M., M., Podhoreck, P., J., "US Specific Self Compacting Concrete for Bridges", Transportation Research Board of the National Academies, Final Report for Highway IDEA Project 89, August 2005.

24. Okamura, H., Ouchi, M., "Self-Compacting Concrete Development, Present Use and Future", International RILEM symposium on self-compacting concrete No1, Stockholm, 1999, pp 3-14.

25. Okamura H., Ouchi, M., "Self-Compacting Concrete", Journal of Advanced Concrete Technology, Vol.1, No.1, April 2003, pp 5-15.

26. Ouchi, M., Nakamura, S., Osteeberg, T., Hallberg, S., E., Lwin, M., "Applications of Self-Compacting Concrete in Japan, Europe, and the United States, ISHPC, 2003, pp 1-20.

27. Ouyang, C., and Shah, S., P., "Geometry dependent R curve for quasi-brittle materials", Journal of American Ceramics Society, 74(11), 1991, pp 2831-2836.

28. Ozbay, E., Oztas, A., Baykasoglu, A., Ozbebek, H., "Investigating Mix Proportions of High Strength Self Compacting Concrete by Using Taguchi Method", Construction and Building Materials 23, 2009, pp 694-702.

29. Ozyildirim, C., Lane, D., S., "Final Report: Evaluation of Self-Consolidating Concrete", Virginia Transportation Research Council, U.S. Department of Transportation Federal Highway Administration, VTRC 03-R13, June 2003.

30. Ozyildirim, C., "Bulb-T Beams with Self Consolidating Concrete on the Route 33 Bridge Over the Pamunkey River in Virginia", Virginia Transportation Research Council, Final Report VTRC 09-R5, November 2008.

31. RILEM Technical Committee, "Durability of Self-Compacting Concrete", Materials and Structures 41, Final Report of RILEM TC 205-DSC, 2008, pp 225-233.

32. Ruiz, E., D., Floyd, R., W., Staton, B., W., Do, N., H., Hale, W., M., "Prestress Losses in Prestressed Bridge Girders Cast with Self-Consolidating Concrete", Mack-Blackwell Rural Transportation Center, US Department of Transportation, Report No. MBTC-2071, July 2008.

33. See, H., T., Attiogbe, E., K., "Performance of Self-Consolidating Concrete under Restrained Shrinkage", ACI Special Publications, SP-227-14, 2005, pp 303-315.

34. Shuguang, H., Xhen, H., Wenquan, L., Huaquan, Y., Wen, Z., "Investigation of the Free and Restrained Shrinkage of Self-Compacting Concrete", Journal of Wuhan University of Technology-Mater: Sci. Ed., 2006, pp 9-14.

35. Suksawang, N., Nassif, H., H., Najm, H., S., "Evaluation of Mechanical Properties for Self-Consolidating, Normal, and High-Performance Concrete", Journal of the Transportation Research Board, No. 1979, 2006, pp 36-45.

36. Turcry, P., Loukili, A., Haidar, K., Pijaudier-Cabot, G., Belarbi, A., "Cracking Tendency of Self-Compacting Concrete Subjected to Restrained Shrinkage: Experimental Study and Modeling", Journal of Materials in Civil Engineering, ASCE 18:1, January-February 2006, pp 46-54.

37. Weiss, W., J., Yang, W., Shah, S., P., "Influence of Specimen Size/Geometry on Shrinkage Cracking of Rings", Journal of Engineering Mechanics, Vol. 126, No.1, 2000, pp 93-101.

38. Wustholz, T., Reinhardt, H., W., "Deformation Behavior of Self-Compacting Concrete under Tensile Loading", Materials and Structures 40, October 2007, pp 965-977.